1-1-2005

# Phase diagrams of stoichiometric polyelectrolyte-surfactant complexes.

Michael J. Leonard
*University of Massachusetts Amherst*

# PHASE DIAGRAMS OF STOICHIOMETRIC POLYELECTROLYTE–SURFACTANT COMPLEXES

A Dissertation Presented

by

MICHAEL J. LEONARD

Submitted to the Graduate School of the
University of Massachusetts Amherst in partial fulfillment
of the requirements for the degree of

DOCTOR OF PHILOSOPHY

September 2005

Department of Polymer Science and Engineering

# PHASE DIAGRAMS OF STOICHIOMETRIC POLYELECTROLYTE–SURFACTANT COMPLEXES

A Dissertation Presented

by

MICHAEL J. LEONARD

Approved as to style and content by:

Helmut H. Strey, Chair

David A. Hoagland, Member

Surita R. Bhatia, Member

Shaw L. Hsu, Department Head
Polymer Science and Engineering

## DEDICATION

To my family, for their tireless love and support.

## ACKNOWLEDGMENTS

I would like to express my deepest appreciation to my advisor, Professor Helmut Strey, for his many years of guidance, support, and patience as this work was conceptualized, carried out, and documented. I would also like to express my gratitude to the members of my committee, Professors David Hoagland and Surita Bhatia, for their insightful comments and suggestions in all aspects of the research presented here. Thanks are also due to my colleagues in the Strey research group, especially Richard Nause, for their support and camaraderie during my career as a graduate student. I also gratefully acknowledge the support of Professor Alan Lesser, as well as that of John Domian in the Departmental machine shop. Finally, I would like to recognize the financial support of the Polymer Science and Engineering Department and the National Science Foundation Materials Research Science and Engineering Center at the University of Massachusetts Amherst.

## ABSTRACT

## PHASE DIAGRAMS OF STOICHIOMETRIC POLYELECTROLYTE–SURFACTANT COMPLEXES

SEPTEMBER 2005

MICHAEL J. LEONARD, B.S., ROANOKE COLLEGE

Ph.D., UNIVERSITY OF MASSACHUSETTS AMHERST

Directed by: Professor Helmut H. Strey

When a water-soluble polyelectrolyte is combined with an oppositely-charged surfactant solution at a stoichiometric charge ratio, self-assembly into a highly ordered, water-insoluble complex can occur. These materials exhibit phase structures which are analogous to their pure surfactant components, and significant effort has been made in the past several decades to characterize, predict, and control the various morphologies observed in these systems. However, a truly comprehensive understanding of the phase behavior of these systems is lacking.

The purpose of this project is to establish general phase diagrams for self-assembled, stoichiometric poly(acrylate-*co*-acrylamide)–cetyltrimethylammonium halide (PAAm–CTAX) complexes by studying phase structure as a function of ionic strength, salt type, polyelectrolyte charge density, temperature, and applied osmotic pressure with small-angle X-ray scattering (SAXS). By developing a deeper understanding of the phase behavior and energetics of such a model system, it is hoped that general trends can be extrapolated to other polyelectrolyte–surfactant systems, such

as polysaccharide–surfactant systems, which may provide the means to template desired structures in nanoporous, biocompatible matrices. Materials such as these may be attractive targets for drug delivery and nanoscale separation applications.

## TABLE OF CONTENTS


Page

ACKNOWLEDGMENTS ..... v

ABSTRACT ..... vi

LIST OF TABLES ..... xi

LIST OF FIGURES ..... xiii

CHAPTER

1. INTRODUCTION ..... 1

1.1 Self-Assembly in Polymer–Surfactant Systems ..... 1
1.2 Principal Experimental Techniques ..... 4

1.2.1 The Osmotic Stress Method ..... 4
1.2.2 Small-Angle X-Ray Scattering ..... 6

2. PHASE DIAGRAMS OF MODEL STOICHIOMETRIC POLYELECTROLYTE–SURFACTANT COMPLEXES ..... 21

2.1 Introduction ..... 21
2.2 Experimental ..... 22

2.2.1 Materials ..... 22
2.2.2 Methods ..... 22
2.2.3 Measurements ..... 24
2.2.4 Crystallographic Interpretation of SAXS Data ..... 25

2.3 Results and Discussion ..... 26

2.3.1 General Phase Sequence ..... 26
2.3.2 Phase Behavior in 10 mM and 100 mM Salt ..... 28

2.3.2.1 Osmotic Stress Effects ..... 28
2.3.2.2 Coexistence Regions ..... 29
2.3.2.3 Charge Density Effects ..... 30
2.3.2.4 Effects of Ionic Strength and Salt Type ..... 31

2.3.3 Phase Behavior in 1M Salt ..... 33
2.3.4 Phase Behavior at Higher Osmotic Pressures ..... 34
2.3.5 Temperature-Dependent Phase Behavior ..... 35

2.4 Conclusions ..... 35

3. PHASE DIAGRAMS OF STOICHIOMETRIC BIOPOLYMER–SURFACTANT COMPLEXES ..... 77

3.1 Introduction ..... 77
3.2 Experimental ..... 79

3.2.1 Materials ..... 79
3.2.2 Methods ..... 80
3.2.3 Measurements ..... 81

3.3 Results and Discussion ..... 82

3.3.1 Alginate–CTAX Complexes ..... 82

3.3.1.1 Osmotic Stress Effects ..... 82
3.3.1.2 Effects of Ionic Strength and Salt Type ..... 83

3.3.2 Chitosan–SDS Complexes ..... 84

3.4 Conclusions ..... 85

4. ENERGETICS OF THE CUBIC-TO-HEXAGONAL TRANSITION IN POLYELECTROLYTE–SURFACTANT COMPLEXES ..... 98

4.1 Introduction ..... 98

4.1.1 Energetics of Amphiphilic Monolayers ..... 98
4.1.2 Free Energy Measurement ..... 100

4.2 Experimental ..... 101

4.2.1 Materials ..... 101
4.2.2 Methods ..... 102

4.2.2.1 Sample preparation ..... 102

4.2.2.1.1 Hydration experiments ..... 102
4.2.2.2.2 Osmotic stress experiments ..... 104

4.2.3 Measurements ..... 104

4.3 Results and Discussion ..... 105

4.3.1 Osmotic Stress and Hydration Experiments ..... 105
4.3.2 Energetics of the Transition ..... 106

4.4 Conclusions ..... 110

APPENDIX: TEMPERATURE DEPENDENCE OF POLYELECTROLYTE–SURFACTANT COMPLEX STRUCTURE ..... 124

A.1 Introduction ..... 124
A.2 Experimental ..... 125
A.3 Results and Discussion ..... 126
A.4 Conclusions ..... 127

BIBLIOGRAPHY ..... 135

## LIST OF TABLES


Table

Page

2.1. Unit Cell Sizes of PAAm–CTABr Complexes in 100 mM NaBr at Varying Polyelectrolyte Charge Densities ..... 37

2.2. Unit Cell Sizes of PAAm–CTABr Complexes in 10 mM NaBr at Varying Polyelectrolyte Charge Densities ..... 38

2.3. Unit Cell Sizes of PAAm–CTACl Complexes in 100 mM NaCl at Varying Polyelectrolyte Charge Densities ..... 39

2.4. Unit Cell Sizes of PAAm–CTACl Complexes in 10 mM NaCl at Varying Polyelectrolyte Charge Densities ..... 40

2.5. Unit Cell Sizes of PAAm–CTACl Complexes in 1 M NaCl at Varying Polyelectrolyte Charge Densities ..... 41

2.6. Exponential Decay Length Data for PA–CTAX Complexes ..... 42

2.7. Exponential Decay Length Data for 70% Charge PAAm–CTAX Complexes ..... 43

2.8. Exponential Decay Length Data for 40% Charge PAAm–CTAX Complexes ..... 44

2.9. Interplanar Spacings for PA–CTAX Complexes Exposed to Saturated Salt Solution Vapor ..... 45

2.10. Interplanar Spacings for 70% Charge PAAm–CTAX Complexes Exposed to Saturated Salt Solution Vapor ..... 46

2.11. Interplanar Spacings for 40% Charge PAAm–CTAX Complexes Exposed to Saturated Salt Solution Vapor ..... 47

3.1. Unit Cell Sizes of Alginate–CTABr Complexes ..... 86

3.2. Unit Cell Sizes of Alginate–CTACl Complexes ..... 87

3.3. Exponential Decay Length Data for Alginate–CTAX Complexes ..... 88

4.1. Sample Preparation Data for Hydration Experiments ..... 111

4.2. Structural Data from Replicate Hydration Experiments ..... 112

4.3. Structural Data from Replicate Osmotic Stress Experiments ..... 113

4.4. Bending Moduli of Various Lipid–Water Systems..... 114

4.5. Lipid and Solvent Abbreviations..... 115

## LIST OF FIGURES


Figure

Page

1.1. Proposed approach for producing a nanostructured hydrogel ..... 11

1.2. Schematic illustration of an osmotic stress experiment ..... 12

1.3. Key components of SAXS apparatus ..... 13

1.4. Comparison of SAXS patterns obtained from divergent and focused beams ..... 14

2.1. Structures of the polyelectrolytes and surfactants used for the phase behavior model study ..... 48

2.2. 2-D SAXS Image and angular-averaged scattering profile for a typical PA–CTACl complex in 10 mM NaCl ..... 49

2.3. 2-D SAXS Image and angular-averaged scattering profile for a typical PA–CTACl complex in 10 mM NaCl at an approximate osmotic pressure of 112 atm ..... 50

2.4. 2-D SAXS Image and angular-averaged scattering profile for a typical PA–CTACl complex at an approximate osmotic pressure of 1000 atm ..... 51

2.5. Correlation of measured and predicted $(a/d)^2$ values with Miller index sums for PA–CTACl unit cells in 10 mM NaCl at 2 osmotic pressures ..... 52

2.6. Phase diagram for PA–CTABr complexes in 10 mM NaBr and 100 mM NaBr ..... 53

2.7. Phase diagram for 70% charge PAAm–CTABr complexes in 10 mM NaBr and 100 mM NaBr ..... 54

2.8. Phase diagram for 40% charge PAAm–CTABr complexes in 10 mM NaBr and 100 mM NaBr ..... 55

2.9. Phase diagram for PA–CTACl complexes in 10 mM NaCl and 100 mM NaCl ..... 56

2.10. Phase diagram for 70% charge PAAm–CTACl complexes in 10 mM NaCl and 100 mM NaCl..... 57

2.11. Phase diagram for 40% charge PAAm–CTACl complexes in 10 mM NaCl and 100 mM NaCl..... 58

2.12 Angular-averaged scattering profiles for PA–CTACl complexes in 10 mM NaCl and 70% charge PAAm–CTABr complexes in 100 mM NaBr..... 59

2.13 Angular-averaged scattering profiles for 40% charge PAAm–CTACl complexes in 100 mM NaCl..... 60

2.14. Phase diagram for PA–CTACl complexes in 1 M NaCl..... 61

2.15. Phase diagram for 70% charge PAAm–CTACl complexes in 1 M NaCl..... 62

2.16. Phase diagram for 40% charge PAAm–CTACl complexes in 1 M NaCl..... 63

2.17. Angular-averaged scattering profiles for PA–CTACl and 70% charge PAAm–CTACl complexes under osmotic stress in 1 M NaCl..... 64

2.18. Phase diagram for PA–CTACl complexes exposed to saturated salt solution vapor..... 65

2.19. Phase diagram for 70% charge PAAm–CTACl complexes exposed to saturated salt solution vapor..... 66

2.20. Phase diagram for 40% charge PAAm–CTACl complexes exposed to saturated salt solution vapor..... 67

2.21. Angular-averaged scattering profiles for PA–CTACl complexes exposed to saturated salt solution vapor..... 68

2.22. Angular-averaged scattering profiles for 70% charge PAAm–CTACl complexes exposed to saturated salt solution vapor..... 69

2.23. Angular-averaged scattering profiles for 40% charge PAAm–CTACl complexes exposed to saturated salt solution vapor..... 70

2.24. Schematic polyelectrolyte–surfactant complex phase diagram..... 71

3.1. Structures of the polyelectrolytes and surfactants used for the polysaccharide–surfactant study ..... 89

3.2. Phase diagram for alginate–CTABr complexes in 100 mM NaBr and 100 mM NaBr ..... 90

3.3. Phase diagram for alginate–CTABr complexes in 10 mM NaBr and 100 mM NaBr ..... 91

3.4. Angular-averaged scattering profiles for alginate–CTABr complexes in 10 mM NaBr and 100 mM NaBr ..... 92

3.5. Angular-averaged scattering profiles for alginate–CTACl complexes in 10 mM NaCl and 100 mM NaCl ..... 93

3.6. 2-D SAXS Image and angular-averaged scattering profiles for chitosan–SDS complexes in 100 mM NaCl at 2 osmotic pressures ..... 94

4.1. Angular-averaged SAXS profiles for 70% charge PAAm–CTACl complexes at 100 mM ionic strength under osmotic stress ..... 116

4.2. Angular-averaged SAXS profiles for 70% charge PAAm–CTACl complexes at 100 mM ionic strength under controlled hydration ..... 117

4.3. Unit cell volume versus water content for *Pm*3*n* and hcpc systems ..... 118

4.4. Characterization of the cubic-to-hexagonal transition in PAAm–CTACl complexes at 100 mM ionic strength under osmotic stress ..... 119

4.5. Water content versus Bragg spacing for PAAm–CTACl complexes at 100 mM ionic strength ..... 120

A.1. Temperature-dependent, angular-averaged scattering profiles for PA–CTACl and 70% charge PAAm–CTABr complexes at 100 mM ionic strength and 5 wt % PEG ..... 129

A.2. Temperature-dependent Bragg spacings for 70% charge PAAm–CTABr complexes at 100 mM ionic strength ..... 130

A.3. Temperature-dependent Bragg spacings for PA–CTACl complexes at 100 mM ionic strength ..... 131

A.4. Bragg spacings for PA–CTACl complex at 100 mM ionic strength throughout a temperature cycle ..... 132

A.5. Angular-averaged scattering profiles for PA–CTACl complexes at 100 mM ionic strength at the beginning and end of a temperature cycle..... 133

# CHAPTER 1

# INTRODUCTION

## 1.1 Self-Assembly in Polymer–Surfactant Systems

Interaction between macroions of opposite charge is a recurring concept in biological self-assembly[1]. Examples include complexation of DNA with histone proteins inside cell nuclei[2], protamine-induced DNA condensation inside sperm heads[3-5], and the formation of arterial plaque—a complex between positively charged low-density lipoprotein and negatively charged polysaccharides[6,7]. Throughout the past several decades, researchers have recognized the potential of electrostatically driven self assembly as a facile structure-forming tool, and significant efforts have been made to elucidate assembly mechanisms, as well as to characterize the wide variety of observed structures.

Complexes between polyelectrolytes and oppositely charged, small-molecule surfactants provide especially good examples of electrostatic self-assembly, and as such, have attracted a significant amount of attention, both theoretically[8-11] and experimentally[12-18]. Complexes formed between flexible, highly charged polyelectrolytes and oppositely charged surfactants at stoichiometric charge ratios have been of particular experimental interest, since they often form water-insoluble complexes possessing long-range nanoscopic order[19-26].

While purely electrostatic interactions undoubtedly play a role during complexation, counterion release is believed to be the major driving force for the self-

assembly process in these and other highly charged systems[27-33]. Prior to complexation, the polyelectrolyte and surfactant counterions are restricted to regions close to the surfaces of both the surfactant micelles and the polyelectrolyte chains, a phenomenon known as Manning condensation[34]. Upon adsorption of a polyelectrolyte chain to the surface of the ionic surfactant micelle, the counterions bound to both species are released into the bulk solution, which gives rise to a significant increase in the overall entropy of the system. Other possible contributions to the free energy include the conformational entropy of the polyelectrolyte, the elastic energy of the surfactant surface, and hydrophobic and steric interactions between the polyelectrolyte chain and the surfactant. The combination of these driving forces makes polyelectrolyte–surfactant binding significantly more favorable than micelle formation. This point is evidenced by the fact that, in the presence of polyelectrolytes, critical aggregation concentrations (cac) of surfactants in dilute solution tend to be orders of magnitude lower than critical micelle concentrations (cmc)[35,36]. Major portions of this thesis are dedicated to developing comprehensive phase diagrams for model polyelectrolyte–surfactant complexes, and to characterizing the structural transitions that occur in these materials.

Because they exhibit such rich phase behavior, stoichiometric polyelectrolyte–surfactant complexes may serve as attractive precursors for nanostructured materials for potential drug delivery and molecular separation applications. Self-assembled colloidal systems have long been used as templates for creating mesoporous and nanoporous materials. Common approaches to these materials

have involved the self-assembly of surfactants[37-41] and block copolymers[42] in the presence of various silica species, followed by the sintering of the silica phase. Since the temperatures used for the sintering process often exceed 500 °C, the material comprising the organic template completely decomposes, leaving a rigid nanoporous matrix. Surfactant–templated siliceous materials have also been prepared under milder conditions that do not involve high-temperature sintering[43,44]. In both types of systems, pore sizes tend to be monodisperse, as they are dictated by the self-assembled amphiphile structure. Materials possessing monodisperse nanopores are attractive because they may allow for improved size-based selectivity and filtering capabilities over materials with broad distributions of pore sizes.

The amphiphilic templating approach described above has also been used to create non-siliceous mesostructured and nanostructured materials[45-49], but has been met with much more limited success. Removal of amphiphilic templates from non-siliceous, soft matter systems has proven to be especially challenging, since these materials are much less chemically and structurally stable than aluminosilicates. However, the potential of non-siliceous nanostructures materials is extremely high, especially in the area of biocompatible materials for drug delivery and molecular filtration.

Self-assembled polyelectrolyte–surfactant complexes may provide a route to such materials. Crosslinkable, biocompatible polyelectrolytes (e.g. charged polysaccharides) may provide the means to "lock in" the desired structure prior to removal of the surfactant template. The resulting hydrogel should be biocompatible

and would possess relatively monodisperse nanopores. This proposed 3-step process—complexation, matrix crosslinking, and surfactant removal—is illustrated schematically in Figure 1.1. A portion of this thesis is devoted to characterizing the phase behavior of charged polysaccharide–surfactant systems that may be useful for these types of applications.

## 1.2 Principal Experimental Techniques

The following sections of this chapter give brief introductions to the osmotic stress method and to the specialized small-angle X-ray scattering instrument that was used for all phase characterization work presented in this thesis.

### 1.2.1 The Osmotic Stress Method

The osmotic stress method provides a means for the direct investigation of the microscopic and thermodynamic details of intermolecular interactions[50], and has been successfully employed to measure intermolecular forces in lamellar stacks of lipid bilayers[51,52] and in hexagonal arrays of semi-stiff biopolymers, such as DNA[4,5,53], collagen[54], and various polysaccharides[55,56]. The essence of the method involves the controlled removal of water from macromolecular samples in aqueous environments via the application of osmotic pressure from an inert hydrophilic species, otherwise known as a neutral osmolyte. The thermodynamic work required to dehydrate the sample is equivalent to the work required to push its constituent molecules closer together. This work is equivalent to the chemical potential difference between the sample subject to

stress and the osmolyte, and can be expressed in terms of the osmotic pressure and the accompanying volume change within the sample (at fixed pressure, temperature, and solvent activity):

$$\Delta\mu\,(T, p, a) = -\Pi\,\Delta V \tag{1.1}$$

Therefore, if the molecular dimensions of the sample as a function of osmotic pressure can be tracked with X-ray scattering, information regarding the free energy of the system can be obtained by integrating the resulting equation of state[57].

A schematic picture of an osmotic stress experiment is shown in Figure 1.2. Experimentally, samples are equilibrated against a large excess of polymer solution whose osmotic pressure is known as a function of concentration, either through a dialysis membrane or across the solid-liquid phase boundary in phase-separated samples. Neutral and highly water-soluble polymers, such as poly(ethylene glycol) (PEG) and dextran, are well suited for use as osmotic stressing agents. For most charged biopolymer systems, higher molecular weight PEG is excluded from the interior of the sample as long as its radius of gyration is larger than the average distance between two polymer chains inside the sample. Under such conditions, osmotic pressures in excess of 300 atm can be achieved.

At this point, it is appropriate to acknowledge one of the key differences between osmotic pressure and hydrostatic pressure. In an osmotic stress experiment, changes in volume are due entirely to mass transfer between the osmolyte and the sample being stressed. Under hydrostatic pressure, on the other hand, volume changes are entirely due to material compressibility; mass is held fixed. Other researchers have

investigated the interesting effects of hydrostatic pressure on soft matter systems[58-62], but it may difficult to relate experimental data from hydrostatic pressure measurements directly to data obtained from osmotic stress experiments.

Using polymer solutions to apply osmotic stress has several advantages over the water vapor pressure method. While the osmotic pressure is set by the polymer concentration in the stressing solution, the salt activity can be fixed independently by adding salt to this solution. Since all activities are controlled by the stressing solution, the phase of the sample will thus be precisely specified–there can be no phase coexistence according to the Gibbs phase rule. Structural characterization of a single phase is typically much more straightforward than the characterization of two coexisting phases, but the latter can be accomplished with some extra effort if the structures of the coexisting species are known.

### 1.2.2 Small-Angle X-Ray Scattering

Small-angle X-ray scattering (SAXS) is a nondestructive structural characterization technique for solid and fluid materials exhibiting nanoscopic periodicity from ten to a few thousand Ångstroms. While there is no requirement for sample crystallinity with SAXS, the technique is best suited for samples which exhibit some degree of order. Stoichiometric polyelectrolyte–surfactant complexes are soft matter systems, and it can be a challenge to obtain the higher-order scattering peaks which are required for structure determination using common sealed-tube X-ray sources with divergent beams. Because of their material characteristics, the vast majority of

work that has been done to investigate stoichiometric polyelectrolyte–surfactant phase behavior has involved the use of high intensity synchrotron radiation. Synchrotron sources, however, are located at relatively few sites in the United States and, at most of these locations, competitive demand for experimental beam time is quite high. Conducting research at these facilities can also be very costly, due to the time and expense involved with frequent traveling. Since the routine use of synchrotron radiation was not possible at the time these studies began, a rotating anode X-ray instrument was purchased and customized to meet our specific experimental requirements. The camera and many of the components contained within it were designed by our group and custom-built in the Polymer Science and Engineering Department's machine shop. Photographs of the key instrument components are presented in Figure 1.3, and are described below.

Target motor and anode housing: This compartment houses the electron gun and rotating copper anode. It is kept under high vacuum (~ $10^{-9}$ torr) by a turbomolecuar pump, so as to avoid scattering of the generated X-rays by air as well as to prevent detrimental "arcing" between the electron gun and the target. A rotating anode instrument is generally a more intense source of radiation than a sealed-tube generator, since there is less heat built up on a constantly moving anode surface at the electron beam focal point than on a fixed surface. It is this heating of the anode at the electron beam focal spot that limits the maximum power of the generator.

Multilayer focusing optic: Laboratory X-ray sources emit radiation equally in all directions. Thus, the beam of radiation that passes through the anode housing

shutter is inherently divergent. Focusing of this "raw" beam can be accomplished through the use of an appropriate optic. The focusing optic chosen for our instrument was a Confocal Max-Flux optic, manufactured by Osmic, Inc. This optic uses a multilayer focusing scheme, with two orthogonal, laterally-grated reflectors that focus the beam symmetrically in two dimensions. This arrangement is similar to a traditional Kirkpatrick-Baez total reflection scheme[63], but because the two orthogonal reflectors are physically connected (i.e. one mirror cannot move independently of the other), alignment of this optic is relatively simple, compared to the traditional scheme, which uses two offset, independently adjustable mirrors. The Max-Flux optic also provides some degree of monochromatization by eliminating Cu Kβ radiation and a significant amount of low-energy background scattering compared to other total reflection schemes. In the Kirkpatrick-Baez scheme, the focusing mirror that is farthest from the source will intercept the least amount of radiation and will therefore limit the amount that can be focused on the detector. With the Max-Flux optic, on the other hand, both mirrors are an equivalent distance from the X-ray source so that the maximum amount of radiation is intercepted and focused on the detector. For our particular instrument, the beam size at the detector was $(100\ \mu m)^2$.

Camera enclosure: This enclosure consisted of 1/4-inch aluminum walls which were caulked with silicone; this configuration was sufficient to sustain a vaccum of approximately 6 torr. An optical rail was affixed to the bottom of the enclosure to

allow for variable positioning of the sample, detector, beamstop, and guard slits. As such, this camera was also well-suited for wide-angle experiments.

Guard slits: Two sets of slits were used at the camera's beam entrance point; each slit assembly consisted of four, independently adjustable tantalum blades. These slits block out low-angle, high-energy radiation that is co-emitted with the desired Cu Kα radiation. Without these slits, this undesirable high-energy radiation can give rise to large, extremely bright streaks near the center of the X-ray pattern which can obscure important diffraction signals due to the sample.

Variable-position sample holder: This brass sample holder was desgined to accommodate several types of sample cells, such as capillary tubes and Mylar-sandwiched cells. The holder was also equipped with a thermo-electric Peltier heating device, and the entire metal surface of the holder was water-cooled. A temperature range of 10–60 °C was accessible with this device. In addition, the vertical and horizontal position of the sample holder could be adjusted for optimum placement in the beam.

Variable-position beamstop: The beamstop consisted of a lead disc with a small hole cut in the center which was glued to a thin nickel plate. The attenuated incident X-ray beam was therefore visible on the image plate as a reference point for the center of the image. This beamstop assembly was fixed onto a thin, X-ray transparent polyimide strip and was attached to a U-shaped aluminum frame. In this geometry, none of the scattered radiation was blocked by the beamstop support, and full 360° angular

averages of the scattering patterns could be obtained. The vertical and horizontal position of the beamstop could be adjusted for optimum placement in the beam.

Image plate holder: This component simply consisted of an aluminum platform that secured the image plate in a vertical position at the end of the camera with two thumbscrews. An image plate is a thin piece of plastic coated with a phosphor-like material which is sensitive to high-energy radiation. After a scattering pattern is acquired, the plate is removed from the camera, and a digitized image of the X-ray pattern is generated by a specialized image plate scanning system. Image plates are significantly more sensitive than conventional X-ray film, and are much more convenient to use, as lengthy film development steps are unnecessary and processing of the digitized image can be done immediately after acquisition. In addition, used image plates can be erased by exposure to white fluorescent light and re-used indefinitely.

After its completion, this instrument provided significantly higher structural resolution with decreased exposure times versus the Department's existing SAXS equipment, as illustrated in Figure 1.4.

## Figures

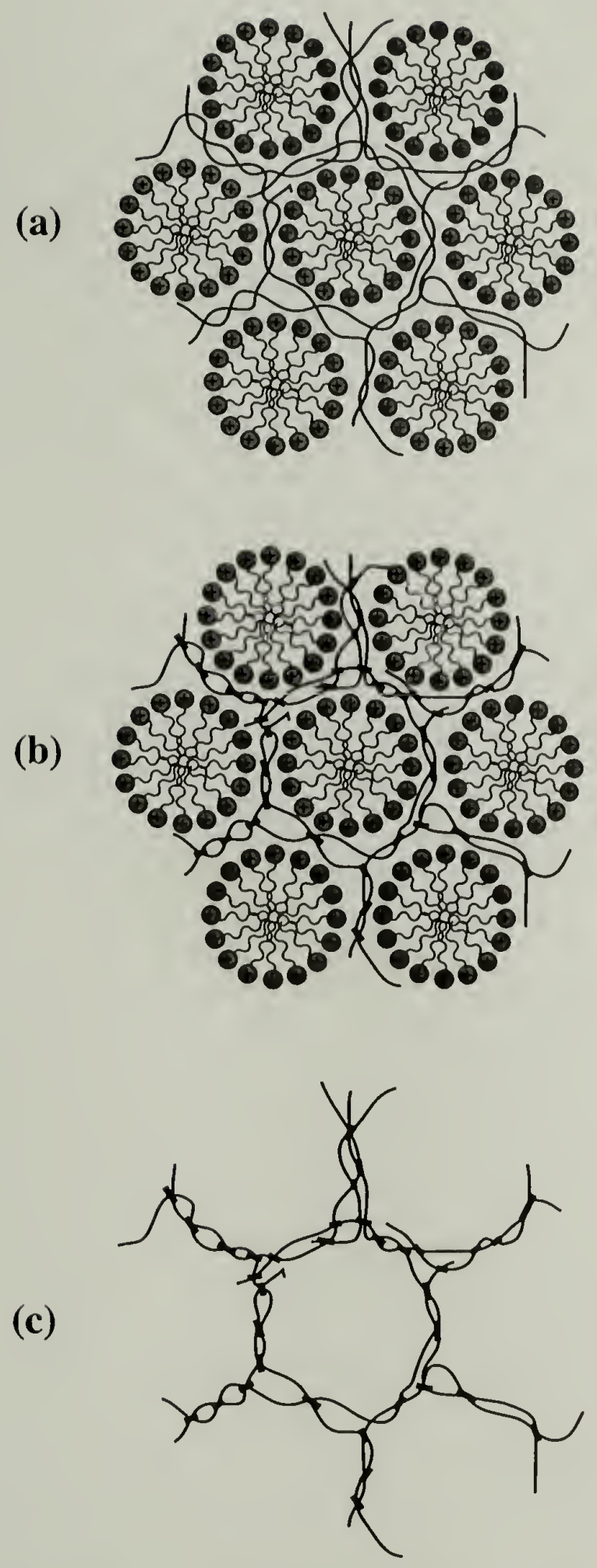


**Figure 1.1:** Proposed approach for producing a nanostructured hydrogel: (a) self-assembly (b) polymer crosslinking by chemical or physical means (c) surfactant removal, leaving a nanoporous polymer matrix.

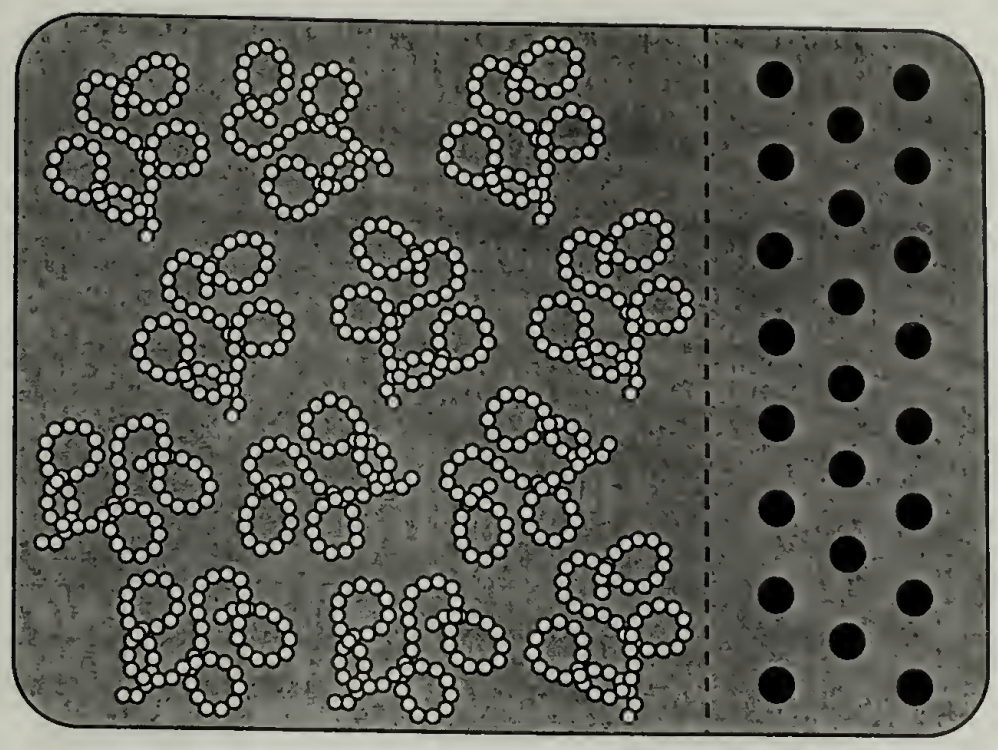

**Figure 1.2:** Schematic illustration of an osmotic stress experiment. A large reservoir of stressing solution, consisting of PEG (white coils) dissolved in a salt solution (shaded background) is equilibrated through a semipermeable membrane (dashed line) against an ordered sample (dark circles). If the sample and solution are phase-separated, the phase boundary can replace the semipermeable membrane as long as the macromolecular stressing agent does not have access to the aqueous spaces within the sample.

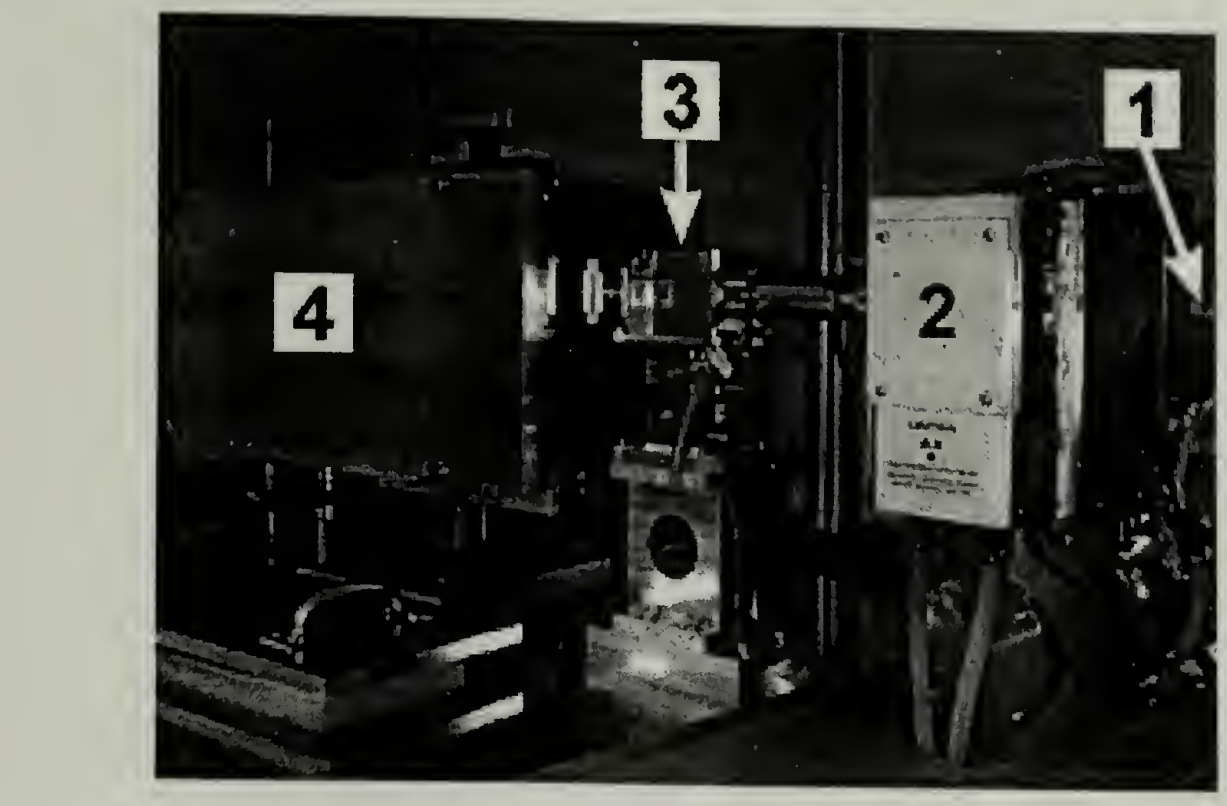


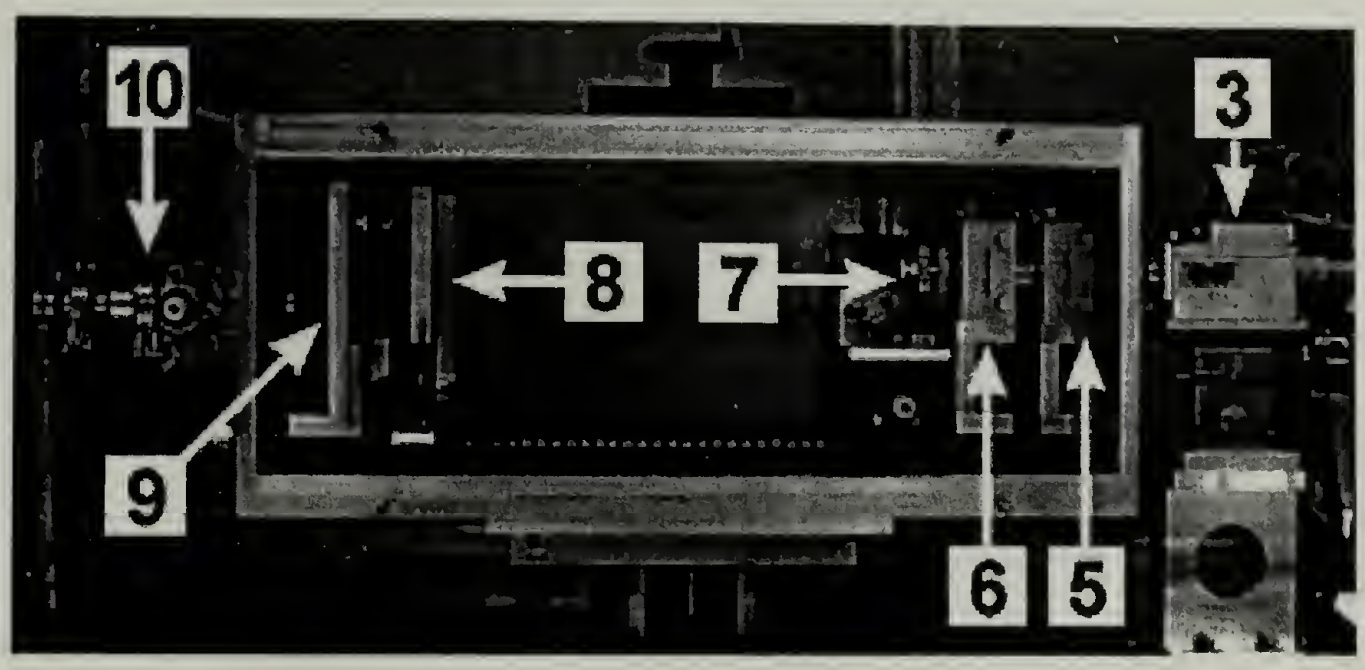


**Figure 1.3:** Key components of SAXS apparatus: target motor (1), anode housing (2), focusing optic (3), and camera (4). Camera components: guard slits (5,6), sample holder (7), beamstop (8), image plate holder (9), and vacuum inlet (10).

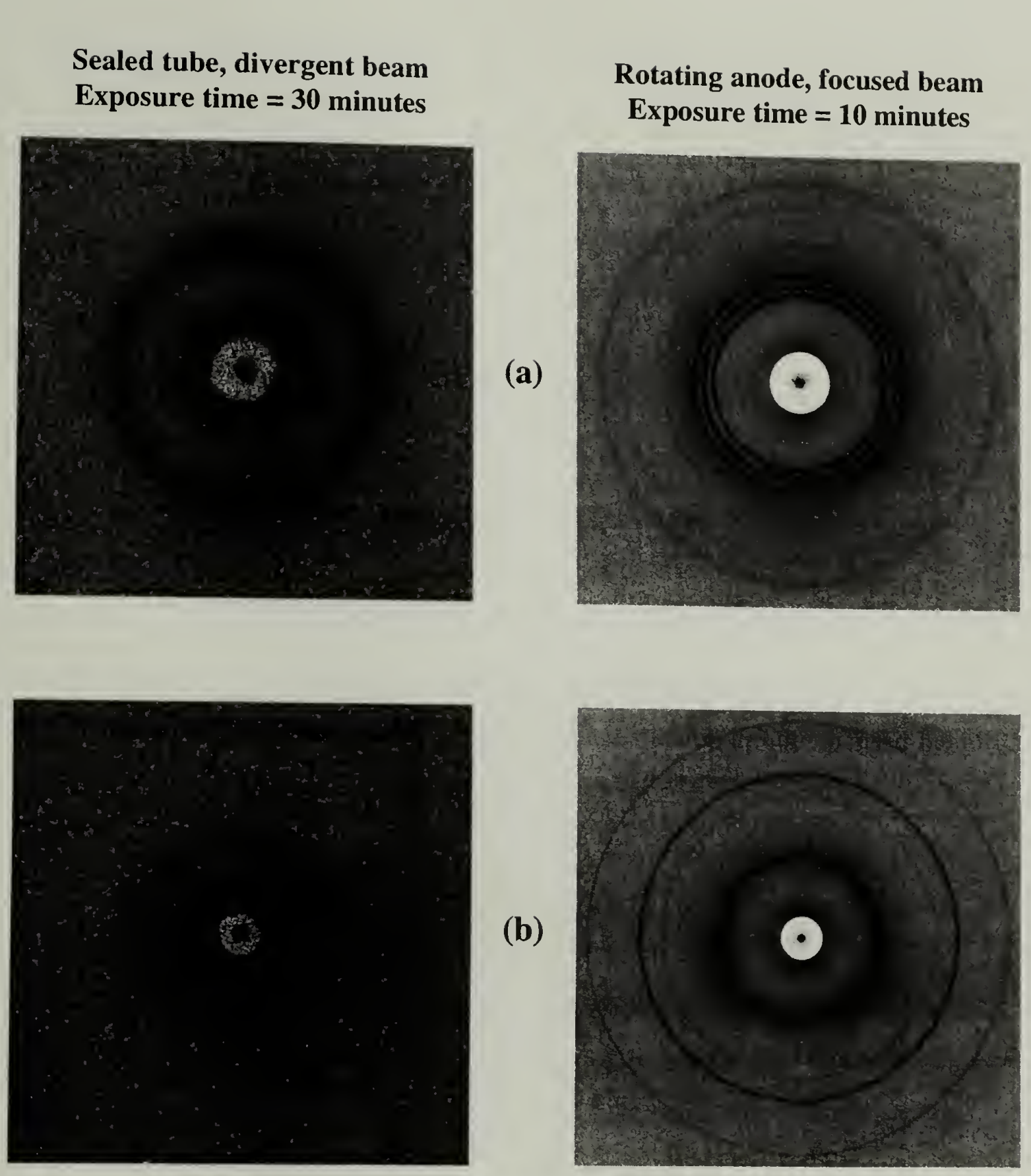


**Figure 1.4:** Comparison of SAXS patterns obtained from divergent (sealed-tube source) and focused (rotating anode source) beams. The peak positions are indicative of the (a) *Pm*3*n* cubic and (b) hexagonally close-packed cylindrical structures.

## References


[1] *Electrostatic Effects in Soft Matter and Biophysics*; Holm, C.; Kékicheff, P.; Podgornik, R., Eds.; Kluwer Academic Publishers: Dordrecht, The Netherlands, 2001.

[2] Darnell, J.; Lodish, H.; Baltimore, D. *Molecular Cell Biology,* Second ed.; Scientific American Books: New York, 1990.

[3] Bloomfield, V. A. DNA Condensation. *Curr. Opin. Struc. Biol.* **1996,** *6,* 334-341.

[4] Strey, H. H.; Podgornik, R.; Rau, D. C.; Parsegian, V. A. DNA-DNA interactions. *Curr. Opin. Struc. Biol.* **1998,** *8,* 309-313.

[5] Podgornik, R.; Strey, H. H.; Parsegian, V. A. Colloidal DNA. *Curr. Opin. Colloid In.* **1998,** *3,* 534-539.

[6] Camejo, G.; Fager, G.; Rosengren, B.; Hurtcamejo, E.; Bondjers, G. Binding of Low-Density Lipoproteins by Proteoglycans Synthesized by Proliferating and Quiescent Human Arterial Smooth-Muscle Cells. *J. Biol. Chem.* **1993,** *268,* 14131-14137.

[7] Camejo, G.; Lopez, A.; Lopez, F.; Quinones, J. Interaction of Low-Density Lipoproteins with Arterial Proteoglycans - the Role of Charge and Sialic-Acid Content. *Atherosclerosis* **1985,** *55,* 93-105.

[8] Diamant, H.; Andelman, D. Onset of self-assembly in polymer-surfactant systems. *Europhys. Lett.* **1999,** *48,* 170-176.

[9] Diamant, H.; Andelman, D. Self-Assembly in Mixtures of Polymers and Small Associating Molecules. *Macromolecules* **2000,** *33,* 8050-8061.

[10] Hansson, P. Self-Assembly of Ionic Surfactants in Polyelectrolyte Solutions: A Model for Mixtures of Opposite Charge. *Langmuir* **2001,** *17,* 4167-4180.

[11] Wallin, T.; Linse, P. Polyelectrolyte-Induced Micellization of Charged Surfactantts. Calculations Based on a Self-Consistent Field Model. *Langmuir* **1998,** *14,* 2940-2949.

[12] Ober, C. K.; Wegner, G. Polyelectrolyte-Surfactant Complexes in the Solid State: Facile Building Blocks for Self-Organizing Materials. *Adv. Mat.* **1997,** *9,* 17-31.

[13] Thalberg, K.; Lindman, B. Gel Formation in Aqueous Systems of a Polyanion and an Oppositely Charged Surfactant. *Langmuir* **1991,** *7,* 277-283.

[14] Thalberg, K.; Lindman, B.; Bergfeldt, K. Phase Behavior of Systems of Polyelectrolyte and Cationic Surfactants. *Langmuir* **1991,** *7,* 2893-2898.

[15] Goddard, E. D. Polymer-Surfactant Interaction Part II. Polymer and Surfactant of Opposite Charge. *Colloids Surf.* **1986,** *19,* 301-329.

[16] Isogai, N.; Narita, T.; Chen, L.; Hirata, M.; Gong, J.; Osada, Y. Polymer-surfactant interactions: their cooperativity and stoichiometry. *Colloids Surf. A* **1999,** *147,* 189-201.

[17] Ilekti, P.; Martin, T.; Cabane, B.; Piculell, L. Effects of Polyelectrolytes on the Structures and Interactions of Surfactant Aggregates. *J. Phys. Chem. B* **1999,** *103,* 9831-9840.

[18] Faul, C. F. J.; Antonietti, M. Ionic Self-Assembly: Facile Synthesis of Supramolecular Materials. *Adv. Mat.* **2003,** *15,* 673-683.

[19] Antonietti, M.; Conrad, J.; Thünemann, A. Polyelectrolyte-Surfactant Complexes: A New Type of Solid, Mesomorphous Material. *Macromolecules* **1994,** *27,* 6007-6011.

[20] Zhou, S.; Yeh, F.; Burger, C.; Chu, B. Nanostructures of Polyelectrolyte Gel-Surfactant Complexes. *J. Polym. Sci. B: Polym. Phys.* **1999,** *37,* 2165-2172.

[21] Zhou, S.; Yeh, F.; Burger, C.; Chu, B. Highly Ordered Supramolecular Structures from Self-Assembly of Ionic Surfactants in Oppositely Charged Polyelectrolyte Gels. *ACS Sym. Ser.* **2000,** *739,* 244-260.

[22] Kogej, K.; Theunissen, E.; Reynaers, H. Effect of Polyion Charge Density on the Morphology of Nanostructures in Polyelectrolyte-Surfactant Complexes. *Langmuir* **2002,** *18,* 8799-8805.

[23] Kogej, K.; Evmenenko, G.; Theunissen, E.; Berghmans, H.; Reynaers, H. Investigation of Structures in Polyelectrolyte/Surfactant Complexes by X-ray Scattering. *Langmuir* **2001,** *17,* 3175-3184.

[24] Sokolov, E. L.; Yeh, F.; Khokhlov, A. R.; Grinberg, V. Y.; Chu, B. Nanostructure Formation in Polyelectrolyte-Surfactant Complexes. *J. Phys. Chem. B* **1998,** *102,* 7091-7098.

[25] Leonard, M.; Hong, H. M.; Easwar, N.; Strey, H. H. Soft matter under osmotic stress. *Polymer* **2001,** *42,* 235-239.

[26] Dembo, A. T.; Yakunin, A. N.; Zaitsev, V. S.; Mironov, A. V.; Starodoubtsev, S. G.; Khokhlov, A. R.; Chu, B. Regular Microstructures in Gel-Surfactant Complexes: Influence of Water Content and Comparison with the Surfactant Structure in Water. *J. Polym. Sci. B: Polym. Phys.* **1996,** *34,* 2893-2898.

[27] Wagner, K.; Harries, D.; May, S.; Kahl, V.; Rädler, J. O.; Ben-Shaul, A. Direct Evidence for Counterion Release upon Cationic Lipid-DNA Condensation. *Langmuir* **2000,** *16,* 303-306.

[28] Sens, P.; Joanny, J.-F. Counterion Release and Electrostatic Adsorption. *Phys. Rev. Lett.* **2000,** *84,* 4862-4865.

[29] Joanny, J.-F.; Castelnovo, M.; Netz, R. Adsorption of charged polymers. *J. Phys.: Condens. Matter* **2000,** *12,* A1-A7.

[30] Konop, A. J.; Colby, R. H. Role of Condensed Counterions in the Thermodynamics of Surfactant Micelle Formation with and without Oppositely Charged Polyelectrolytes. *Langmuir* **1999,** *15,* 58-65.

[31] Meier-Koll, A. A.; Fleck, C. C.; Grünberg, v. The counterion-release interaction. *J. Phys.: Condens. Matter* **2004,** *16,* 6041-6052.

[32] Wang, C.; Tam, K. C.; Jenkins, R. D.; Tan, C. B. Interactions between Methacrylic Acid/Ethyl Acrylate Copolymers and Dodecyltrimethylammonium Bromide. *J. Phys. Chem. B* **2003,** *107,* 4667-4675.

[33] Wang, C.; Tam, K. C. New Insights on the Interaction Mechanism within Oppositely Charged Polymer/Surfactant Systems. *Langmuir* **2002,** *18,* 6484-6490.

[34] Manning, G. S. Counterion binding in polyelectrolyte theory. *Acc. Chem. Res.* **1979,** *12,* 443-449.

[35] Kosmella, S.; Kötz, J.; Shirahama, K.; Liu, J. Cooperative Nature of Complex Formation in Mixed Polyelectrolyte-Surfactant Systems. *J. Phys. Chem. B* **1998,** *102,* 6459-6464.

[36] Li, Y.; Dubin, P. L.; Havel, H. A.; Edwards, S. L.; Dautzenberg, H. Complex Formation between Polyelectrolyte and Oppositely Charged Mixed Micelles: Soluble Complexes vs Coacervation. *Langmuir* **1995,** *11,* 2486-2492.

[37] Beck, J. S.; Vartulli, J. C.; Roth, W. J.; Leonowicz, M. E.; Kresge, C. T.; Schmitt, K. D.; Chu, C. T.-W.; Olson, D. H.; Sheppard, E. W.; McCullen, S. B.; Higgins, J. B.; Schlenker, J. L. A New Family of Mesoporous Molecular Sieves Prepared with Liquid Crystal Templates. *J. Am. Chem. Soc.* **1992,** *114,* 10834-10843.

[38] Pantazis, C. C.; Trikalitis, P. N.; Pomonis, P. J.; Hudson, M. J. A method of synthesis of silicious inorganic ordered materials (MCM-41–SBA-1) employing polyacrylic acid–$C_n$TAB–TEOS nanoassemblies. *Microporous Mesoporous Mat.* **2003,** *66,* 37-51.

[39] Lapeña, A. M.; Gross, A. F.; Tolbert, S. H. Examining the Role of Surfactant Packing in Phase Transformations of Periodic Templated Silica/Surfactant Composites. *Langmuir* **2005,** *21,* 470-480.

[40] Corma, A. From Microporous to Mesoporous Molecular Sieve Materials and Their Use in Catalysis. *Chem. Rev.* **1997,** *97,* 2373-2419.

[41] Ciesla, U.; Schüth, F. Ordered mesoporous materials. *Microporous Mesoporous Mat.* **1999,** *27,* 131-149.

[42] Zhao, D.; Feng, J.; Huo, Q.; Melosh, N.; Fredrickson, G. H.; Chmelka, B. F.; Stucky, G. D. Triblock Copolymer Synthesis of Mesoporous Silica with Periodic 50 to 300 Angstrom Pores. *Science* **1998,** *279,* 548-552.

[43] McGrath, K. M.; Dabbs, D. M.; Yao, N.; Aksay, I. A.; Gruner, S. M. Formation of a Silicate $L_3$ Phase with Continuously Adjustable Pore Sizes. *Science* **1997,** *277,* 552-556.

[44] Monnier, A.; Schüth, F.; Huo, Q.; Kumar, D.; Margolese, D.; Maxwell, R. S.; Stucky, G. D.; Krishnamurty, M.; Petroff, P.; Firouzi, A.; Janicke, M.; Chmelka, B. F. Cooperative Formation of Inorganic–Organic Interfaces in the Synthesis of Silicate Mesostructures. *Science* **1993,** *261,* 1299-1303.

[45] Schüth, F. Non-siliceous Mesostructured and Mesoporous Materials. *Chem. Mater.* **2001,** *13,* 3184-3195.

[46] Ganeva, D.; Antonietti, M.; Faul, C. F. J.; Sanderson, R. Polymerization of the Organized Phases of Polyelectrolyte–Surfactant Complexes. *Langmuir* **2003,** *19,* 6561-6565.

[47] Faul, C. F. J.; Antonietti, M.; Sanderson, R.; Hentze, H.-P. Directed Polymerization in Mesophases of Polyelectrolyte–Surfactant Complexes. *Langmuir* **2001,** *17,* 2031-2035.

[48] Liu, T.; Burger, C.; Chu, B. Nanofabrication in polymer matrices. *Prog. Polym. Sci.* **2003,** *28,* 5-26.

[49] Aksay, I. A.; Trau, M.; Manne, S.; Homma, I.; Yao, N.; Zhou, L.; Fenter, P.; Eisenberger, P. M.; Gruner, S. M. Biomimetic Pathways for Assembling Inorganic Thin Films. *Science* **1996,** *273,* 892-898.

[50] Parsegian, V. A.; Rand, R. P.; Fuller, N. L.; Rau, D. C. Osmotic Stress for the Direct Measurement of Intermolecular Forces. In *Methods in Enzymology*; Packer, L., Ed.; Academic Press, Inc., 1986; Vol. 127; pp 400-416.

[51] Parsegian, V. A.; Fuller, N. L.; Rand, R. P. Measured Work of Deformation and Repusion of Lecithin Bilayers. *Proc. Natl. Acad. Sci. U.S.A.* **1979,** *76,* 2750-2754.

[52] Lis, L. J.; McAlister, M.; Fuller, N. L.; Rand, R. P.; Parsegian, V. A. Interactions between neutral phospholipid bilayer membranes. *Biophys J.* **1982,** *37,* 657-665.

[53] Leikin, S.; Rau, D. C.; Parsegian, V. A. Measured entropy and enthalpy of hydration as a function of distance between DNA double helices. *Phys. Rev. A* **1991,** *44,* 5272-5278.

[54] Leikin, S.; Rau, D. C.; Parsegian, V. A. Direct Measurement of Forces Between Self-Assembled Proteins - Temperature-Dependent Exponential Forces Between Collagen Triple Helices. *Proc. Natl. Acad. Sci. U.S.A.* **1994,** *91,* 276-280.

[55] Rau, D. C.; Parsegian, V. A. Direct Measurement of Forces Between Linear Polysaccharides Xanthan and Schizophyllan. *Science* **1990,** *249,* 1278-1281.

[56] Bonnet-Gonnet, C.; Leikin, S.; Chi, S.; Rau, D. C.; Parsegian, V. A. Measurement of Forces between Hydroxypropylcellulose Polymers: Temperature Favored Assembly and Salt Exclusion. *J. Phys. Chem. B* **2001,** *105,* 1877-1886.

[57] Strey, H. H.; Parsegian, V. A.; Podgornik, R. Equation of State for Lyotropic Polymer Liquid Crystals: Theory and Experiment. *Phys. Rev. E* **1999,** *59,* 999-1008.

[58] Gleeson, J. T.; Polcyn, A. D.; Gruner, S. M. Structure of Phospholipid Suspensions under Negative Pressure. *J. Colloid Interface Sci.* **1993,** *156,* 430-432.

[59] Gruner, S. M. Intrinsic Curvature Hypothesis for Biomembrane Lipid Compositions: A Role for Nonbilayer Lipids. *Proc. Natl. Acad. Sci. U.S.A.* **1985,** *82,* 3665-3669.

[60] Gruner, S. M. Stability of Lyotropic Phases with Curved Interfaces. *J. Phys. Chem.* **1989,** *93,* 7562-7570.

[61] Gruner, S. M. Soft Materials and Biomaterials Under Pressure: Putting the Squeeze on Biology. In *High-Pressure Crystallography*; Katrusiak, A., McMillan, P., Eds.; Kluwer Academic Publishers: Dordrecht, The Netherlands, 2004; pp 543-556.

[62] Toombes, G. E. S.; Finnefrock, A. C.; Tate, M. W.; Gruner, S. M. Determination of Lamellar-Hexagonal Phase Transition Temperature for 1,2-Dioleoyl-sn-Glycero-3-Phosphatidylethanolamine. *Biophys J.* **2002,** *82,* 2504-2510.

[63] Howells, M. R.; Cambie, D.; Duarte, R. M.; Irick, S.; MacDowell, A. A.; Padmore, H. A.; Renner, T. R.; Rah, S.; Sandler, R. Theory and practice of elliptically bent X-ray mirrors. *Opt. Eng.* **2000,** *39,* 2748-2762.

# CHAPTER 2

# PHASE DIAGRAMS OF MODEL STOICHIOMETRIC POLYELECTROLYTE–SURFACTANT COMPLEXES

## 2.1 Introduction

Polyelectrolyte–surfactant complexation has been known for quite some time, but virtually no truly systematic studies regarding the phase diagrams of stoichiometric, insoluble complexes have been reported. Previous work concerning stoichiometric complexes has involved the detailed study of morphological changes under relatively limited conditions, such as the variation of polymer charge density[1-5], ionic strength[6], and surfactant tail length[7-9], and involved the exposure of crosslinked polyelectrolyte gels to low concentrations (below cmc) of aqueous surfactant[3,8,10-12]. Other studies have considered polyelectrolyte–surfactant complex phase behavior as a function of surfactant concentration, with the stoichiometric complex representing one of several concentration regimes[13-15].

The main objective of this research was to establish comprehensive phase diagrams of stoichiometric polyelectrolyte–surfactant complexes by studying the thermodynamics and structure of a single model system of fixed composition while manipulating several environmental variables. Specifically, our model system consisted of a series of poly(acrylate-*co*-acrylamide)–cetyltrimethylammonium halide (PAAm–CTAX) complexes whose phase behavior was monitored as a function of ionic strength, salt type, osmotic pressure, and linear polyelectrolyte charge density.

## 2.2 Experimental

### 2.2.1 Materials

Polyacrylate, sodium salt (PA, Aldrich, $M_n$= 30,000 g mol$^{-1}$, 40 wt % aqueous solution), Poly(acrylate-*co*-acrylamide) (PAAm, Polysciences, 70%, 40%, and 10% carboxylate contents, $M_n$= 200,000, 10,000,000, and 200,000 g mol$^{-1}$, respectively), sodium chloride (Mallinckrodt), cetyltrimethylammonium chloride (CTACl, Aldrich, 1.04 M aqueous solution), poly(ethylene glycol) (PEG, Fluka, $M_n$ = 8,000 g mol$^{-1}$), and ethylenediaminetetraacetic acid (EDTA, Sigma molecular biology grade) were used as received. Tris(hydroxymethylaminomethane) (TRIS base, Sigma molecular biology grade) was adjusted to pH 7.0 (HCl) before use. Concentrated solutions of PAAm were prepared in 10 mM, 100 mM, and 1 M NaCl and NaBr and were buffered in a mixture of 10 mM TRIS base/1 mM EDTA (10-1 TE). The 70%, 40%, and 10% carboxylate content PAAm solutions were prepared at concentrations of 5 wt %, 1 wt %, and 5 wt %, respectively. All aqueous solutions were prepared using water purified via reverse osmosis. The relevant polyelectrolyte and surfactant structures are shown in Figure 2.1.

### 2.2.2 Methods

Polyelectrolyte–surfactant complexes were prepared by combining 1.04 M CTACl solution with a stoichiometric amount (based on charge) of concentrated polyelectrolyte solution, followed by vigorous mixing. Immediately upon the addition of approximately 10 mL of water to these mixtures, a fine white precipitate formed.

The precipitatates were isolated by centrifugation, washed with three 50 mL aliquots of water to remove excess ions, and were allowed to air dry for approximately 8 hours. Pieces of the dried complexes were then placed in large reservoirs of aqueous sodium bromide and sodium chloride solutions (10 mM, 100 mM, and 1 M) with PEG concentrations in each solution ranging from 0 wt % to 50 wt % corresponding to an approximate osmotic pressure range of 0 to 112 atm at room temperature. The relationship between osmotic pressure and PEG 8000 concentration, $G$ [wt %], was determined by Michel[16], who showed that

$$\Pi\ [\text{atm}] = -1.29\, G^2 T + 140\, G^2 + 4\, G \qquad (2.1)$$

where 5 °C < $T$ < 40 °C. Each of these solutions were buffered in 10-1 TE at a pH of 7. The samples were then allowed to equilibrate with the stressing solutions for one month at room temperature. During this time, samples were periodically vortexed to ensure PEG solution homogeneity. Cetyltrimethylammonium bromide (CTABr) was generated in situ by exchange of the CTACl chloride ion with the free bromide ions in the NaBr/PEG solutions. In order to access higher osmotic pressures than solution stress could provide, pieces of vacuum-dried 40%, 70%, and 100% charge complexes were placed in separate, sealed polyethylene chambers containing saturated aqueous solutions of NaBr, $CH_3CO_2Na$, and KCl, having relative humidities (RH) of 57%, 77%, and 89%, respectively[17] (approximate corresponding osmotic pressures were 200, 450, and 1000 atm, respectively). Samples were suspended above each saturated salt solution on a small platform inside these chambers, and the complexes were allowed to

equilibrate with the salt solution vapor for one month. It is important to note that no salt was intentionally added to these complexes either before or after equilibration.

### 2.2.3 Measurements

Small angle X-ray scattering (SAXS) measurements were performed with a Rigaku RU-H3R rotating anode X-ray diffractometer operating at 1.2 kW. The diffractometer was equipped with a Confocal Max-Flux multilayer focusing optic (point focus = $(100\ \mu m)^2$; Osmic Inc., type CMF23-46Cu8) and a custom-built evacuated Statton-type scattering camera. The sample cell used for the solution osmotic stress measurements consisted of a Teflon card sandwiched between two thin Mylar windows which allowed the solid samples to remain in equilibrium with the stressing solutions during the measurements while simultaneously isolating the samples from vacuum. For complexes equilibrated against saturated salt solution vapor, a Mylar-windowed polyethylene sample cell consisting of two connected chambers was used. This particular cell allowed the sample to remain in an equilibrated saturated salt vapor environment during the X-ray measurements. For all measurements, the sample-to-detector distance was 460 mm, which corresponds to a $q$ range of $0.0698\ Å^{-1} \leq q \leq 0.625\ Å^{-1}$ with $q = (4\pi/\lambda)\sin(\theta/2)$, where $\theta$ is twice the Bragg angle. The incident beam wavelength was 1.54 Å, corresponding to 8 keV Cu K$\alpha$ radiation, and an exposure time of 10 minutes was used for all samples. Scattering patterns were acquired with 10 cm × 15 cm Fujifilm ST-VA image plates in conjunction with a Fujifilm BAS-2500 image plate scanner. Profiles of intensity versus $q$ were obtained from radial averages of the 2-

D scattering patterns, using procedures developed by our research group for the Igor Pro software package (Wavemetrics, Inc.; Lake Oswego, OR).

### 2.2.4 Crystallographic Interpretation of SAXS Data

The regular pattern in a crystal gives rise to a sequence of Bragg-like peaks in the scattering data, the relative locations of which depend on the structure of the crystal's repeat unit. The peaks in the scattering patterns are the results of interplanar spacings $d_{hkl}$ in the crystal, where $h$, $k$, and $l$ are integers denoted by the Miller indices, such that the peak positions are located at $q_{hkl} = 2\pi/d_{hkl}$. For the $Pm3n$ cubic unit cell, these interplanar spacings are given by

$$\frac{1}{d_{hkl}^2} = \frac{h^2 + k^2 + l^2}{a^2} \tag{2.2}$$

Using the (210) diffraction signal, the $Pm3n$ unit cell parameter can be calculated as $a = \sqrt{5}d_{210}$. For the hcpc unit cell, which is a 2-dimensional hexagonal array of long rods, $l = 0$ and the interplanar spacings are given by

$$\frac{1}{d_{hk0}^2} = \frac{4}{3}\left(\frac{h^2 + k^2 + hk}{a^2}\right) \tag{2.3}$$

Using the (100) diffraction signal, the hcpc unit cell parameter is calculated as $a = 2/\sqrt{3}d_{100}$. Throughout this paper, the Bragg spacings referenced above are denoted as $d_B$.

## 2.3 Results and Discussion

### 2.3.1 General Phase Sequence

Compression of a soft phase through the application of osmotic stress can eventually give rise to phase transformations, due to reductions in spontaneous curvature and the accompanying driving force for increased molecular packing efficiency. Most of the stoichiometric polyelectrolyte–surfactant complexes considered for this study exhibited both high and low degrees of nanoscopic order, depending on the experimental conditions. For well-ordered complexes, we observed the following general sequence of structures as a function of decreasing water content: *Pm*3*n* cubic ↔ hexagonally close-packed cylinders (hcpc) ↔ lamellar. Experimentally-obtained SAXS patterns for each of these structures are shown in Figures 2.2-2.4. The ratios between the peak positions follow the characteristic patterns for each structure: $\sqrt{2}$, $\sqrt{4}$, $\sqrt{5}$, $\sqrt{6}$, $\sqrt{8}$, $\sqrt{10}$, $\sqrt{12}$, $\sqrt{14}$ for *Pm*3*n*; 1, $\sqrt{3}$, $\sqrt{4}$, $\sqrt{7}$, $\sqrt{9}$ for hcpc; 1, 2, 3 for lamellar. Note that the (110) diffraction signal—the $\sqrt{2}$ peak—is the first observable peak in the scattering profile for the *Pm*3*n* cubic structure. The high level of correlation between the measured and predicted peak positions for these two phases is shown in Figure 2.5.

In contrast to the phase sequence observed here, the progression of structures in aqueous surfactant systems tends to follow a slightly different sequence: micellar ↔ hexagonal (spheres or cylinders) ↔ orthorhombic ↔ lamellar[18,19] as a function of increasing amphiphile concentration. In these systems, the interaction between surfactant moieties is dominated by electrostatic interactions, whereas the sequence of

structures in stoichiometrie polyeleetrolyte–surfactant complexes ean be explained by the competition of spontaneous curvature (which favors the formation of spherical micelles) and moleeular paeking constraints (which favor the formation of lamellar structures).

Another morphologieal differenee between a pure surfactant system and the polyelectrolyte–surfactant systems studied here is the occurrenee of a *Pm*3*n* cubie phase. This phase, whieh is also known as the A15 lattiee and thc β tungsten latticc, is known to oecur at high water eontents, and is thought to consist of either a bimodal distribution of spherical and oblate mieelles packed into the lattiee[20], or a monomodal distribution of 8 prolate mieelles packed into the same lattice[21]. The *Pm*3*n* phasc has been observed frequently in polyelectrolyte–surfactant eomplexes[3,5,6,12-14,22] and relatcd hard core/soft corona colloidal systems[23]. Its existenee has been addressed theoretieally by Kamien and co-workers[24], who used a modified hard-eore/soft shell potential to model its evolution from close-packed cubic structures. The *Pm3n* phase is believed to arise from frustration between the hard-core excluded volume interaction and the surface interaction due to overlapping soft eoronas and as such, illustratcs the so-calld "close packing versus minimal area" principle. In our case, polyelectrolyte ehains surrounding the surfactant micelles comprise the soft shell.

### 2.3.2 Phase Behavior in 10 mM and 100 mM Salt

#### 2.3.2.1 Osmotic Stress Effects

Osmotic pressure versus Bragg distance curves were constructed from SAXS data obtained from the complexes bathed in PEG solutions containing either sodium bromide or sodium chloride. These results are shown in Figures 2.6-2.11. Each of the curves indicate an exponential relationship between osmotic pressure and distance, where increased osmotic pressure consistently brought about a reduction in unit cell size. Tables 2.1-2.4 show the range of unit cell parameters obtained under all conditions. This type of exponential relationship is frequently observed in osmotic stress experiments[25-28], either because of screened electrostatic interactions, or due to short-range hydration forces.

Length scales of the exponential forces present between surfactant moieties are directly related to the decay lengths of the experimental pressure versus distance curves. Such decay lengths are also indicative of complex compressibilities—large decay lengths indicate a higher degree of compressibility than do smaller decay lengths. Decay lengths were calculated as $\lambda = 1/[m \ln(10)]$ where $m$ is the slope of the linear portion of the pressure versus distance curve. Values of $\lambda$ for each system are summarized in Tables 2.6-2.8. It is interesting to note that the decay lengths obtained from our experiments are extremely small, ranging from a few Ångstroms at low charge densities to tenths of Ångstroms at high charge densities. These length scales may

reflect the monomer–monomer repulsion distances between polyelectrolyte chains, as they are much smaller than any electrostatic or hydration screening lengths.

### 2.3.2.2 Coexistence Regions

As shown in Figures 2.7, 2.9, and 2.10, phase transitions from *Pm*3*n* cubic to hexagonal cylinders often proceeded through two-phase coexistence regions. Other groups have observed this sort of cubic–hexagonal coexistence for polyelectrolyte–surfactant complexes in which surfactant concentration was being increased[1,15,29], but this is the first time it has been observed in stoichiometric polyelectrolyte–surfactant complexes of fixed composition. The SAXS traces shown in Figure 2.12 illustrate how the hexagonal phase evolves from the cubic phase as osmotic pressure is increased in two different systems, as the (100), (110), and (200) hcpc diffraction signals increase in intensity as osmotic pressure is increased.

In addition to inducing order–order transitions within well-structured complexes, the application of osmotic stress to a poorly-ordered system can promote the formation of a well-ordered phase. Figure 2.13 shows the evolution of a well-ordered *Pm*3*n* cubic phase from an indeterminate, poorly-ordered structure in the 40% charge PAAm–CTACl system as osmotic pressure was increased.

As mentioned earlier, the well-defined thermodynamic conditions under which osmotic stress experiments are carried out preclude the existence of two-phase regions as per the Gibbs phase rule–all chemical potentials are fixed and must be identical at equilibrium. However, it is quite possible that the systems which exhibit cubic-

hexagonal coexistence regions have not yet reached their true equilibrium states. This would be a likely scenario if the two phases are energetically similar, or if the kinetic barriers associated with the transition are sufficiently large. Such behavior is analogous to the topologically-hindered structural transitions of liquid crystalline lipid-water systems that have been studied as functions of hydrostatic pressure[30-32] and temperature[33].

### 2.3.2.3 Charge Density Effects

At 10% polyelectrolyte charge content, no precipitate could be isolated after following the preparatory procedures described earlier. This result can be explained by Manning theory[34], which maintains that counterion condensation will not occur unless polyelectrolyte charge density is above a certain threshold value. This charge density parameter is defined as $\xi = l_B/b$, where $l_B$ is the Bjerrum length defined as $l_B = e^2/4\pi\varepsilon\varepsilon_0 k_B T$, and $b$ is the linear charge spacing. Applying the critical condition for counterion condensation, $\xi = 1$, the critical linear charge spacing equals the Bjerrum length, which is 7.1 Å in aqueous solution. However, it has been shown that this critical spacing is not achieved in partially ionized PA systems unless the charge content is roughly 35%[35]. Therefore, at 10% charge content, there is little to no driving force for binding, due to the absence of condensed counterions on the PAAm chain.

Decreasing the polyelectrolyte charge density while holding other factors fixed tended to increase unit cell sizes by as many as several Ångstroms, as shown in Tables 2.1-2.5. Presumably, at low charge densities, more neutral monomers will be allowed

to fill the spaces between surfactant moieties than at higher charge contents, thereby increasing the overall unit cell size. These data also show that an increase in polymer charge density (while holding other conditions fixed) shifts the phase sequence towards more densely-packed structures. For example, a cubic phase will be converted to a hexagonal phase as polymer charge density is increased, and Figures 2.9-2.11 reflect this increase in phase density with increasing charge content explicitly.

As shown in Tables 2.6-2.8, decay lengths tended to decrease with increasing charge density. It seems reasonable that an increase in charge density should render the complexes less compressible—decreased compressibility follows directly from a decrease in the density of neutral monomers packed between surfactant moieties.

### 2.3.2.4 Effects of Ionic Strength and Salt Type

For both salts investigated, decreasing the ionic strength while holding all other factors fixed brought about a reduction in unit cell size within each observed phase–a clear indication of counterion release[36-42]. This is reasonable, considering that at higher bulk ionic strengths, the entropic gain of the counterions upon adsorption of the polyelectrolyte chain will be reduced relative to lower ionic strengths.

Tables 2.6-2.7 show that exponential decay lengths generally increased as bromide concentration was increased from 10 mM to 100 mM. This could be related to the fact that bromide has a particularly strong affinity for the quaternary ammonium ion[43,44]. This driving force to bind with the surfactant headgroup may be so strong as to bring about the displacement of small sections of the polyelectrolyte chain that are

bound to the surfactant as it competes for the same binding sites. In this way, the presence of bromide ions would reduce the effective charge density of the surfactant. Therefore, as more bromide ions are introduced into the system, we would expect to see a decrease in unit cell size and increased complex compressibility. Indeed, this is what we have observed experimentally.

For the complexes equilibrated in chloride ion, it seems strange that higher ionic strengths should bring about smaller decay lengths, since unit cell sizes for the *Pm*3*n* and hcpc phases at fixed pressures tend to be larger at higher chloride concentration. One may reasonably expect that larger unit cell sizes would lead to increased compressibility. However, this is not what we have observed, and the reason for this sort of behavior is unclear.

These results also show that the morphology of the complex is influenced by the counterion type. For example, at a charge density of 100%, hexagonal cylinders were observed at all osmotic pressures in both 10 mM and 100 mM bromide, whereas a combination of cubic and hexagonal phases are observed for the same systems in chloride. This is due to the well-documented ability of the bromide ion to shield the surfactant headgroup repulsion more efficiently than the chloride ion. However, when charge density is reduced below 100%, the *Pm*3*n* phase was observed to coexist with the hcpc phase.

### 2.3.3 Phase Behavior in 1M Salt

In 1 M NaBr, solid CTABr precipitated from each sample, leaving no discernable complex for analysis. However, ordered complexes were obtained in the presence of 1 M NaCl, and osmotic pressure versus distance curves for these systems are shown in Figures 2.14-2.16. The complexes remained soluble at osmotic pressures below 5 atm, but became organized into hexagonal cylindrical phases as osmotic pressure was increased. In contrast to the results obtained in 10 mM and 100 mM salt, the curves obtained in 1 M salt are not smoothly exponential—unit cell size depends on osmotic pressure in a more complicated way. Unit cell size ranges for these systems are presented in Table 2.5. Note that these ranges are different from those obtained at 100 mM NaCl (Table 2.3), as the complexes are compressible over a considerably larger range at 1 M salt. At this ionic strength, we also observed the occurrence of the hcpc phase at 40% polyelectrolyte charge content; at 10 and 100 mM ionic strengths, only the *Pm*3*n* phase was observed at 40% charge. In addition, note that the osmotic pressure versus distance curves for each system can essentially be superimposed; the effect of charge density on unit cell dimensions is relatively insignificant in this case.

Small-angle X-ray scattering profiles obtained at each osmotic pressure for the 100% and 70% charge systems are shown in Figure 2.17. From these data, we note that the degree of long-range order tended to decrease in 1 M salt relative to the same systems at lower ionic strengths, as fewer higher-order peaks were observed in this regime. Moreover, a coexistence region of hexagonal cylinders and *Pm*3*n* cubic structures was observed at high osmotic pressures in the 70% charge system.

Considering these results, as well the fact that CTABr precipitated from all samples in 1 M bromide, it is likely that the complexes become non-stoichiometric under high-salt conditions. Other studies concerning polyelectrolyte–surfactant complexes at high ionic strengths[45-48] have postulated this departure from stoichiometry. Clearly, the trends observed for complexes in 10 mM and 100 mM salt cannot be extended to this high-salt, presumably non-stoichiometric regime.

### 2.3.4 Phase Behavior at Higher Osmotic Pressures

In an effort to access higher osmotic pressures than solution stress could provide, complexes were equilibrated against saturated salt solution vapor at three different relative humidities. As mentioned in the Experimental section, salt was not intentionally added to these complexes prior to equilibration, and as such, the effect of ionic strength in this regime could not be considered. Phase diagrams for these systems are shown in Figures 2.18-2.20 and the associated angular-averaged scattering profiles are shown in Figures 2.21-2.23; the diffraction peaks are labeled with their corresponding structures and Miller indices. Tables 2.9-2.11 show the measured Bragg distances and peak position ratios that were used to identify the structures. From these data, we identified a phase progression of coexisting cubic and hcpc phases for the 40% charge system at 80% RH to a pure lamellar phase for the 100% charge system at 57% RH. These transitions proceeded through hcpc–lamellar coexistence regions; indeed, most samples analyzed in this high osmotic pressure regime exhibited some degree of phase coexistence. This trend toward decreasing curvature with increasing osmotic

pressure and polyelectrolyte charge density is consistent with observations made earlier in this chapter. However, it is important to mention that there is not enough resolution in the phase diagrams presented here to comment on the nature of the forces between assemblies, or on the precise locations of the phase boundaries.

It should be noted that a few extraneous peaks were observed in the scattering profile for the 70% charge PAAm–CTAX system at 57% RH (Figure 2.22). These peaks were located at $q$ = 0.187, 0.202, and 0.367 $Å^{-1}$ and could not be assigned to a specific structure. The presence of these peaks is puzzling and cannot be easily rationalized; the 2-D scattering image obtained from this sample shows that these peaks were completely isotropic (i.e. no "spotting" was observed). As such, they are not likely due to crystallized salt or surfactant.

### 2.3.5 Temperature-Dependent Phase Behavior

A small portion of this study considered the influence of temperature on PAAm–CTAX complex structure. Background information and findings from these experiments are presented in the Appendix.

## 2.4 Conclusions

Self-assembled PAAm–CTAX complexes exhibiting high degrees of nanoscopic order have been prepared, and comprehensive phase diagrams of these systems have been mapped as functions of polyelectrolyte charge density, ionic strength, salt type, and osmotic pressure, using a combination of solution osmotic stress

and saturated salt solution vapor; this phase map is presented schematically in Figure 2.24. A phase sequence of *Pm3n* cubic ↔ hexe ↔ lamellar was observed with decreasing complex water content, and the general trends we have observed can be explained in terms of counterion release and the competition between packing constraints and spontaneous curvature. These factors, along with the occurrence of a *Pm3n* phase in our systems, help to distinguish polyelectrolyte–surfactant complexes from pure surfactant systems. The presence of coexistence regions between hexe and *Pm3n* phases under certain conditions suggests that these complexes have not yet reached their true equilibrium states; it is possible that these two phases are energetically similar or that the observation of coexistence is a result of kinetic trapping.

## Tables

**Table 2.1: Unit Cell Sizes of PAAm–CTABr Complexes in 100 mM NaBr at Varying Polyelectrolyte Charge Densities**

| | *a*, hcpc [Å] | | | *a*, *Pm3n* [Å] | | |
|---|---|---|---|---|---|---|
| Π [atm] | 100% | 70% | 40% | 100% | 70% | 40% |
| 0 | 51.98 | — | — | — | 118.29 | — |
| 1 | 51.91 | — | — | — | 118.74 | — |
| 2 | 51.90 | — | — | — | 118.11 | — |
| 4 | 51.90 | 54.16 | — | — | 118.11 | — |
| 8 | 51.90 | 53.87 | — | — | 117.68 | — |
| 13 | 51.72 | 53.35 | — | — | 117.46 | — |
| 21 | 51.60 | 53.08 | — | — | 117.46 | 131.15 |
| 33 | 51.39 | 52.64 | — | — | 117.13 | 127.11 |
| 50 | 51.18 | 52.41 | — | — | 116.88 | 124.75 |
| 75 | 51.00 | 52.17 | — | — | — | 121.65 |
| 112 | 50.89 | 51.60 | — | — | — | 117.52 |

—, no structure observed

**Table 2.2: Unit Cell Sizes of PAAm–CTABr Complexes in 10 mM NaBr at Varying Polyelectrolyte Charge Densities**

| | *a*, hcpc [Å] | | | *a*, *Pm3n* [Å] | | |
|---|---|---|---|---|---|---|
| Π [atm] | 100% | 70% | 40% | 100% | 70% | 40% |
| 0 | 48.39 | — | — | — | 109.46 | — |
| 1 | 48.35 | — | — | — | 109.08 | — |
| 2 | 48.35 | — | — | — | 108.90 | — |
| 4 | 48.31 | — | — | — | 108.72 | — |
| 8 | 48.31 | — | — | — | 108.54 | — |
| 13 | 48.25 | 49.58 | — | — | 108.43 | 110.47 |
| 21 | 48.25 | 49.35 | — | — | 108.27 | 109.86 |
| 33 | 48.25 | 49.07 | — | — | 108.16 | 108.91 |
| 50 | 48.25 | 48.96 | — | — | — | 107.89 |
| 75 | 48.25 | 48.87 | — | — | — | 107.79 |
| 112 | 48.25 | 48.73 | — | — | — | 106.93 |

—, no structure observed

**Table 2.3: Unit Cell Sizes of PAAm–CTACl Complexes in 100 mM NaCl at Varying Polyelectrolyte Charge Densities**

| | *a*, hcpc [Å] | | | *a*, *Pm3n* [Å] | | |
|---|---|---|---|---|---|---|
| Π [atm] | 100% | 70% | 40% | 100% | 70% | 40% |
| 0 | 49.65 | — | — | 110.46 | 111.26 | — |
| 1 | 49.54 | — | — | 110.33 | 110.54 | — |
| 2 | 49.42 | — | — | 110.19 | 110.09 | — |
| 4 | 49.37 | — | — | 110.01 | 110.13 | — |
| 8 | 49.31 | — | — | — | 110.01 | — |
| 13 | 49.22 | — | — | — | 109.79 | — |
| 21 | 49.23 | — | — | — | 109.57 | — |
| 33 | 49.06 | 49.93 | — | — | 109.34 | 111.71 |
| 50 | 49.09 | 49.82 | — | — | — | 111.03 |
| 75 | 48.96 | 49.74 | — | — | — | 110.48 |
| 112 | 48.94 | 49.50 | — | — | — | 109.79 |

—, no structure observed

**Table 2.4: Unit Cell Sizes of PAAm–CTACl Complexes in 10 mM NaCl at Varying Polyelectrolyte Charge Densities**

| | *a*, hcpc [Å] | | | *a*, *Pm*3*n* [Å] | | |
|---|---|---|---|---|---|---|
| Π [atm] | 100% | 70% | 40% | 100% | 70% | 40% |
| 0 | 49.54 | — | — | 108.69 | 108.67 | — |
| 1 | 49.42 | — | — | 108.53 | 108.45 | — |
| 2 | 49.07 | — | — | 108.23 | 107.86 | — |
| 4 | 48.84 | — | — | 107.96 | 107.61 | — |
| 8 | 48.73 | — | — | 107.81 | 107.11 | 109.28 |
| 13 | 48.49 | — | — | 107.59 | 107.06 | 108.61 |
| 21 | 48.37 | — | — | — | 106.84 | 107.43 |
| 33 | 48.20 | 48.73 | — | — | 106.51 | 106.28 |
| 50 | 48.03 | 48.38 | — | — | — | 105.90 |
| 75 | 47.93 | 48.18 | — | — | — | 104.85 |
| 112 | 47.79 | 47.94 | — | — | — | 104.32 |

—, no structure observed

**Table 2.5: Unit Cell Sizes of PAAm–CTACl Complexes in 1 M NaCl at Varying Polyelectrolyte Charge Densities**

| | *a*, hcpc [Å] | | | *a*, *Pm3n* [Å] | | |
|---|---|---|---|---|---|---|
| Π [atm] | 100% | 70% | 40% | 100% | 70% | 40% |
| 0 | — | — | — | — | — | — |
| 1 | — | — | — | — | — | — |
| 2 | — | — | — | — | — | — |
| 4 | 56.27 | 56.28 | 56.15 | — | — | — |
| 8 | 53.14 | 54.42 | 53.98 | — | — | — |
| 13 | 51.14 | 52.41 | 52.56 | — | — | — |
| 21 | 49.65 | 51.67 | 51.56 | — | — | — |
| 33 | 48.84 | 50.90 | 50.62 | — | 102.24 | — |
| 50 | 48.09 | 49.99 | 50.13 | — | 101.65 | — |
| 75 | 47.80 | 49.51 | 49.46 | — | 100.35 | — |
| 112 | 47.46 | 49.05 | 49.01 | — | 99.84 | — |

—, no structure observed

**Table 2.6: Exponential Decay Length Data for PA–CTAX Complexes**

| Ionic strength [mM] | Structure | Π-Range[a] [atm] | λ [Å] | $R^2$ |
|---|---|---|---|---|
| NaBr | | | | |
| 10 | hcpc | 13–112 | 0.00 | 0.96 |
| 100 | hcpc | 13–112 | 0.37 | 0.99 |
| 10 | *Pm*3*n* | — | — | — |
| 100 | *Pm*3*n* | — | — | — |
| NaCl | | | | |
| 10 | hcpc | 1–112 | 0.27 | 0.99 |
| 100 | hcpc | 1–112 | 0.10 | 0.98 |
| 10 | *Pm*3*n* | 1–13 | 0.13 | 0.99 |
| 100 | *Pm*3*n* | 1–4 | 0.07 | 0.98 |

[a]Denotes the linear portion of the phase diagram
—, no structure observed

**Table 2.7: Exponential Decay Length Data for 70% Charge PAAm–CTAX Complexes**

| Ionic strength [mM] | Structure | Π-Range[a] [atm] | λ [Å] | $R^2$ |
|---|---|---|---|---|
| NaBr | | | | |
| 10 | hcpc | 13–112 | 0.35 | 0.98 |
| 100 | hcpc | 15–112 | 0.66 | 0.99 |
| 10 | *Pm3n* | 1–33 | 0.10 | 0.99 |
| 100 | *Pm3n* | 1–50 | 0.18 | 0.98 |
| NaCl | | | | |
| 10 | hcpc | 33–112 | 0.56 | 0.99 |
| 100 | hcpc | 33–112 | 0.32 | 0.97 |
| 10 | *Pm3n* | 1–35 | 0.20 | 0.99 |
| 100 | *Pm3n* | 1–35 | 0.13 | 0.96 |

[a]Denotes the linear portion of the phase diagram
—, no structure observed

**Table 2.8: Exponential Decay Length Data for 40% Charge PAAm–CTAX Complexes**

| Ionic strength [mM] | Structure | Π-Range[a] [atm] | λ [Å] | $R^2$ |
|---|---|---|---|---|
| NaBr | | | | |
| 10 | hcpc | — | — | — |
| 100 | hcpc | — | — | — |
| 10 | *Pm*3*n* | 13–112 | 3.59 | 0.99 |
| 100 | *Pm*3*n* | 21–112 | 0.74 | 0.99 |
| NaCl | | | | |
| 10 | hcpc | — | — | — |
| 100 | hcpc | — | — | — |
| 10 | *Pm*3*n* | 33–112 | 0.88 | 0.99 |
| 100 | *Pm*3*n* | 8–112 | 0.70 | 0.99 |

[a]Denotes the linear portion of the phase diagram
—, no structure observed

**Table 2.9: Interplanar Spacings for PA–CTAX Complexes Exposed to Saturated Salt Solution Vapor**

| | $d_B$ [Å] | | Peak ratios | |
|---|---|---|---|---|
| RH [%] | hcpc | Lamellar | hcpc | Lamellar |
| 57 | — | 25.73 | — | 1 |
| | — | 12.87 | — | 2 |
| | — | 8.57 | — | 3 |
| 77 | 40.91 | 33.32 | 1 | 1 |
| | 24.07 | 16.86 | $\sim\sqrt{3}$ | 2 |
| | 20.83 | — | $\sim\sqrt{4}$ | — |
| 89 | 41.36 | 34.12 | 1 | 1 |
| | 24.01 | 17.05 | $\sqrt{3}$ | 2 |
| | 20.83 | — | $\sqrt{4}$ | — |
| | 15.76 | — | $\sqrt{7}$ | — |
| | 13.92 | — | $\sim\sqrt{9}$ | — |

—, no structure observed

**Table 2.10: Interplanar Spacings for 70% Charge PAAm–CTAX Complexes Exposed to Saturated Salt Solution Vapor**

| | $d_B$ [Å] | | Peak ratios | |
|---|---|---|---|---|
| RH [%] | hcpc | Lamellar | hcpc | Lamellar |
| 57[a] | 41.27 | 24.99 | 1 | 1 |
| | — | 12.68 | — | ~2 |
| | — | 8.50 | — | ~3 |
| 77 | 42.04 | 34.58 | 1 | 1 |
| | 24.44 | 17.37 | ~√3 | 2 |
| | 21.18 | — | ~√4 | — |
| | 16.01 | — | ~√7 | |
| 89 | 42.46 | 35.19 | 1 | 1 |
| | 24.52 | 17.56 | √3 | 2 |
| | 21.24 | — | √4 | — |
| | 16.05 | — | √7 | — |

[a]Peaks at $q \approx 0.187$, 0.202, and 0.367 $Å^{-1}$ could not be attributed to a specific structure

—, no structure observed

**Table 2.11: Interplanar Spacings for 40% Charge PAAm–CTAX Complexes Exposed to Saturated Salt Solution Vapor**

| | $d_B$ [Å] | | | Peak ratios | | |
|---|---|---|---|---|---|---|
| RH [%] | *Pm3n* | hcpc | Lamellar | *Pm3n* | hcpc | Lamellar |
| 57 | — | 41.29 | 35.09 | — | 1 | 1 |
| | — | 23.85 | 17.52 | — | √3 | 2 |
| | — | 20.66 | — | — | √4 | — |
| 77 | — | 42.20 | 35.44 | — | 1 | 1 |
| | — | 24.36 | 17.66 | — | √3 | 2 |
| | — | 21.10 | — | — | √4 | — |
| | — | 15.95 | — | — | √7 | — |
| 89 | 75.96 | 43.33 | — | √2 | 1 | — |
| | 52.78 | 25.04 | — | √4 | √3 | — |
| | 47.33 | 21.69 | — | √5 | √4 | — |
| | — | 16.35 | — | — | √7 | — |

—, no structure observed

## Figures

### Poly(acrylate-*co*-acrylamide) (PAAm)

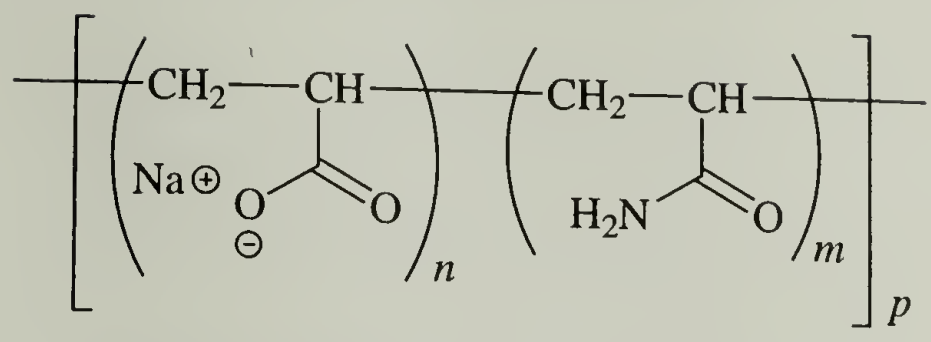

where $n$ = 100% (PA), 70%, 40% or 10%

### Cetyltrimethylammonium ion (CTAX)

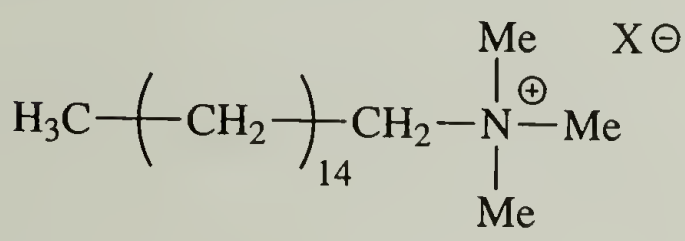

where X= Br or Cl

**Figure 2.1:** Structures of the polyelectrolytes and surfactants used for the phase behavior model study. Polyacrylate (PA) is fully charged ($n$ = 100%).

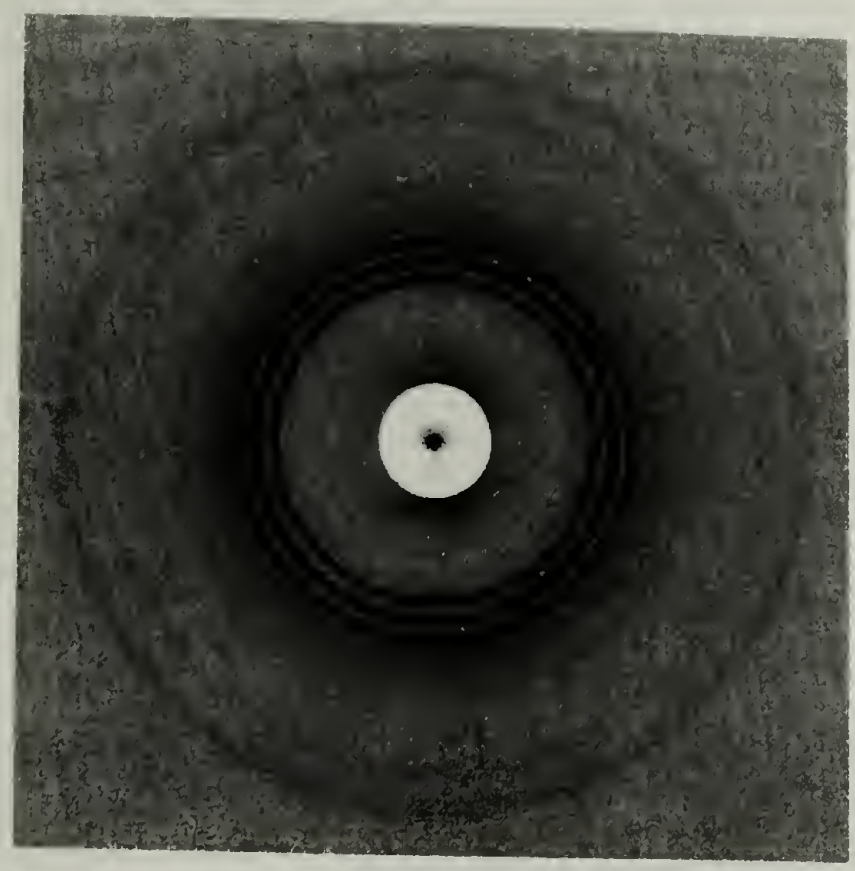

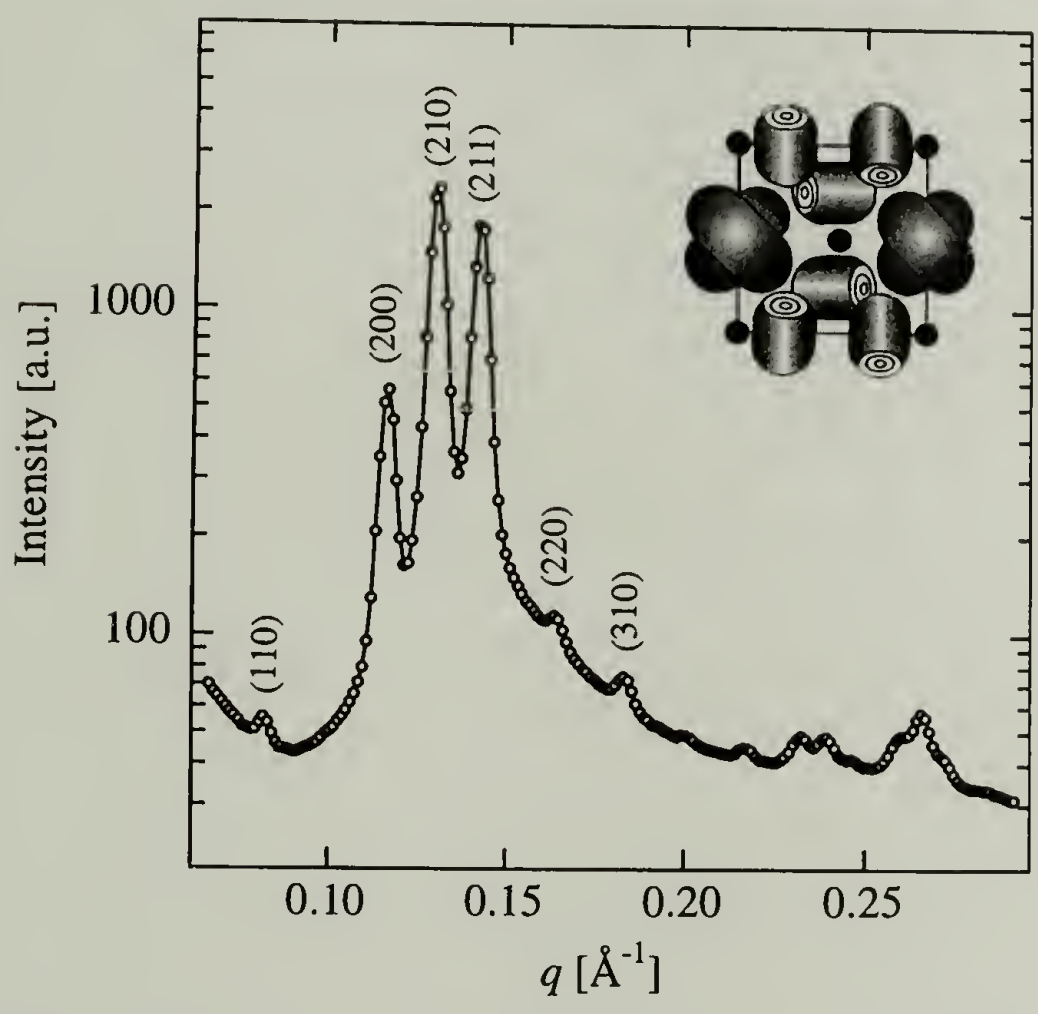


**Figure 2.2:** 2-D SAXS Image and angular-averaged scattering profile for a typical PA–CTACl complex in 10 mM NaCl. The peak positions correspond to a *Pm*3*n* cubic unit cell structure, which is pictured schematically. Miller indices associated with the major peaks are also shown.

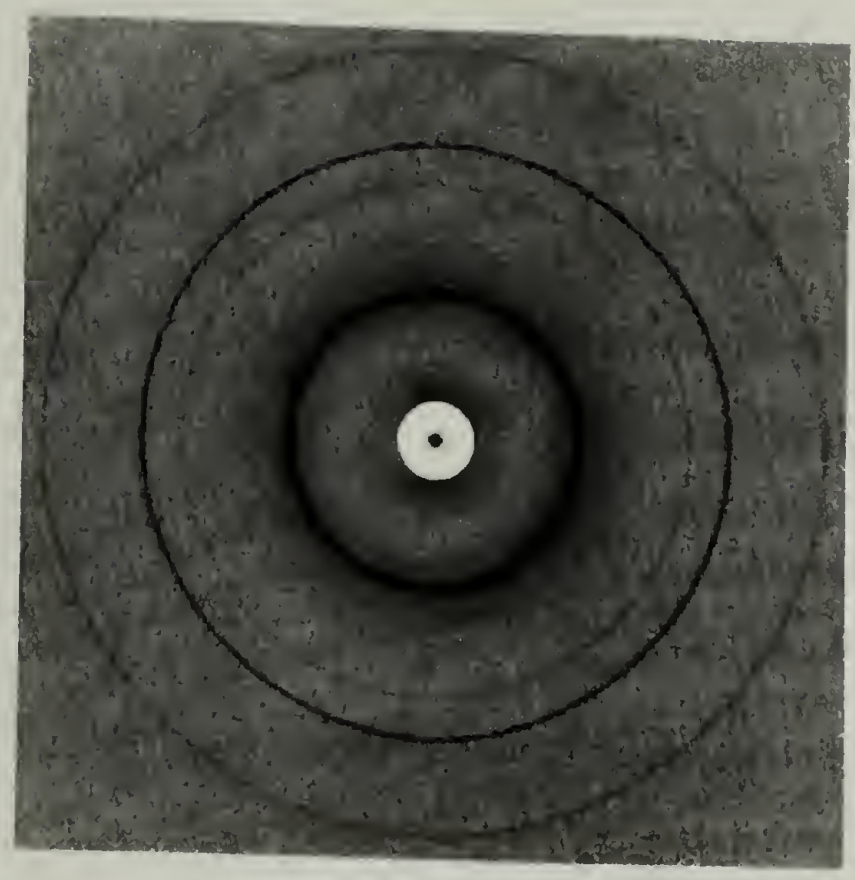

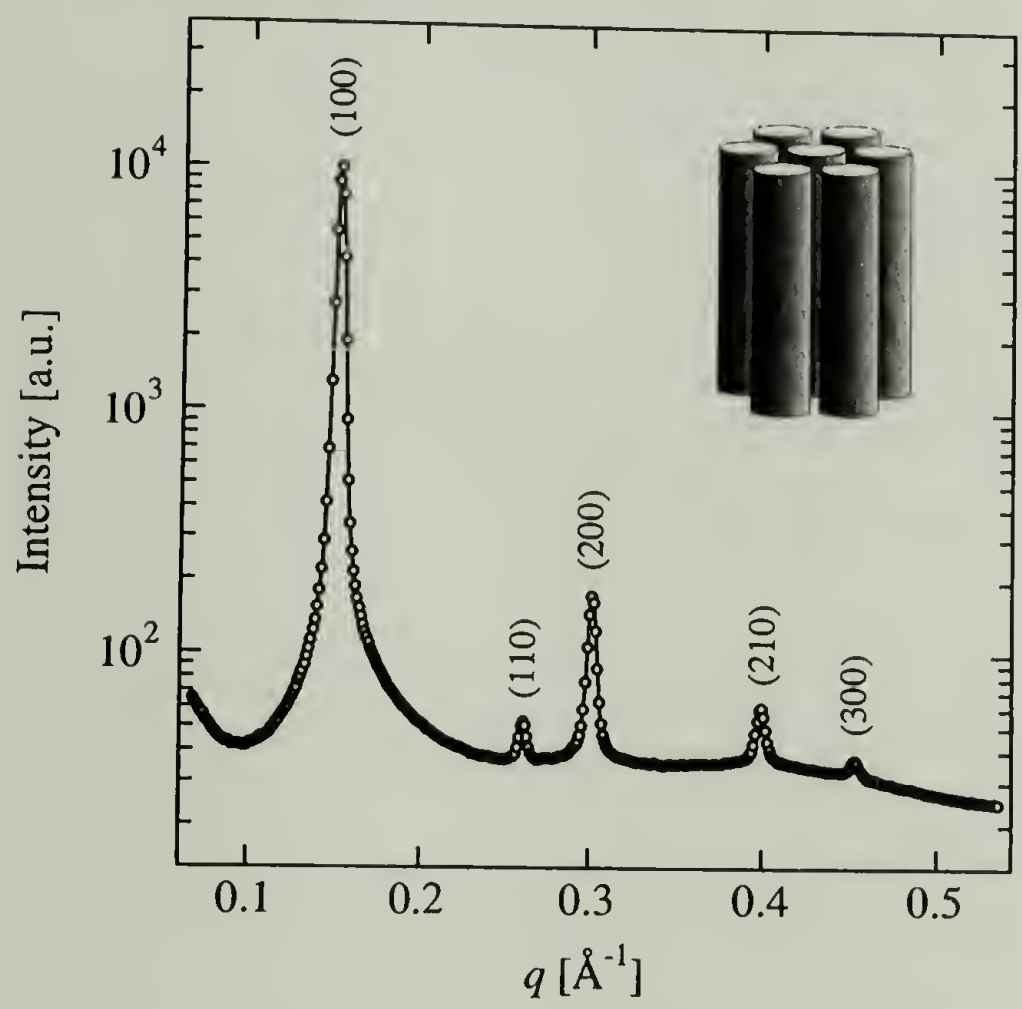


**Figure 2.3:** 2-D SAXS Image and angular-averaged scattering profile for a typical PA–CTACl complex in 10 mM NaCl at an approximate osmotic pressure of 112 atm. The peak positions correspond to a hexagonally close-packed cylindrical (hcpc) unit cell structure, which is pictured schematically. Miller indices associated with the major peaks are also shown.

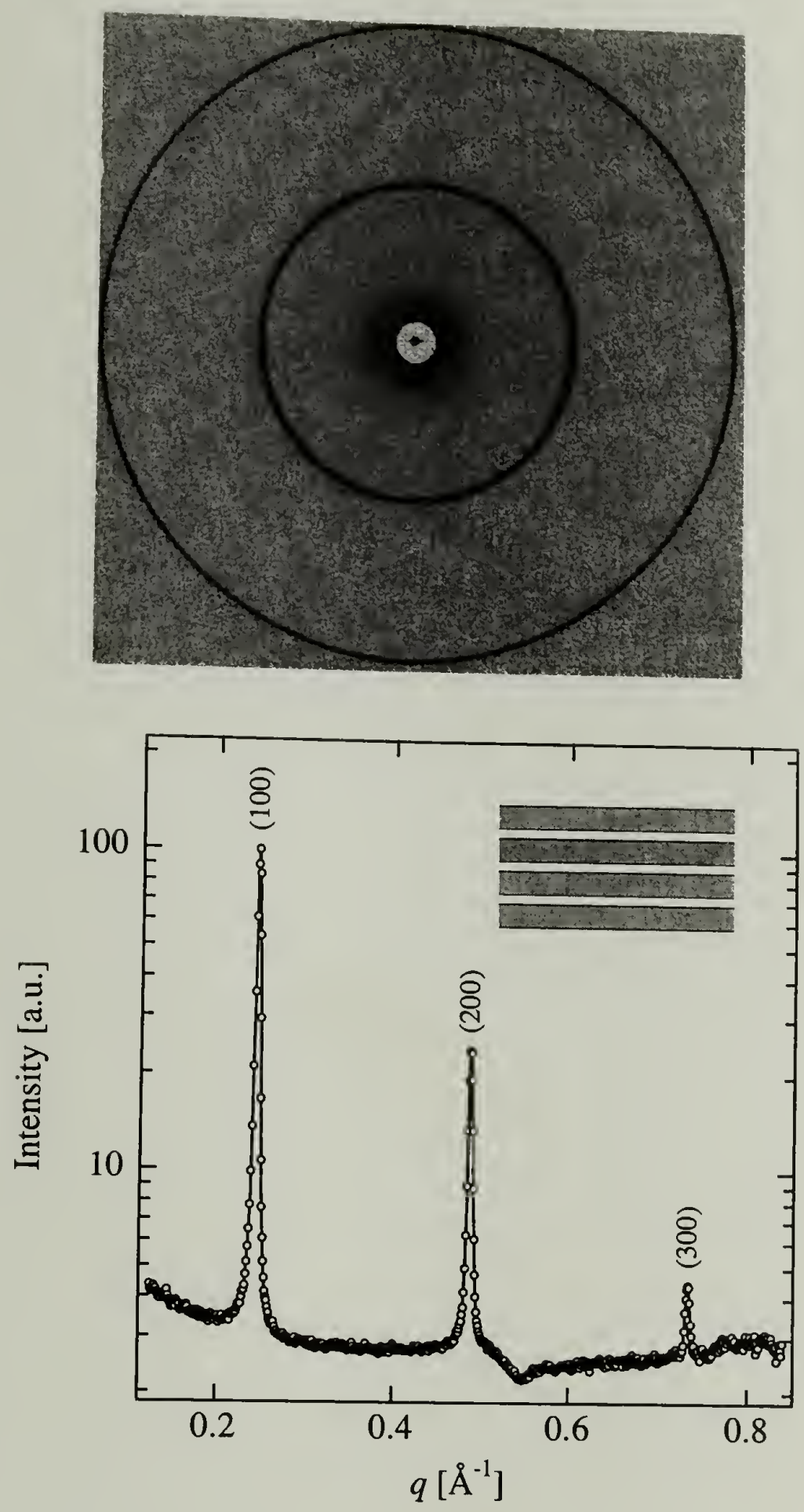


**Figure 2.4:** 2-D SAXS Image and angular-averaged scattering profile for a typical PA–CTACl complex at an approximate osmotic pressure of 1000 atm. The peak positions correspond to a lamellar structure, which is pictured schematically. Miller indices associated with the major peaks are also shown.

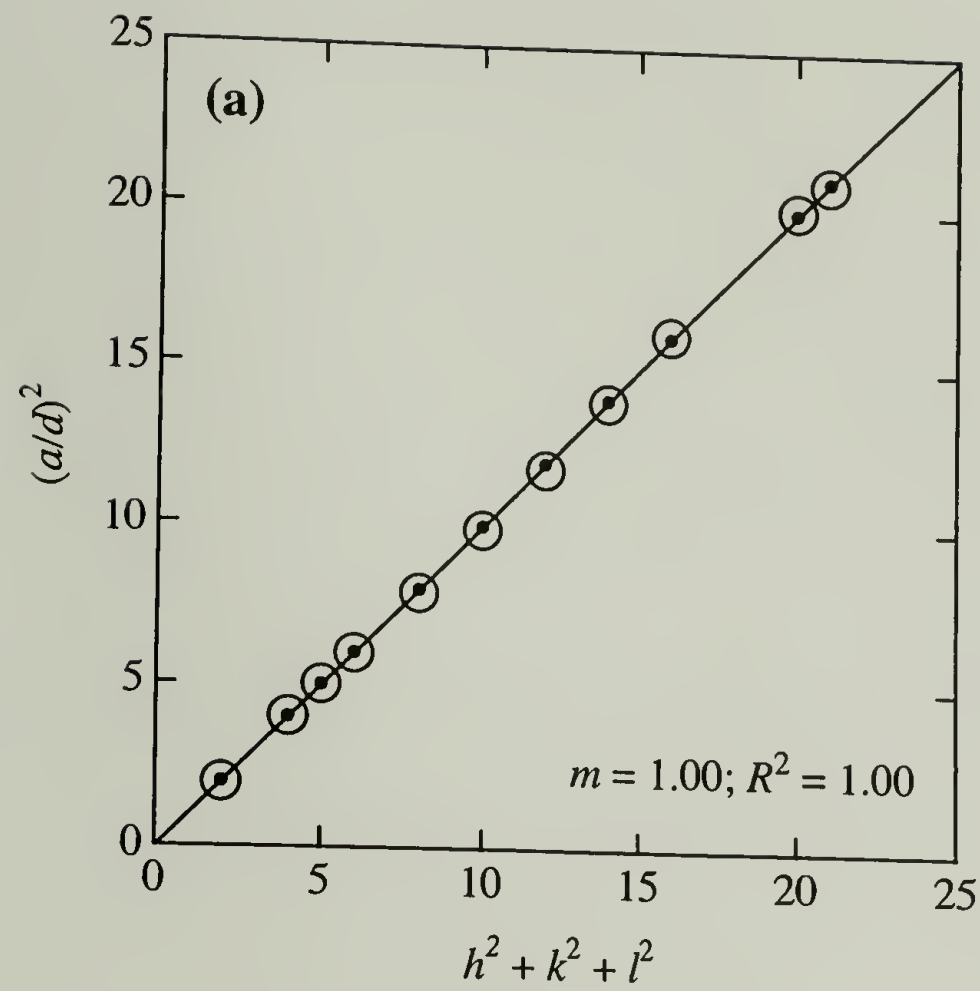


**Figure 2.5:** Correlation of measured (open circles) and predicted (filled dots) $(a/d)^2$ values with Miller index sums for PA–CTACl unit cells in 10 mM NaCl at 2 osmotic pressures: (a) *Pm*3*n* unit cell at 0 atm, and (b) hcpc unit cell at 112 atm. Solid lines are curve fits of the measured data. As per equations 2.2 and 2.3, a slope of 1 was obtained for the *Pm*3*n* phase and a slope of 4/3 was obtained for the hcpc phase.

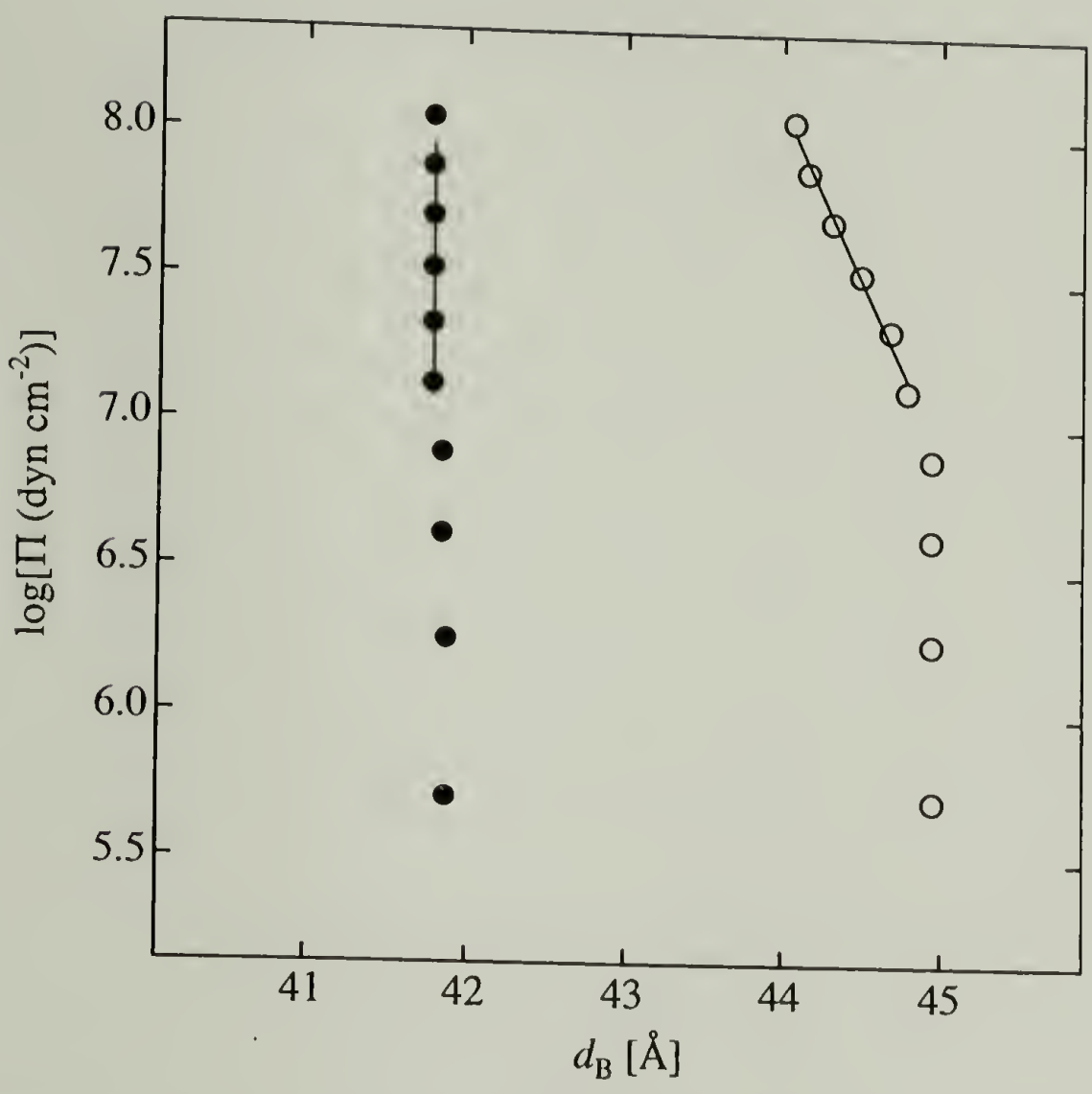


**Figure 2.6:** Phase diagram for PA–CTABr complexes in 10 mM NaBr (filled symbols) and 100 mM NaBr (open symbols). Only the hcpc phase was observed under these conditions, and Bragg spacings were calculated using the (100) hcpc diffraction signals. Exponential decay lengths were determined by fitting the linear portion of each curve; these values are presented in Table 2.6.

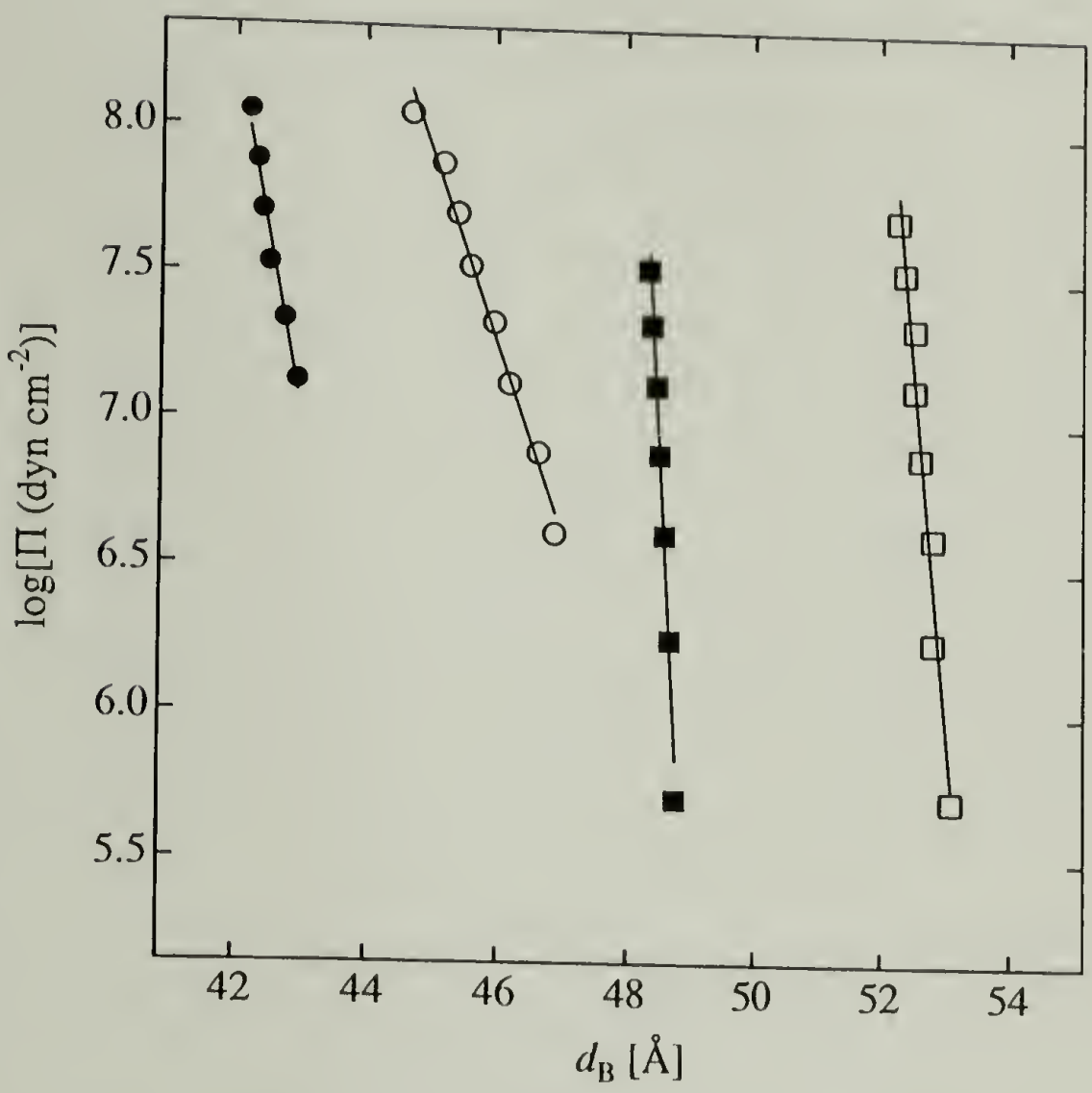


**Figure 2.7:** Phase diagram for 70% charge PAAm–CTABr complexes in 10 mM NaBr (filled symbols) and 100 mM NaBr (open symbols). The hcpc (●,○) and *Pm*3*n* cubic phases (■,□) were observed. Bragg spacings were calculated using the (100) hcpc and the (210) *Pm*3*n* cubic diffraction signals when those phases were present. Exponential decay lengths were determined by fitting the linear portion of each curve; these values are presented in Table 2.7.

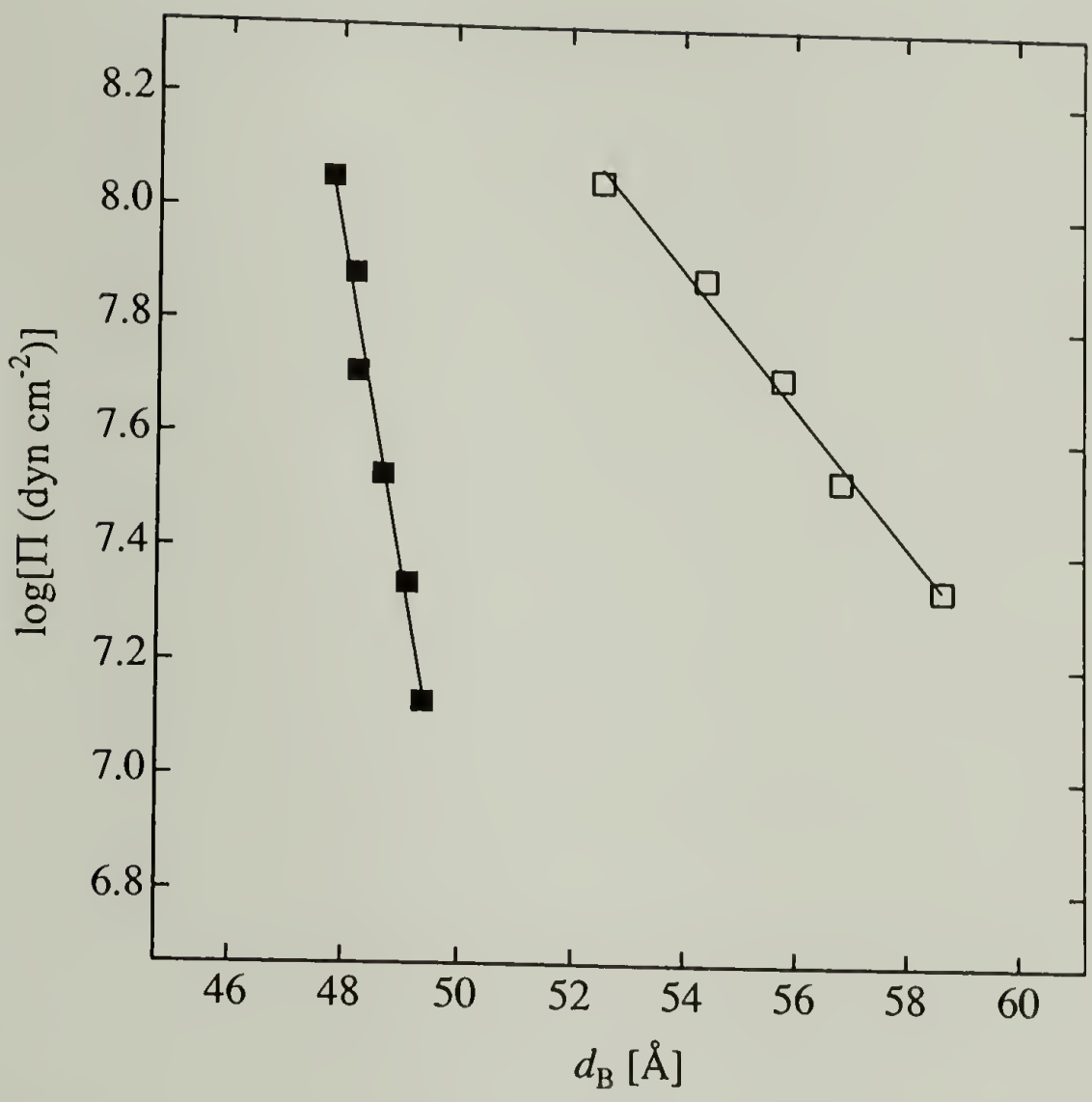


**Figure 2.8:** Phase diagram for 40% charge PAAm–CTABr complexes in 10 mM NaBr (filled symbols) and 100 mM NaBr (open symbols). Only the *Pm*3*n* phase was observed under these conditions, and Bragg spacings were calculated using the (210) *Pm*3*n* diffraction signals. Exponential decay lengths were determined by fitting the linear portion of each curve; these values are presented in Table 2.8.

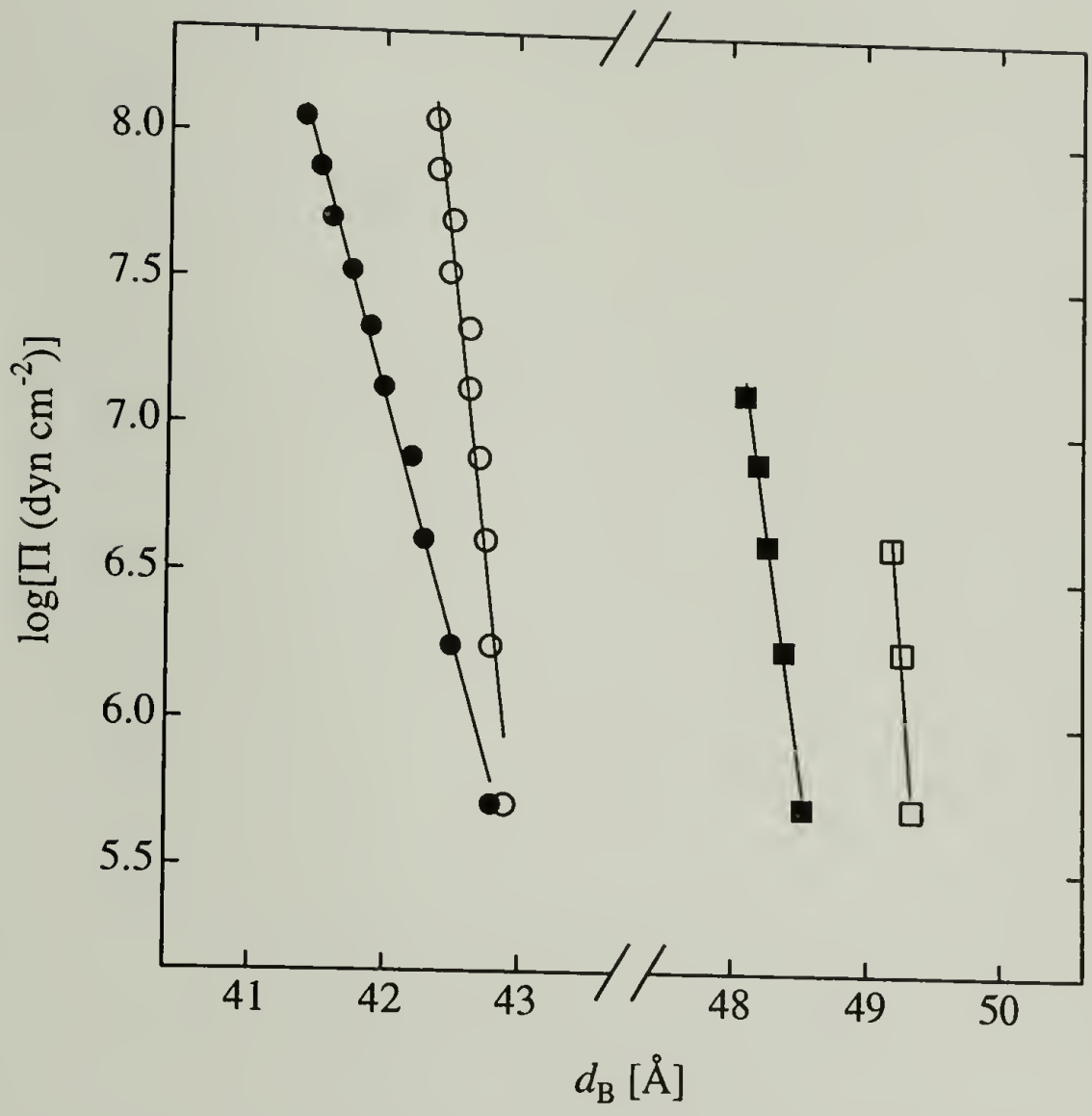


**Figure 2.9:** Phase diagram for PA–CTACl complexes in 10 mM NaCl (filled symbols) and 100 mM NaCl (open symbols). The hcpc (●,○) and *Pm3n* cubic phases (■,□) were observed. Bragg spacings were calculated using the (100) hcpc and the (210) *Pm3n* cubic diffraction signals when those phases were present. Exponential decay lengths were determined by fitting the linear portion of each curve; these values are presented in Table 2.6.

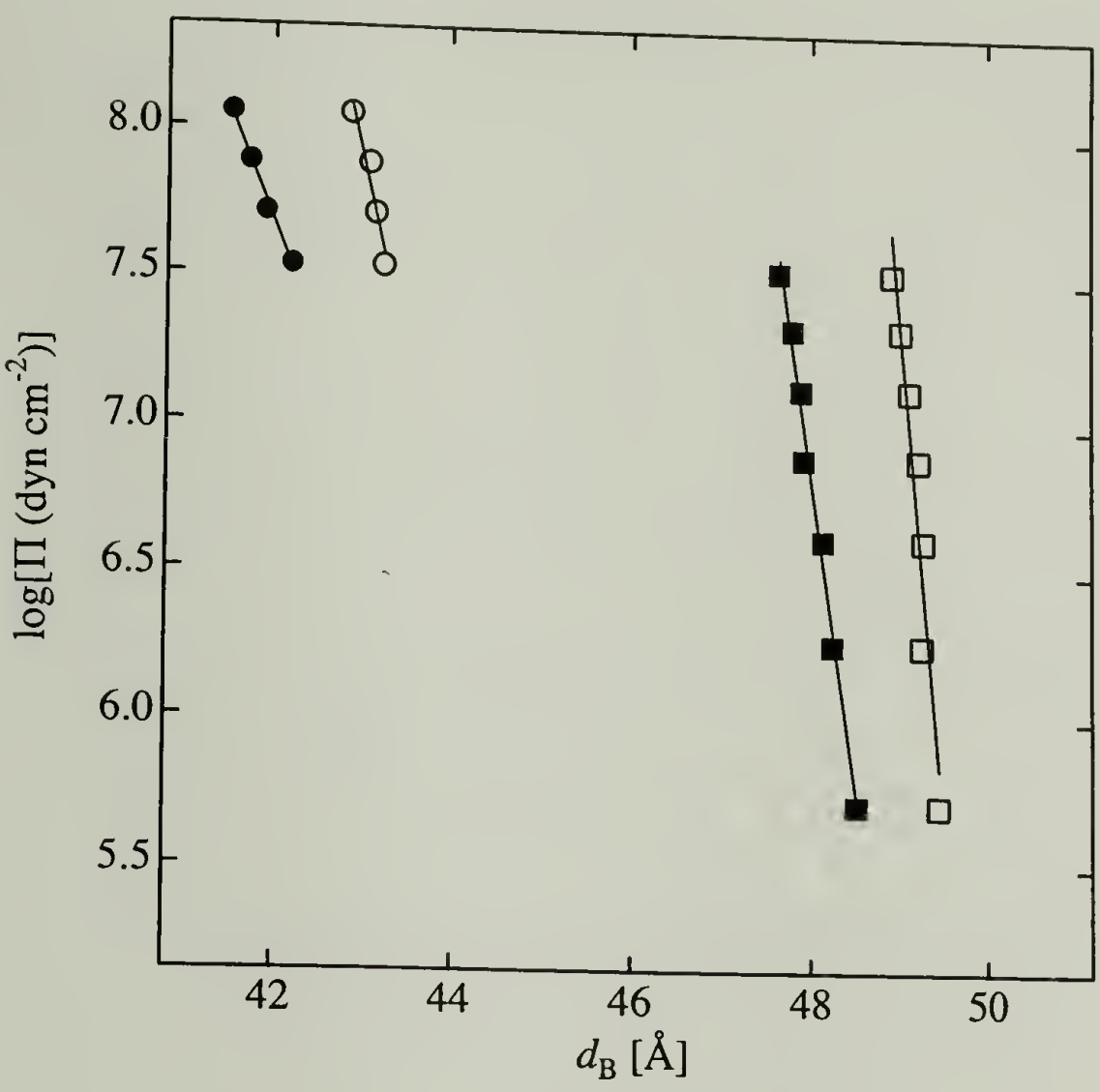


**Figure 2.10:** Phase diagram for 70% charge PAAm–CTACl complexes in 10 mM NaCl (filled symbols) and 100 mM NaCl (open symbols). The hcpc (●,○) and *Pm*3*n* cubic phases (■,□) were observed. Bragg spacings were calculated using the (100) hcpc and the (210) *Pm*3*n* cubic diffraction signals when those phases were present. Exponential decay lengths were determined by fitting the linear portion of each curve; these values are presented in Table 2.7.

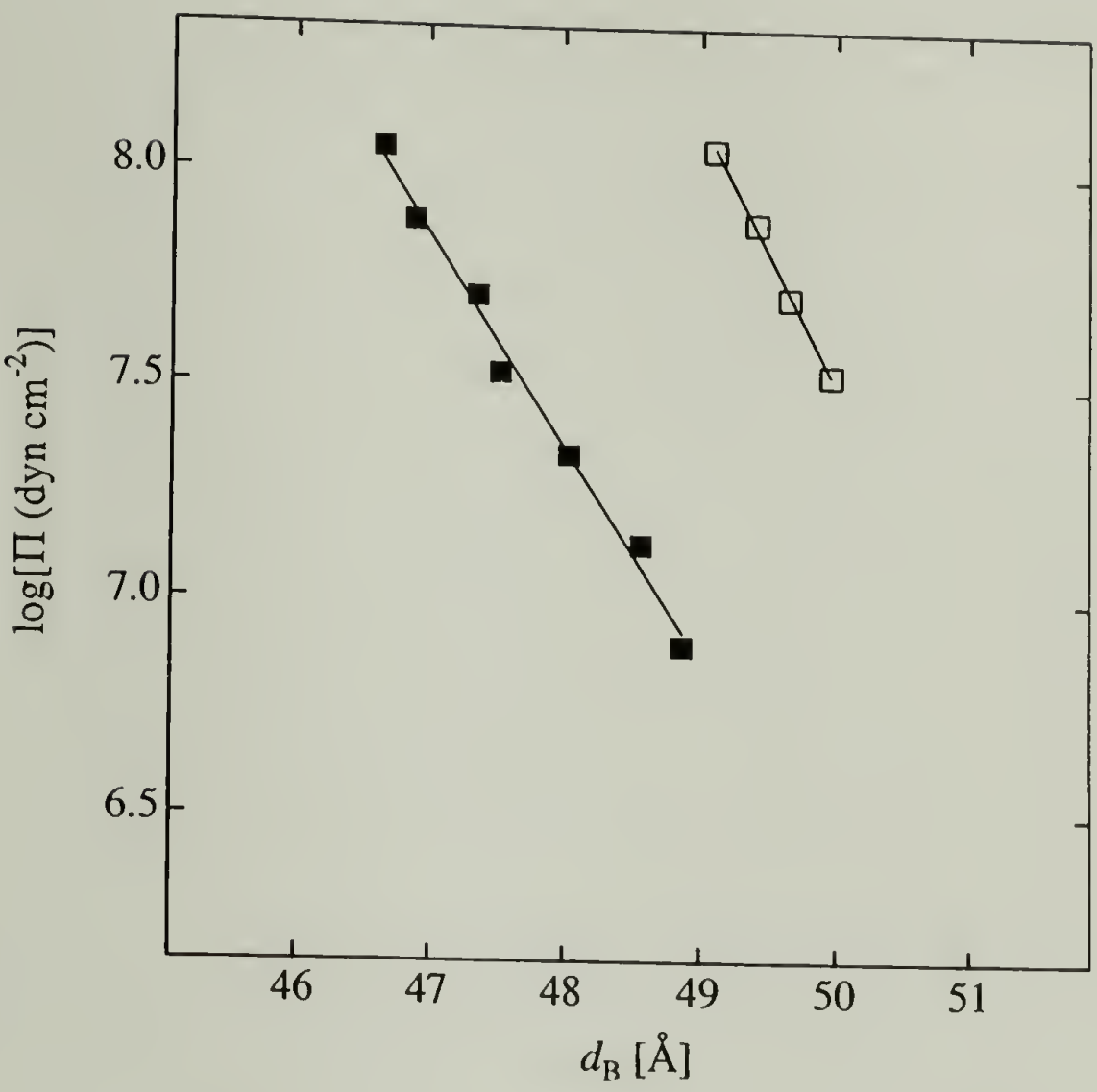


**Figure 2.11:** Phase diagram for 40% charge PAAm–CTACl complexes in 10 mM NaCl (filled symbols) and 100 mM NaCl (open symbols). Only the *Pm*3*n* phase was observed under these conditions, and Bragg spacings were calculated using the (210) *Pm*3*n* diffraction signals. Exponential decay lengths were determined by fitting the linear portion of each curve; these values are presented in Table 2.8.

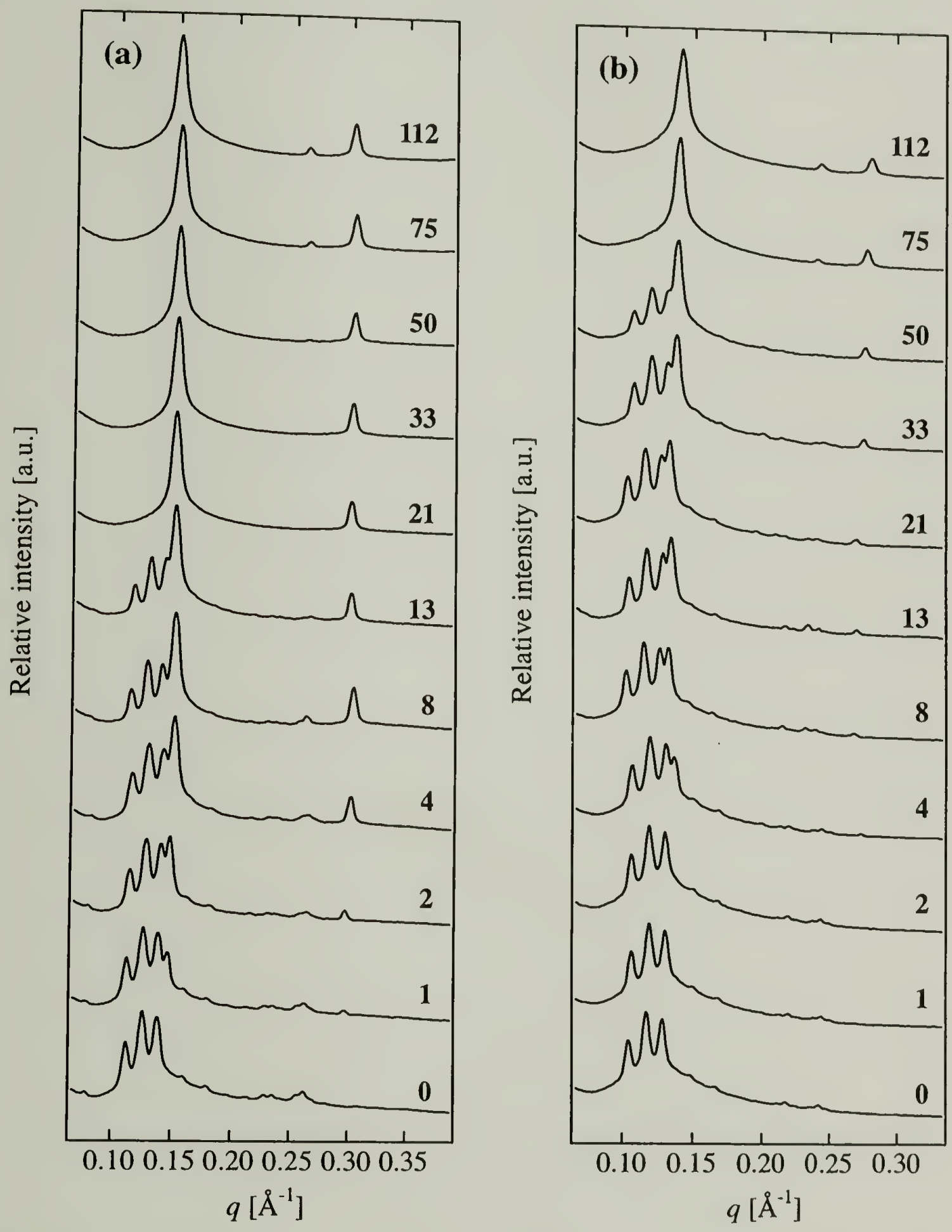


**Figure 2.12:** Angular-averaged scattering profiles for (a) PA–CTACl complexes in 10 mM NaCl and (b) 70% charge PAAm–CTABr complexes in 100 mM NaBr under osmotic stress. Approximate osmotic pressure values in units of atm are associated with each curve.

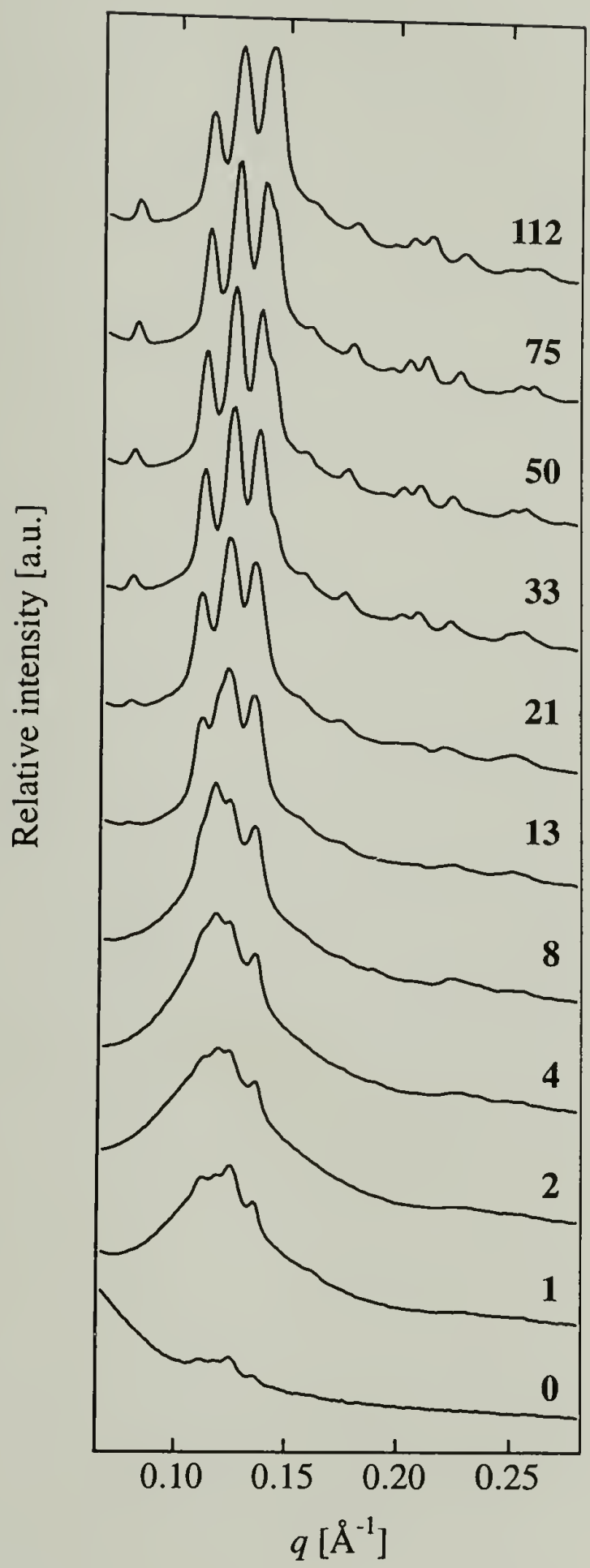


**Figure 2.13:** Angular-averaged scattering profiles for 40% charge PAAm–CTACl complexes in 100 mM NaCl under osmotic stress. Approximate osmotic pressure values in units of atm are associated with each curve.

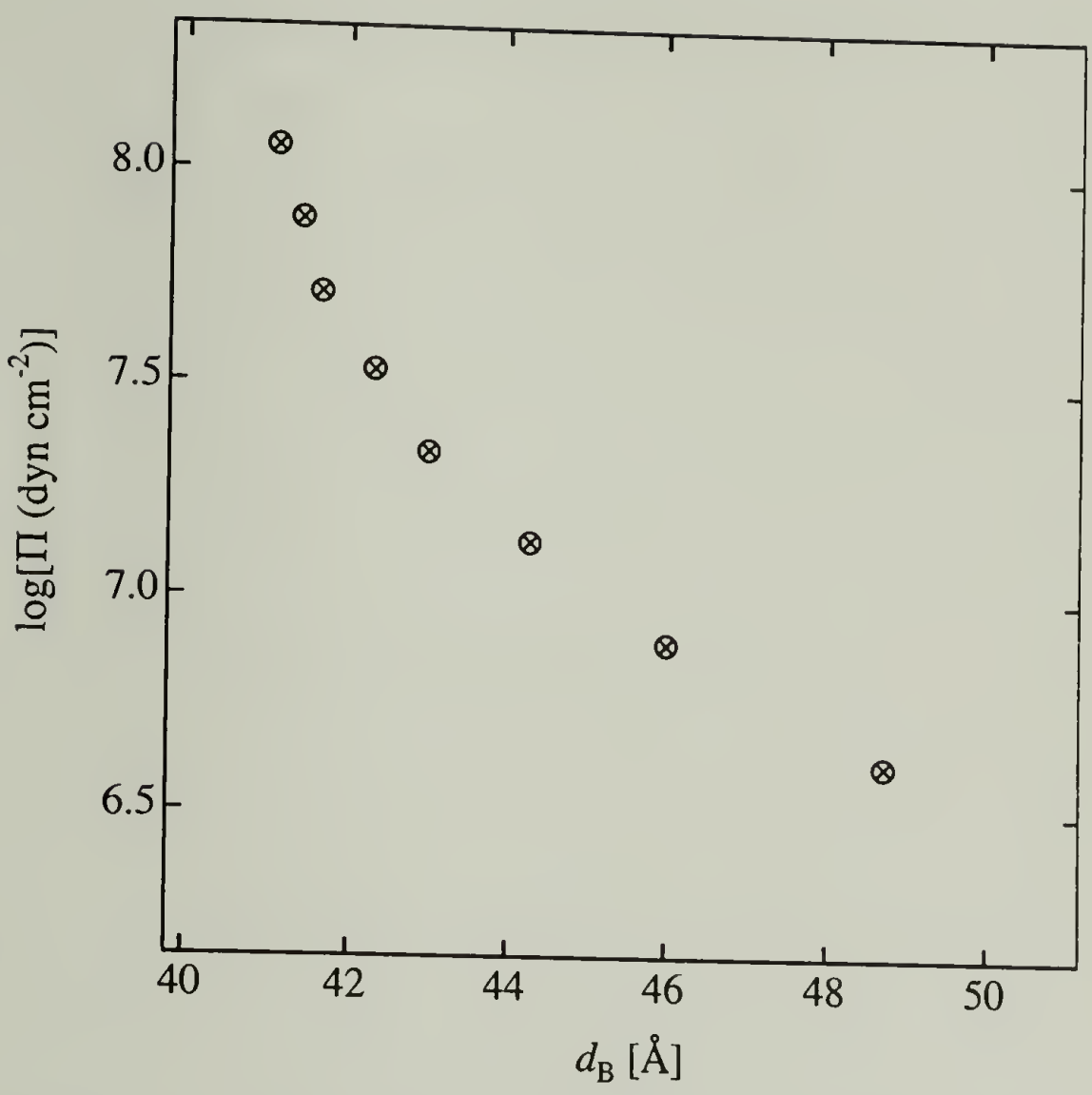


**Figure 2.14:** Phase diagram for PA–CTACl complexes in 1 M NaCl. Only the hcpc phase was observed under these conditions, and Bragg spacings were calculated using the (100) hcpc diffraction signals.

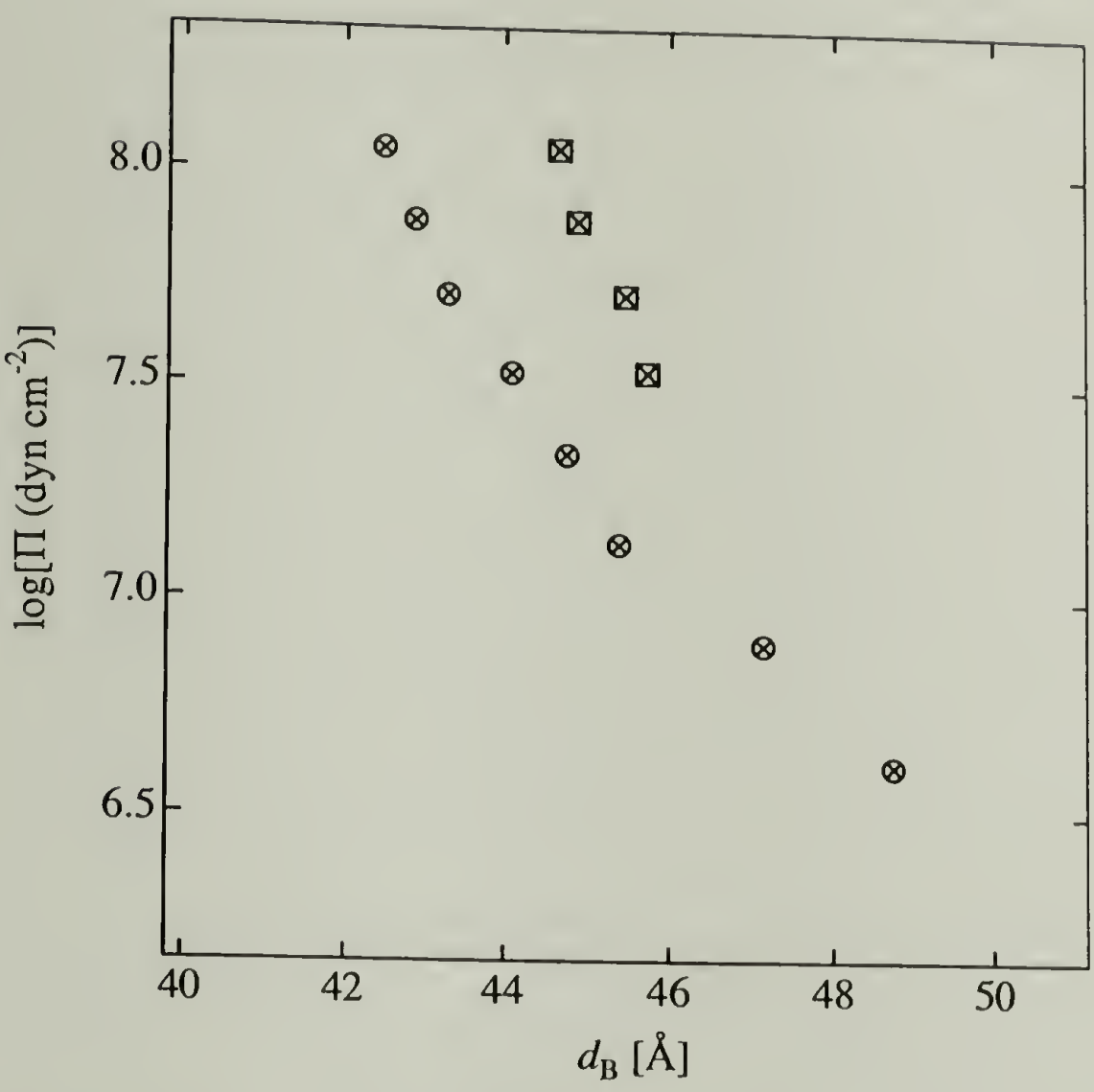


**Figure 2.15:** Phase diagram for 70% charge PAAm–CTACl complexes in 1 M NaCl. The hcpc (⊗) and *Pm*3*n* cubic phases (⊠) were observed. Bragg spacings were calculated using the (100) hcpc and the (210) *Pm*3*n* cubic diffraction signals when those phases were present.

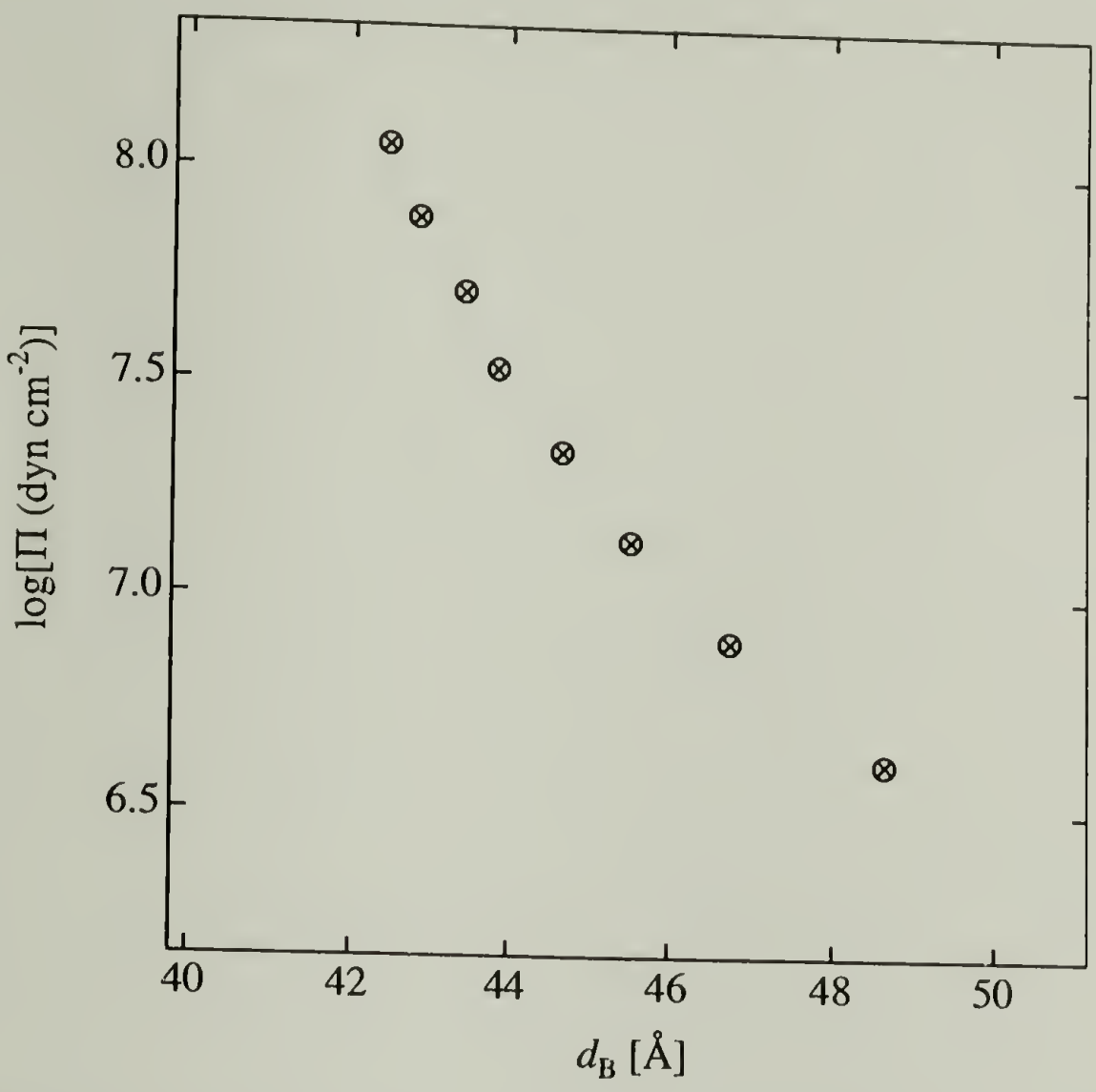


**Figure 2.16:** Phase diagram for 40% charge PAAm–CTACl complexes in 1 M NaCl. Only the hcpc phase was observed under these conditions, and Bragg spacings were calculated using the (100) hcpc diffraction signals.

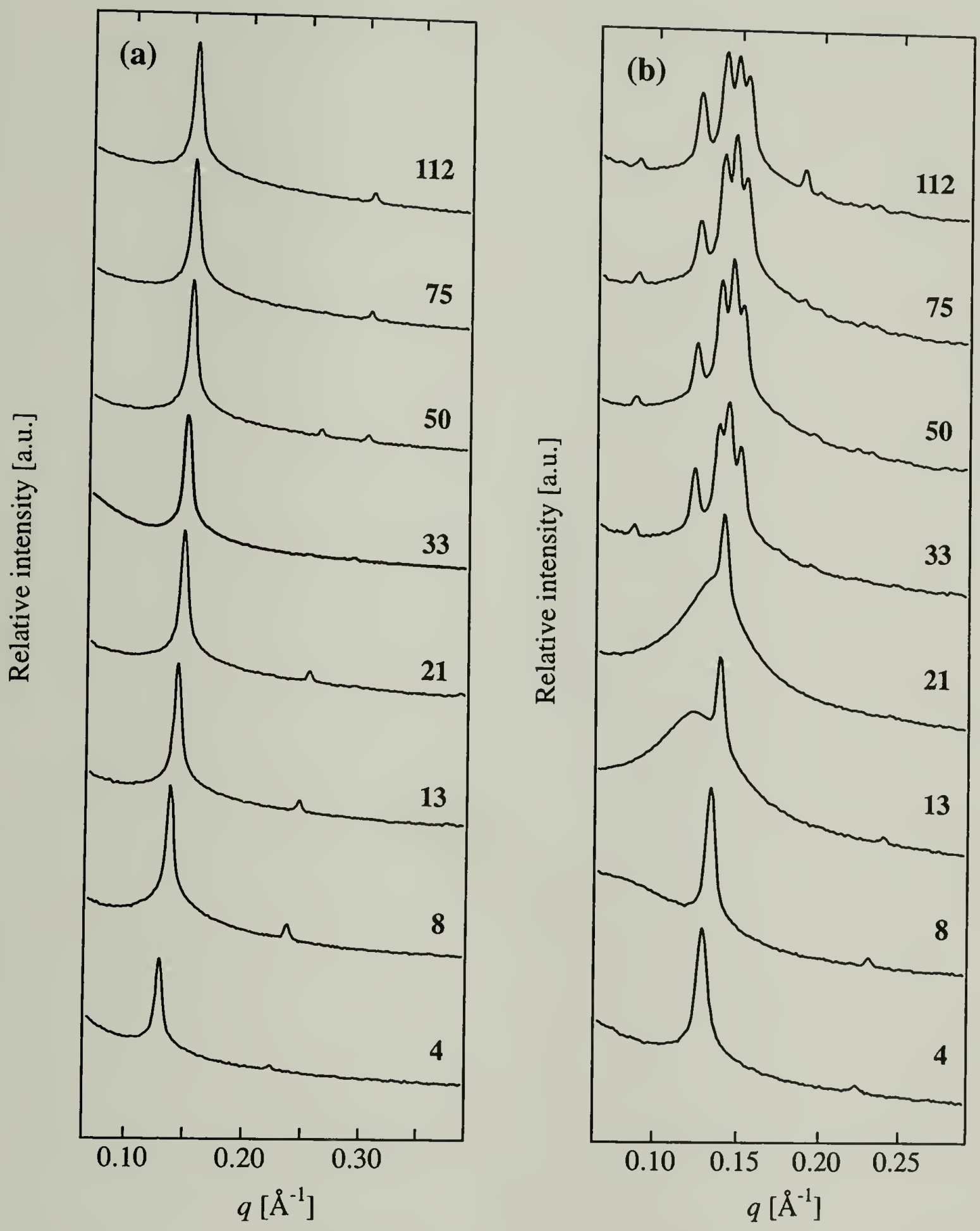


**Figure 2.17:** Angular-averaged scattering profiles for (a) PA–CTACl and (b) 70% charge PAAm–CTACl complexes under osmotic stress in 1 M NaCl. Approximate osmotic pressure values in units of atm are associated with each curve.

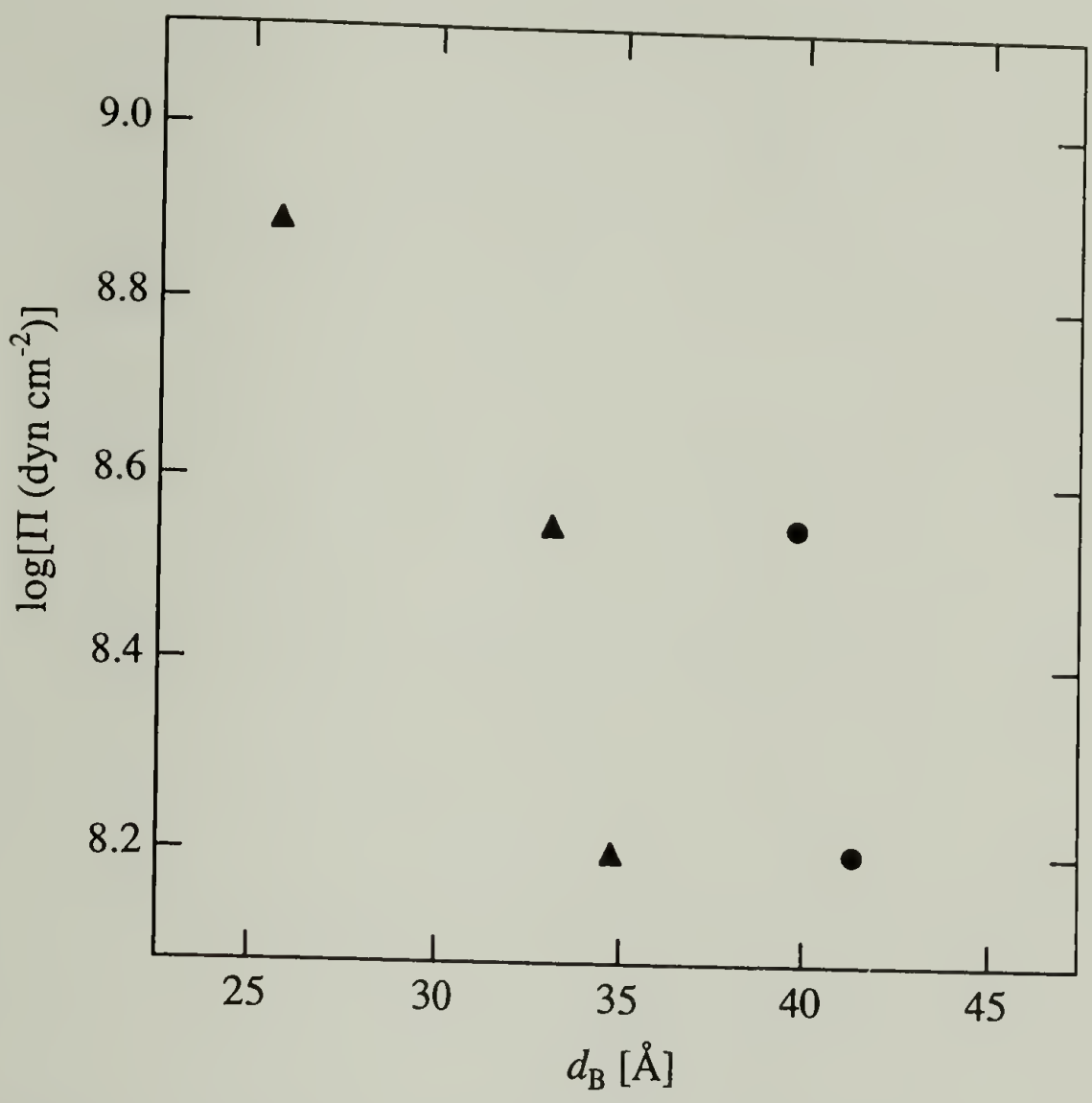


**Figure 2.18:** Phase diagram for PA–CTACl complexes exposed to saturated salt solution vapor. The lamellar (▲) and hcpc phases (●) were observed. Bragg spacings were calculated using the (100) lamellar and the (100) hcpc diffraction signals when those phases were present.

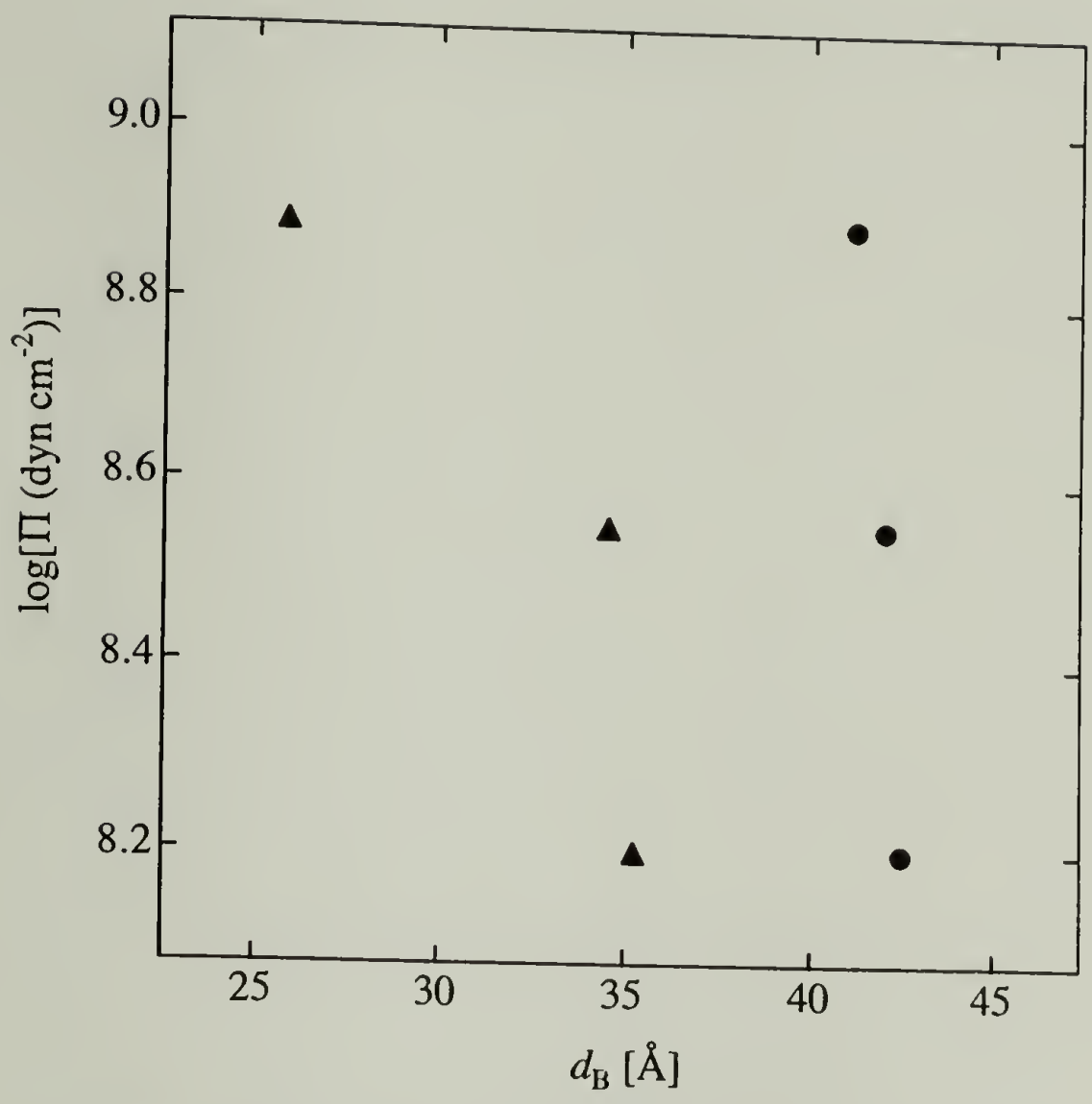


**Figure 2.19:** Phase diagram for 70% charge PAAm–CTACl complexes exposed to saturated salt solution vapor. The lamellar (▲) and hcpc phases (●) were observed. Bragg spacings were calculated using the (100) lamellar and the (100) hcpc diffraction signals when those phases were present.

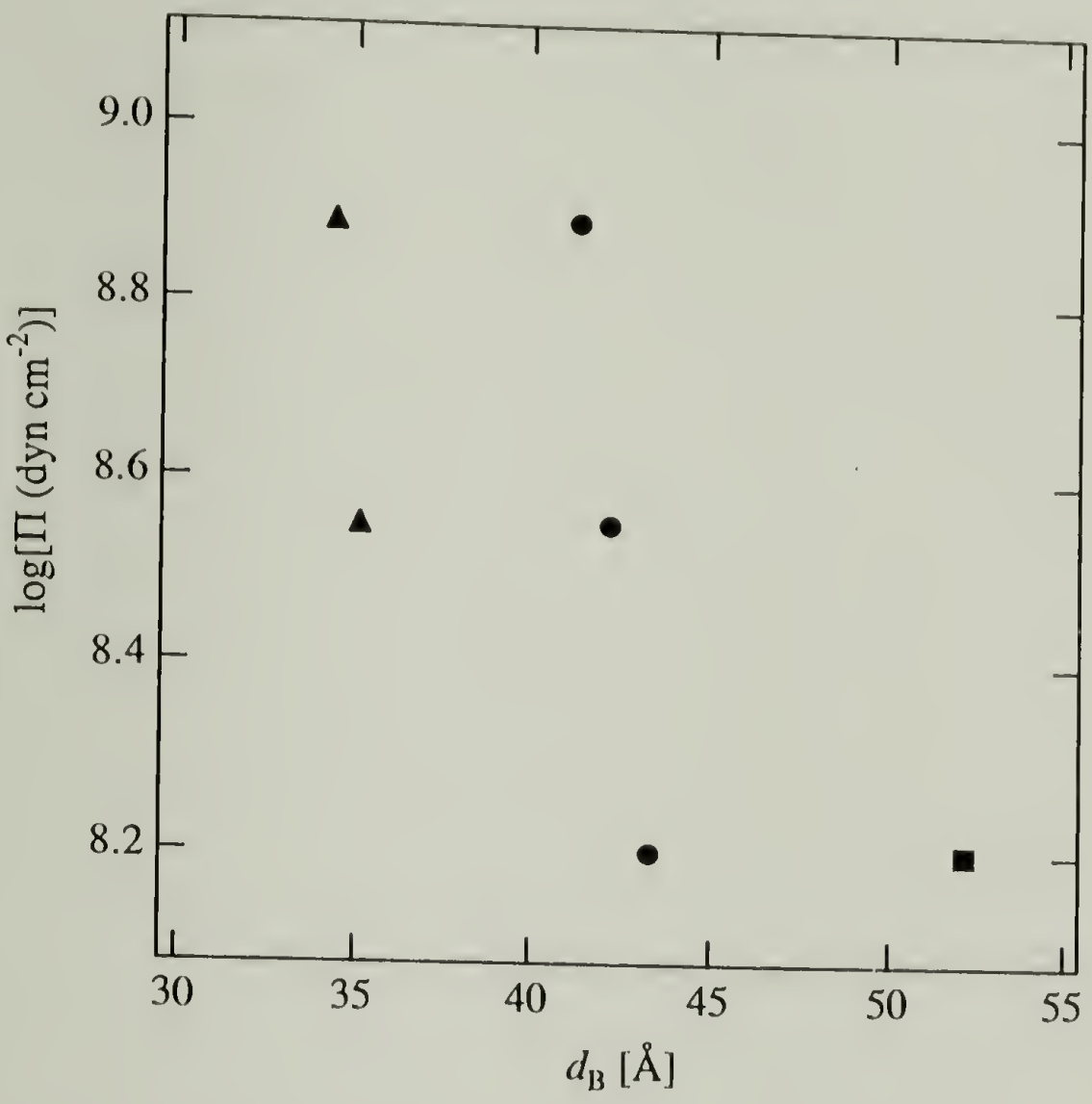


**Figure 2.20:** Phase diagram for 40% charge PAAm–CTACl complexes exposed to saturated salt solution vapor. The lamellar (▲), hcpc (●), and *Pm*3*n* cubic phases (■) were observed. Bragg spacings were calculated using the (100) lamellar, (100) hcpc, and (210) Pm3n diffraction signals when those phases were present.

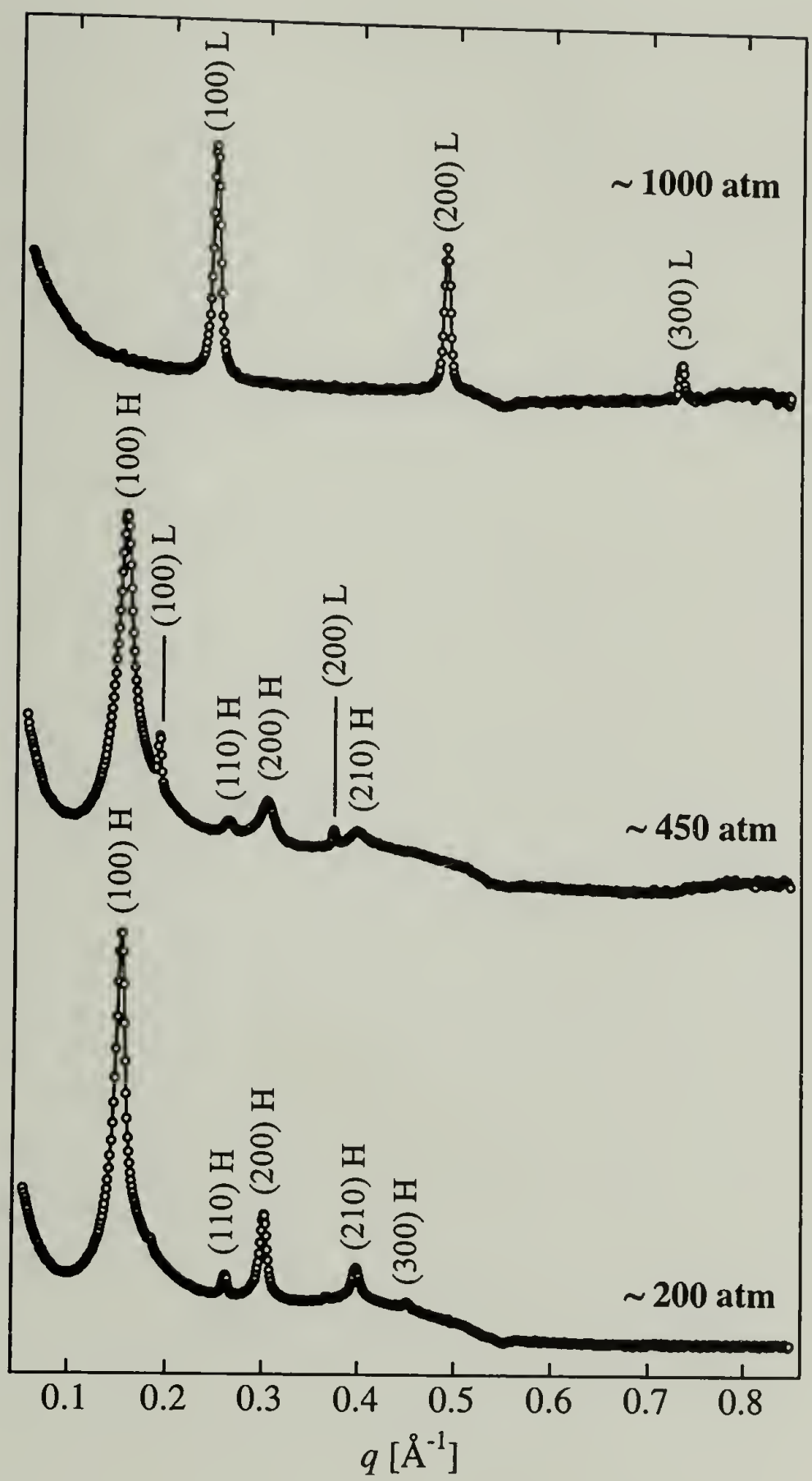


**Figure 2.21:** Angular-averaged scattering profiles for PA–CTACl complexes exposed to saturated salt solution vapor. Approximate osmotic pressure values are associated with each curve, and the Miller indices corresponding to each diffraction peak are shown. Both the lamellar (L) and hcpc (H) phases were observed.

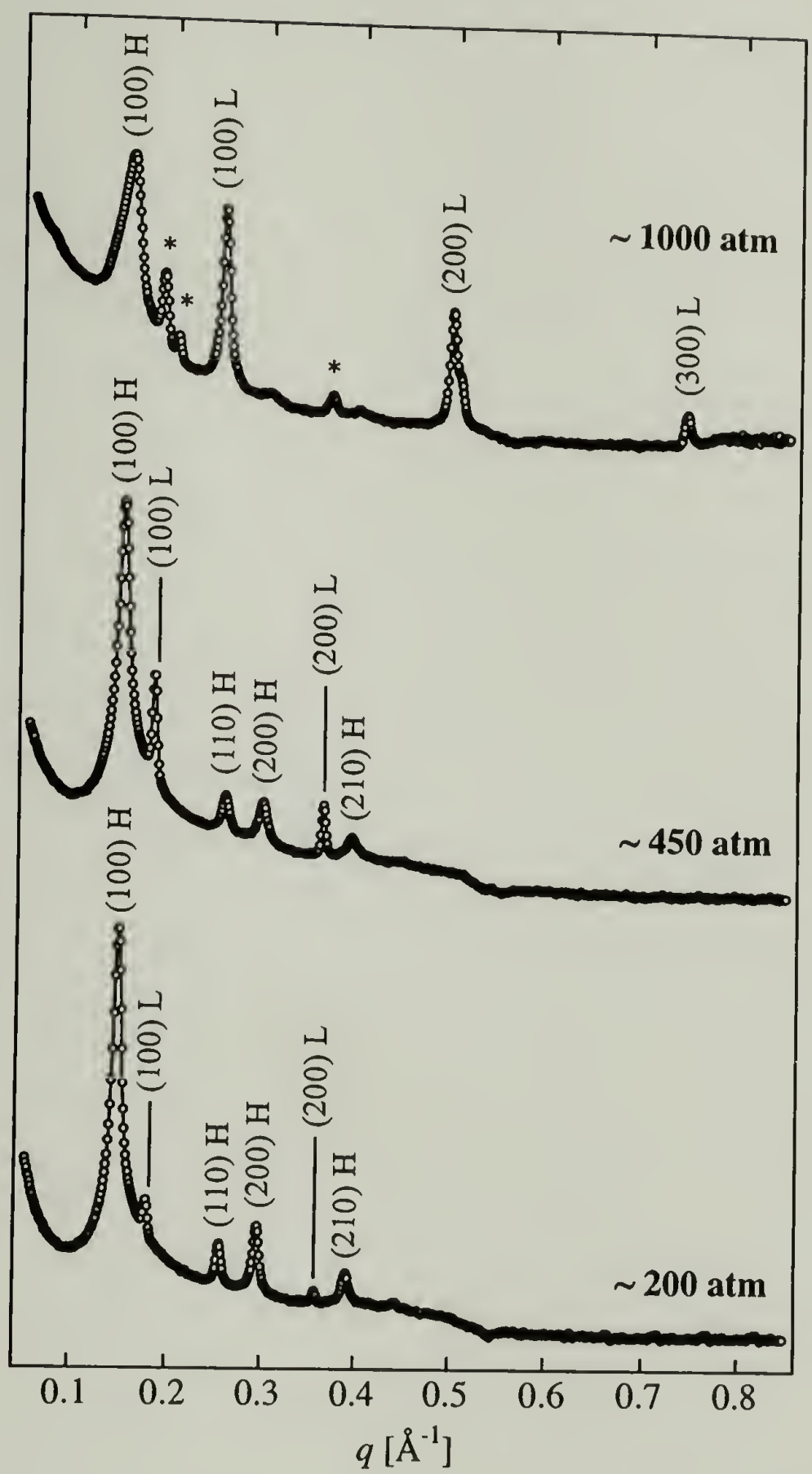


**Figure 2.22:** Angular-averaged scattering profiles for 70% charge PAAm–CTACl complexes exposed to saturated salt solution vapor. Approximate osmotic pressure values are associated with each curve, and the Miller indices corresponding to each diffraction peak are shown. Both the lamellar (L) and hcpc (H) phases were observed. Peaks that could not be assigned to a structure are labeled with an asterisk (*).

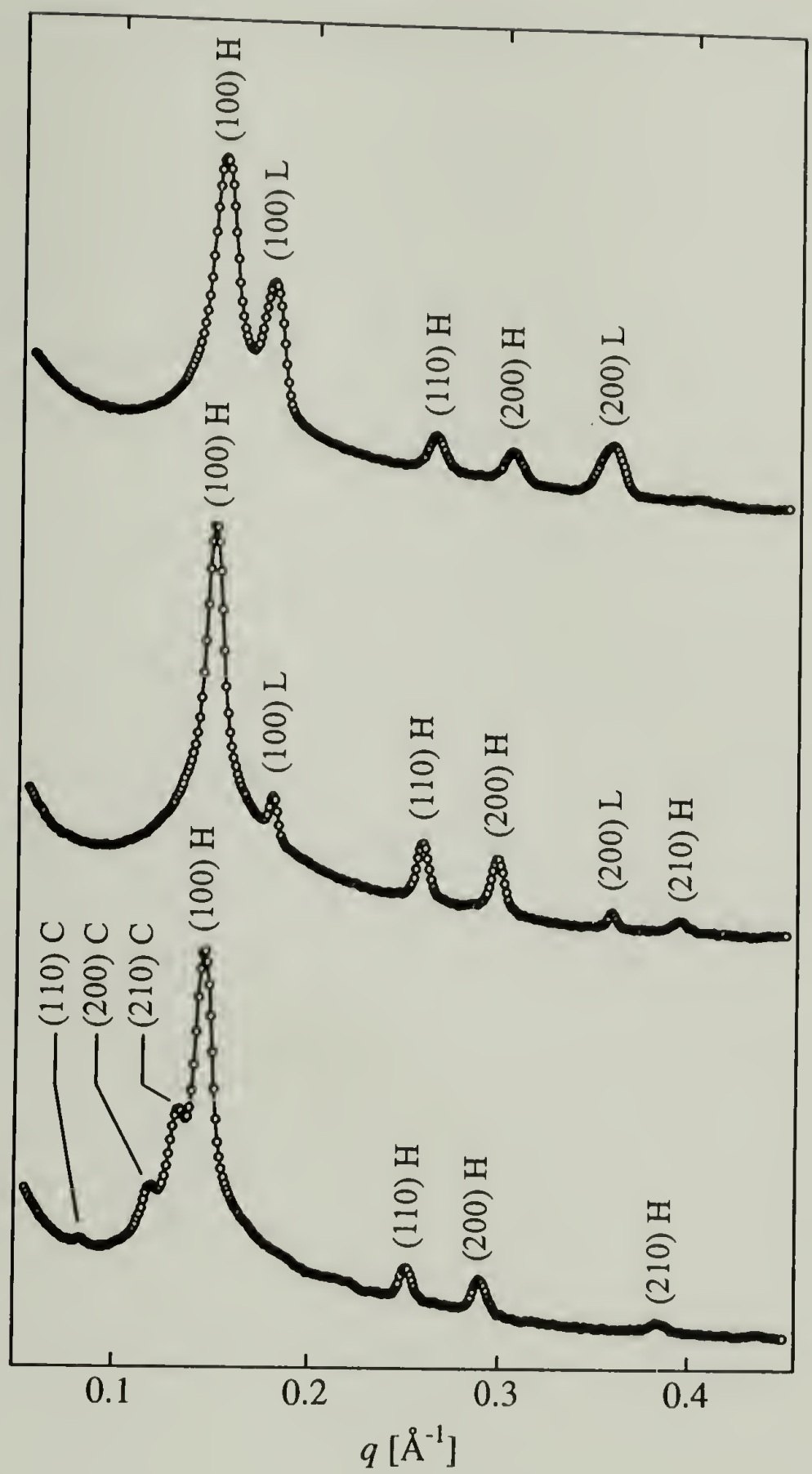


**Figure 2.23:** Angular-averaged scattering profiles for 40% charge PAAm–CTACl complexes exposed to saturated salt solution vapor. Approximate osmotic pressure values are associated with each curve, and the Miller indices corresponding to each diffraction peak are shown. The lamellar (L), hcpc (H), and *Pm*3*n* cubic (C) phases were observed.

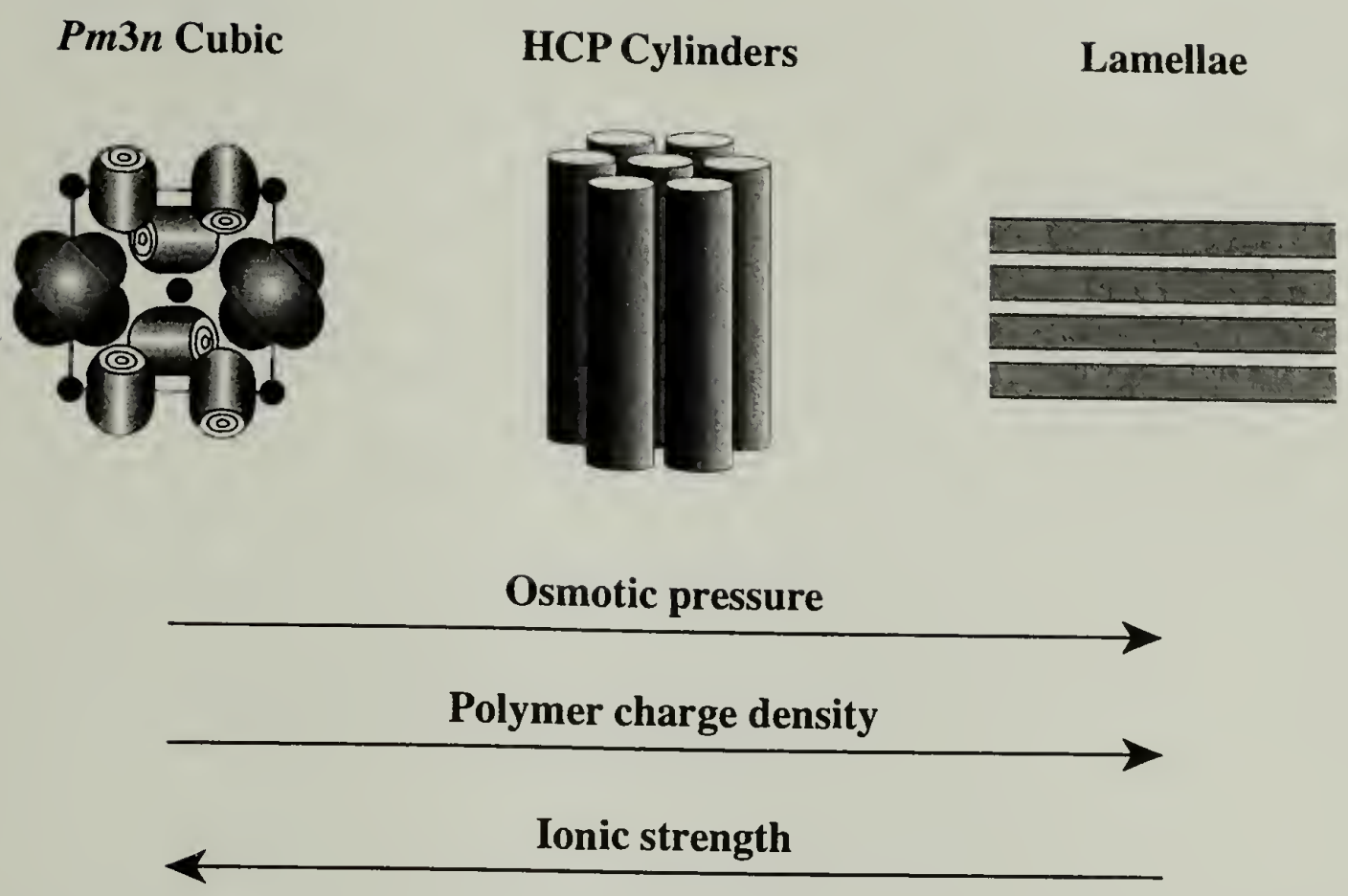


**Figure 2.24:** Schematic polyelectrolyte–surfactant complex phase diagram. Phase curvature decreases from left to right.

## References


[1] Kogej, K.; Theunissen, E.; Reynaers, H. Effect of Polyion Charge Density on the Morphology of Nanostructures in Polyelectrolyte-Surfactant Complexes. *Langmuir* **2002,** *18,* 8799-8805.

[2] Antonietti, M.; Wenzel, A. Structure control of polyelectrolyte-lipid complexes by variation of charge density and addition of cholesterol. *Colloids Surf. A* **1998,** *135,* 141-147.

[3] Zhou, S.; Burger, C.; Yeh, F.; Chu, B. Charge Density Effect of Polyelectrolyte Chains on the Nanostructures of Polyelectrolyte-Surfactant Complexes. *Macromolecules* **1998,** *31,* 8157-8163.

[4] Wang, C.; Tam, K. C. Interaction between Polyelectrolyte and Oppositely Charged Surfactant: Effect of Charge Density. *J. Phys. Chem. B* **2004,** *108,* 8976-8982.

[5] Kogej, K. Study of the Effect of Polyion Charge Density on Structural Properties of Complexes between Poly(acrylic acid) and Alkylpyridinium Surfactants. *J. Phys. Chem. B* **2003,** *107,* 8003-8010.

[6] Sasaki, S.; Koga, S. Order–Disorder Phase Transition of Polyelectrolyte Gel–Surfactant Complexes. *Macromolecules* **2004,** *37,* 3809-3814.

[7] Zhou, S.; Hu, H.; Burger, C.; Chu, B. Phase Structural Transitions of Polyelectrolyte-Surfactant Complexes between Poly(vinylamine hydrochloride) and Oppositely Charged Sodium Alkyl Sulfate. *Macromolecules* **2001,** *34,* 1772-1778.

[8] Zhou, S.; Yeh, F.; Burger, C.; Chu, B. Nanostructures of Polyelectrolyte Gel-Surfactant Complexes. *J. Polym. Sci. B: Polym. Phys.* **1999,** *37,* 2165-2172.

[9] Sokolov, E. L.; Yeh, F.; Khokhlov, A. R.; Chu, B. Nanoscale Supramolecular Ordering in Gel-Surfactant Complexes: Sodium Alkyl Sulfates in Poly(diallyldimethylammonium Chloride). *Langmuir* **1996,** *12,* 6229-6234.

[10] Mironov, A. V.; Starodoubtsev, S. G.; Khokhlov, A. R.; Dembo, A. T.; Yakunin, A. N. Structural study of surfactant aggregates in polyelectrolyte gel. *Colloids Surf. A* **1999,** *147,* 213-220.

[11] Michiotti, P.; Bonicelli, M. G.; Cafarelli, P.; Ceccaroni, G.; Ferragina, C.; La Mesa, C. Complexes of octadecyltrimethylammonium polyacrylate: properties in solution, gel and solid forms. *Colloid Polym. Sci.* **2003,** *281,* 431-438.

[12] Sasaki, S.; Koga, S.; Sugiyama, M.; Annaka, M. Nanostructures of polyelectrolyte gel–surfactant complexes in uniaxially stretched networks. *Phys. Rev. E* **2003,** *68,* 021504.

[13] Ilekti, P.; Martin, T.; Cabane, B.; Piculell, L. Effects of Polyelectrolytes on the Structures and Interactions of Surfactant Aggregates. *J. Phys. Chem. B* **1999,** *103,* 9831-9840.

[14] Svensson, A.; Piculell, L.; Cabane, B.; Ilekti, P. A New Approach to the Phase Bchavior of Oppositely Charged Polymers and Surfactants. *J. Phys. Chem. B* **2002,** *106,* 1013-1018.

[15] Kogej, K.; Evmenenko, G.; Theunissen, E.; Berghmans, H.; Reynaers, H. Investigation of Structures in Polyelectrolyte/Surfactant Complexes by X-ray Scattering. *Langmuir* **2001,** *17,* 3175-3184.

[16] Michel, B. E. Evaluation of the water potentials of solutions of polyethylene glycol-8000 both in the absence and presence of other solutes. *Plant Physiol.* **1983,** *72,* 66-70.

[17] *CRC Handbook of Chemistry and Physics;* 73rd ed.; Lide, D. R., Ed.; CRC Press: Boca Raton, FL, 1993.

[18] Kékicheff, P.; Grabielle-Madelmont, C.; Ollivon, M. Phase Diagram of Sodium Dodecyl Sulfate-Water System. *J. Colloid Interface Sci.* **1989,** *131,* 112-132.

[19] Auvray, X.; Petipas, C.; Anthore, R.; Rico, I.; Lattes, A. X-Ray Diffraction Study of Mesophases of Cetyltrimethylammonium Bromide in Water, Formamide, and Glycerol. *J. Phys. Chem.* **1989,** *93,* 7458-7464.

[20] Vargas, R.; Mariani, P.; Gulik, A.; Luzzati, V. Cubic Phases of Lipid-Containing Systems–The Structure of Phase-Q223 (Space Group *Pm3n*)– An X-Ray Scattering Study. *J. Mol. Biol.* **1992,** *225,* 137-145.

[21] Fontell, K.; Fox, K. K.; Hansson, E. On the Structure of the Cubic Phase I1 in Some Lipid–Water Systems. *Mol. Cryst. Liq. Cryst.* **1985,** *1,* 9-17.

[22] Svensson, A.; Topgaard, D.; Piculell, L.; Söderman, O. Molecular Self-Diffusion in Micellar and Discrete Cubic Phases of an Ionic Surfactant with Mixed Monovalent/Polymeric Counterions. *J. Phys. Chem. B* **2003,** *107,* 13241-13250.

[23] Fontell, K. Cubic phases in surfactant and lipid-containing systems. *Colloid Polym. Sci.* **1990,** *268,* 264-285.

[24] Ziherl, P.; Kamien, R. D. Soap Froths and Crystal Structures. *Phys. Rev. Lett.* **2000,** *85,* 3528-3531.

[25] Parsegian, V. A.; Rand, R. P.; Fuller, N. L.; Rau, D. C. Osmotic Stress for the Direct Measurement of Intermolecular Forces. In *Methods in Enzymology*; Packer, L., Ed.; Academic Press, Inc., 1986; Vol. 127; pp 400-416.

[26] Rau, D. C.; Parsegian, V. A. Direct Measurement of Forces Between Linear Polysaccharides Xanthan and Schizophyllan. *Science* **1990,** *249,* 1278-1281.

[27] Strey, H. H.; Parsegian, V. A.; Podgornik, R. Equation of State for DNA Liquid Crystals: Fluctuation Enhanced Electrostatic Double Layer Repulsion. *Phys. Rev. Lett.* **1997,** *78,* 895-898.

[28] Leikin, S.; Rau, D. C.; Parsegian, V. A. Measured entropy and enthalpy of hydration as a function of distance between DNA double helices. *Phys. Rev. A* **1991,** *44,* 5272-5278.

[29] Hansson, P.; Schneider, S.; Lindman, B. Phase Separation in Polyelectrolyte Gels Interacting with Surfactants of Opposite Charge. *J. Phys. Chem. B* **2002,** *106,* 9777-9793.

[30] So, P. T. C.; Gruner, S. M.; Erramilli, S. Pressure-Induced Topological Phase Transitions in Membranes. *Phys. Rev. Lett.* **1993,** *70,* 3455-3458.

[31] Gleeson, J. T.; Polcyn, A. D.; Gruner, S. M. Structure of Phospholipid Suspensions under Negative Pressure. *J. Colloid Interface Sci.* **1993,** *156,* 430-432.

[32] Gruner, S. M. Soft Materials and Biomaterials Under Pressure: Putting the Squeeze on Biology. In *High-Pressure Crystallography*; Katrusiak, A., McMillan, P., Eds.; Kluwer Academic Publishers: Dordrecht, The Netherlands, 2004; pp 543-556.

[33] Toombes, G. E. S.; Finnefrock, A. C.; Tate, M. W.; Gruner, S. M. Determination of Lamellar-Hexagonal Phase Transition Temperature for 1,2-Dioleoyl-sn-Glycero-3-Phosphatidylethanolamine. *Biophys J.* **2002,** *82,* 2504-2510.

[34] Manning, G. S. Counterion binding in polyelectrolyte theory. *Acc. Chem. Res.* **1979,** *12,* 443-449.

[35] Kiefer, J. J.; Somasundaran, P.; Ananthapadmanabhan, K. P. Interaction of Tetradecyltrimethylammonium Bromide with Poly(acrylic acid) and Poly(methacrylic acid). Effect of Charge Density. *Langmuir* **1993,** *9,* 1187-1192.

[36] Sens, P.; Joanny, J.-F. Counterion Release and Electrostatic Adsorption. *Phys. Rev. Lett.* **2000,** *84,* 4862-4865.

[37] Joanny, J.-F.; Castelnovo, M.; Netz, R. Adsorption of charged polymers. *J. Phys.: Condens. Matter* **2000,** *12,* A1-A7.

[38] Wagner, K.; Harries, D.; May, S.; Kahl, V.; Rädler, J. O.; Ben-Shaul, A. Direct Evidence for Counterion Release upon Cationic Lipid-DNA Condensation. *Langmuir* **2000,** *16,* 303-306.

[39] Konop, A. J.; Colby, R. H. Role of Condensed Counterions in the Thermodynamics of Surfactant Micelle Formation with and without Oppositely Charged Polyelectrolytes. *Langmuir* **1999,** *15,* 58-65.

[40] Meier-Koll, A. A.; Fleck, C. C.; Grünberg, v. The counterion-release interaction. *J. Phys.: Condens. Matter* **2004,** *16,* 6041-6052.

[41] Wang, C.; Tam, K. C. New Insights on the Interaction Mechanism within Oppositely Charged Polymer/Surfactant Systems. *Langmuir* **2002,** *18,* 6484-6490.

[42] Wang, C.; Tam, K. C.; Jenkins, R. D.; Tan, C. B. Interactions between Methacrylic Acid/Ethyl Acrylate Copolymers and Dodecyltrimethylammonium Bromide. *J. Phys. Chem. B* **2003,** *107,* 4667-4675.

[43] Ozeki, S.; Ikeda, S. The Sphere-Rod Transition of Micelles and the Two-Step Micellization of Dodecyltrimethylammonium Bromide in Aqueous NaBr Solutions. *J. Colloid Interface Sci.* **1982,** *87,* 424-435.

[44] Imae, T.; Kamiya, R.; Ikeda, S. Formation of Spherical and Rod-like Micelles of Cetyltrimethylammonium Bromide in Aqueous NaBr Solutions. *J. Colloid Interface Sci.* **1985,** *108,* 215-225.

[45] Thalberg, K.; Lindman, B. Segregation in aqueous systems of a polyelectrolyte and an ionic surfactant. *Colloids Surf. A* **1993,** *76,* 283-288.

[46] Mironov, A. V.; Starodoubtsev, S. G.; Khokhlov, A. R.; Dembo, A. T.; Yakunin, A. N. Ordered Nonstoichiometric Polymer Gel-Surfactant Complexes in Aqueous Medium with High Ionic Strength. *Macromolecules* **1998,** *31,* 7698-7705.

[47] Thalberg, K.; Lindman, B.; Karlström, G. Phase Behavior of a System of Cationic Surfactant and Anionic Polyelectrolyte: The Effect of Salt. *J. Phys. Chem.* **1991,** *95,* 6004-6011.

[48] Skepö, M.; Linse, P. Dissolution of a polyelectrolyte-macroion complex by addition of salt. *Phys. Rev. E* **2002,** *66,* 051807.

# CHAPTER 3

# PHASE DIAGRAMS OF STOICHIOMETRIC BIOPOLYMER–SURFACTANT COMPLEXES

## 3.1 Introduction

Thus far, we have considered the phase behavior of model systems consisting of synthetic polyelectrolyte–surfactant complexes, and have identified important trends in the morphological behavior of these materials. It would be very useful if these trends could be generalized to other polyelectrolyte–surfactant systems, especially those which exhibit potential as biocompatible drug delivery and nanoscale filtration matrices. In this way, we may develop the means to predict and control the self-assembled structures of these materials based on a knowledge of their phase diagrams. Naturally-occurring, charged polysaccharides are especially attractive matrix materials, because they are generally biocompatible, and because they provide a chemical basis for post-assembly crosslinking (e.g. via hydroxyl groups or other functional moieties). Alginate and chitosan are excellent examples of such materials.

Alginate is a cationic block copolymer of (1-4)-linked α-L-guluronic acid and β-D-mannuronic acid (shown in Figure 3.1) and is found in a wide variety of brown seaweeds where it serves as a structural polysaccharide. The major commercial source of this material is the giant kelp, *Macrocystis pyrifera*. The mannuronic and guluronic acid blocks vary in size; alternating segments as well as random blocks may be present. It is this block structure that ultimately dictates the gelling properties of the material,

with high guluronic acid content resulting in soft gels whereas high mannuronic acid content yields more rigid gels. Because of their biocompatibility, low cost, wide availability, and gelling properties—especially in the presence of divalent cations[1-5]—alginates have been frequently used in medical, agricultural, and drug delivery applications. For example, calcium alginate microcapsules have been used to encapsulate cells[6,7], for hybrid artificial organs[8], as hemoglobin carriers, and for macromolecular delivery[9]. However, despite the widespread use of these materials, very little work has been done to characterize the phase behavior of alginate–surfactant systems.

Chitosan is a linear polysaccharide consisting of (1-4)-linked β-D-glucosamine units, as shown in figure 3.1. It is obtained from the alkaline *N*-deacetylation of chitin, which is manufactured from shrimp and crab shells and is the next most abundant natural polysaccharide after cellulose[10]. Chitosan is characterized by an average degree of deacetylation, which is typically a minimum of 70%, and is cationic below an approximate pH of 5. Like alginate, chitosan is inexpensive, biocompatible, biodegradable, and can be chemically functionalized via its constituent hydroxyl groups. Because of these desirable properties, chitosan has found use in many medical applications, especially in the area of drug encapsulation[11-17]. In addition, chitosan is known to exhibit fungistatic and antibacterial activity[18-24]. Interactions between chitosan and sodium dodecyl sulfate (SDS) have been studied by other groups, although the majority of these studies have been limited to the measurement of chitosan–SDS binding isotherms in nonstoichiometric regimes[25-27].

The objective of this study was to characterize the phase behavior of stoichiometric alginate–CTAX and chitosan–SDS complexes as functions of osmotic pressure, ionic strength, and salt type.

## 3.2 Experimental

### 3.2.1 Materials

Low-viscosity sodium alginate (Sigma), chitosan (Aldrich, > 80% *N*-deacetylated), sodium chloride (Mallinckrodt), cetyltrimethylammonium chloride (CTACl, Aldrich, 1.04 M aqueous solution), sodium dodecyl sulfate (SDS, Aldrich), poly(ethylene glycol) (PEG, Fluka, $M_n$ = 8,000 g mol$^{-1}$), ethylenediaminetetraacetic acid (EDTA, Sigma molecular biology grade), sodium chloride (Mallinckrodt), sodium bromide (Aldrich), sodium acetate (Aldrich), and acetic acid (Fisher, glacial) were used as received. Tris(hydroxymethylaminomethane) (TRIS base, Sigma molecular biology grade) was adjusted to pH 7.0 (HCl) before use. Concentrated solutions (2 wt %) of sodium alginate were prepared in 10 mM and 100 mM NaCl and NaBr and were buffered in a mixture of 10 mM TRIS base/1 mM EDTA (10-1 TE). Chitosan solutions (5 wt %) were prepared in 10 mM and 100 mM NaCl and NaBr and were buffered in a 0.5 M acetate–acetic acid solution at pH 6. This solution was gradually reduced to pH 5 by the addition of small amounts of 1 M acetic acid; at this pH, the chitosan was completely soluble. All aqueous solutions were prepared using water purified via

reverse osmosis. The relevant polyelectrolyte and surfactant structures are shown in Figure 3.1. The structure of CTAX was presented previously in Figure 2.1.

### 3.2.2 Methods

Alginate–CTACl complexes were prepared by combining 1.04 M CTACl solution with a stoichiometric amount (based on charge) of 2 wt % sodium alginate solution, followed by vigorous mixing. Chitosan–SDS complexes were prepared by combining 0.34 M SDS solution with a stoichiometric amount (based on charge) of 5 wt % chitosan solution, followed by vigorous mixing. Immediately upon the addition of approximately 10 mL of water to these mixtures, a white precipitate formed. The precipitate obtained from the chitosan–SDS mixture was quite fibrous and was essentially a single congealed mass whereas the alginate–CTACl system yielded qualitatively much finer particles. The precipitates were isolated by centrifugation, washed with three 50 mL aliquots of water to remove excess ions, and were allowed to air dry for approximately 8 hours. Pieces of the dried complexes were then placed in large reservoirs of aqueous sodium bromide and sodium chloride solutions (10 mM, 100 mM, and 1 M) with PEG concentrations in each solution ranging from 0 wt % to 50 wt % corresponding to an approximate osmotic pressure range of 0 to 112 atm. Each of these solutions were buffered in 10-1 TE at a pH of 7. The samples were then allowed to equilibrate with the stressing solutions for one month at room temperature. During this time, samples were periodically vortexed to ensure PEG solution homogeneity.

Cetyltrimethylammonium bromide (CTABr) was generated *in situ* by exchange of the CTACl chloride ion with the free bromide ions in the NaBr/PEG solutions.

### 3.2.3 Measurements

Small angle X-ray scattering (SAXS) measurements were performed with a Rigaku RU-H3R rotating anode X-ray diffractometer operating at 1.2 kW. The diffractometer was equipped with a multilayer focusing optic (point focus = 100 $\mu m^2$; Osmic Inc., type CMF23-46Cu8) and a custom-built evacuated Statton-type scattering camera. The sample cell used for the solution osmotic stress measurements consisted of a Teflon card sandwiched between thin Mylar windows which allowed the solid samples to remain in equilibrium with the stressing solutions during the measurements while isolating the samples from vacuum. The sample-to-detector distance was 460 mm, which corresponds to a $q$ range of $0.0698\ Å^{-1} \leq q \leq 0.625\ Å^{-1}$ with $q = (4\pi/\lambda)\sin(\theta/2)$, where $\theta$ is twice the Bragg angle, and the incident beam wavelength was 1.54 Å, corresponding to 8 keV Cu K$\alpha$ radiation. Scattering patterns were acquired with 10 cm × 15 cm Fuji ST-VA image plates in conjunction with a Fuji BAS-2500 image plate scanner. The scattering intensity profiles were obtained from radial averages of the scattering pattern intensities, using procedures developed by our research group for the Igor Pro software package (Wavemetrics, Inc.; Lake Oswego, OR). Crystallographic interpretation of SAXS data was performed according to the procedures set forth in section 2.2.4.

## 3.3 Results and Discussion

### 3.3.1 Alginate–CTAX Complexes

The alginate–CTAX complexes considered for this study exhibited moderate to high degrees of nanoscopic order, depending on the experimental conditions. At low osmotic pressures, a moderately well-ordered *Pm*3*n* cubic phase was observed, as shown in Figures 3.4 and 3.5. However, this structure was not as well-ordered as the *Pm*3*n* phase observed in the PAAm–CTAX model system. This lower degree of order may be due to the increased heterogeneity and blockiness of the alginate chains relative to the PAAm chains. As water content of the complexes was decreased, *Pm*3*n*-to-hcpc phase transitions were observed; these transitions proceeded through 2-phase coexistence regions, as was observed with the model system. As before, this suggests that hcpc and *Pm*3*n* phases are energetically similar. The hcpc and *Pm*3*n* unit cell dimensions of the alginate–CTAX complexes were also generally larger than those of the corresponding 100% or 70% charge PAAm–CTAX complexes under all conditions, as shown in Tables 3.1 and 3.2. This may be advantageous for crosslinking purposes, as a larger unit cell size implies a higher density of polymer chains between surfactant moieties—and therefore a better medium for crosslinking—than smaller unit cell sizes.

#### 3.3.1.1 Osmotic Stress Effects

Osmotic pressure versus distance curves for alginate–CTAX complexes equilibrated in NaBr and NaCl are shown in Figures 3.2 and 3.3, respectively. As was

the case with the model system, each of the curves indicated a smoothly exponential relationship between osmotic pressure and distance, where increased osmotic pressure consistently brought about a reduction in unit cell size. The measured exponential decay lengths for these systems are shown in Table 3.3. Comparing these data with model system decay length data from Tables 2.6–2.8, we see that the alginate–CTAX complexes—regardless of unit cell structure—are generally more compressible than the corresponding 100% charge and 70% charge PAAm–CTAX complexes. However, the decay lengths obtained for the alginate–CTAX complexes were still quite small and are well out of the length scale range of electrostatic screening lengths or hydration forces.

### 3.3.1.2 Effects of Ionic Strength and Salt Type

For both salt types investigated, increasing the ionic strength while holding other factors fixed tended to increase unit cell sizes for the alginate–CTAX complexes, as shown in Tables 3.1 and 3.2. This is similar to what was observed in the model system, and underscores the fact that counterion release plays a significant role in polyelectrolyte–surfactant binding.

As expected, the morphology of the alginate–CTAX complex was also influenced by counterion type. In 100 mM NaBr, only the hcpc phase was observed at all osmotic pressures for the alginate–CTAX system; this is consistent with the behavior of the PAAm–CTAX model system under the same conditions. In addition, the dimensions of the *Pm*3*n* and hcpc structures in chloride were smaller than the corresponding structures exposed to bromide ion. Complex compressibility was also

consistently reduced in chloride ion relative to bromide, as shown in Table 3.3. These results reinforce the earlier hypothesis that the strong affinity of the bromide ion for the cetyltrimethylammonium cation might bring about displacement of the polyelectrolyte chain and result a reduction in the degree of polyelectrolyte–surfactant binding. This decrease in binding brings about in an increase in unit cell size.

### 3.3.2 Chitosan–SDS Complexes

In contrast to the alginate–CTAX complexes described above, chitosan–SDS complexes formed a poorly-ordered, indiscriminate phase that was insensitive to osmotic pressure, ionic strength, and salt type. Representative SAXS traces for these complexes at low and high osmotic pressures are shown in Figure 3.6, along with a typical 2-D SAXS image. From Figure 3.6, we note that the first-order scattering peaks in both systems ($d_B \approx 35$ Å) are very broad, indicative of poor long-range order. Second-order peaks are discernable in both systems ($d_B \approx 18$ Å), but these peaks are quite weak and are very broad. Although the 1:2 ratio between these peak positions fit the characteristic pattern of a lamellar structure, these data are still relatively ambiguous; many possible structures include the 1:2 ratio as part of their characteristic patterns. Additionally, the broad, diffuse scattering peaks we have observed are not unlike those obtained from ordered liquids. Thus, it is not possible to assign a specific structure based solely on these data. It is interesting to note that the position of the first-order peak shown in Figure 3.6 does not appear to change with osmotic pressure. The relative insensitivity of chitosan–SDS complexes to ionic strength, temperature, and

other environmental variables has been previously reported[27]. It is currently unclear which factors are responsible for the relative lack of long-range order in stoichiometric chitosan–SDS complexes, but one possibility is that the chitosan chains are fairly stiff and have a strong tendency to self-associate independently of the surfactant mesophase.

## 3.4 Conclusions

Phase diagrams of well-ordered stoichiometric alginate–CTAX complexes were mapped as functions of osmotic pressure, ionic strength, and salt type. A phase sequence of *Pm*3*n* cubic ↔ hcpc was observed with decreasing complex water content, and the trends that were identified in the model system studied in Chapter 2 appear to be generally applicable to the alginate–CTAX complexes studied in this chapter. In contrast, stoichiometric chitosan–SDS complexes formed poorly-ordered structures that were insensitive to osmotic pressure, ionic strength, and salt type.

## Tables

**Table 3.1: Unit Cell Sizes of Alginate–CTABr Complexes**

| | *a*, hcpc [Å] | | *a*, *Pm*3*n* [Å] | |
|---|---|---|---|---|
| Π [atm] | 10 mM | 100 mM | 10 mM | 100 mM |
| 0 | — | 56.35 | 113.44 | — |
| 1 | — | 56.35 | 113.41 | — |
| 2 | — | 55.54 | 113.19 | — |
| 4 | — | 54.61 | 112.70 | — |
| 8 | — | 54.16 | 112.55 | — |
| 13 | — | 53.60 | 112.19 | — |
| 21 | 47.34 | 53.36 | 111.70 | — |
| 33 | 47.05 | 53.10 | — | — |
| 50 | 46.82 | 52.72 | — | — |
| 75 | 46.77 | 52.37 | — | — |
| 112 | 46.53 | 52.22 | — | — |

—, no structure observed

**Table 3.2: Unit Cell Sizes of Alginate–CTACl Complexes**

| | *a*, hcpc [Å] | | *a*, *Pm3n* [Å] | |
|---|---|---|---|---|
| Π [atm] | 10 mM | 100 mM | 10 mM | 100 mM |
| 0 | — | — | — | — |
| 1 | — | — | — | — |
| 2 | — | — | — | — |
| 4 | — | 52.08 | — | 120.97 |
| 8 | — | 51.40 | 112.06 | 118.96 |
| 13 | — | 50.96 | 111.45 | 118.22 |
| 21 | — | 50.25 | 110.96 | 116.89 |
| 33 | 46.36 | 49.83 | 110.89 | — |
| 50 | 46.30 | 49.46 | 110.35 | — |
| 75 | 46.07 | 49.09 | — | — |
| 112 | 45.96 | 48.91 | — | — |

—, no structure observed

**Table 3.3: Exponential Decay Length Data for Alginate–CTAX Complexes**

| Ionic strength [mM] | Structure | Π-Range[a] [atm] | λ [Å] | $R^2$ |
|---|---|---|---|---|
| NaBr | | | | |
| 10 | hcpc | 21–112 | 0.42 | 0.98 |
| 100 | hcpc | 0–112 | 0.69 | 0.99 |
| 10 | *Pm3n* | 0–13 | 0.33 | 0.97 |
| 100 | *Pm3n* | — | — | — |
| NaCl | | | | |
| 10 | hcpc | 33–112 | 0.33 | 0.97 |
| 100 | hcpc | 4–112 | 0.87 | 0.99 |
| 10 | *Pm3n* | 8–50 | 0.40 | 0.98 |
| 100 | *Pm3n* | 4–21 | 1.07 | 0.99 |

[a]Denotes the linear portion of the phase diagram
—, no structure observed

## Figures

**Sodium alginate**

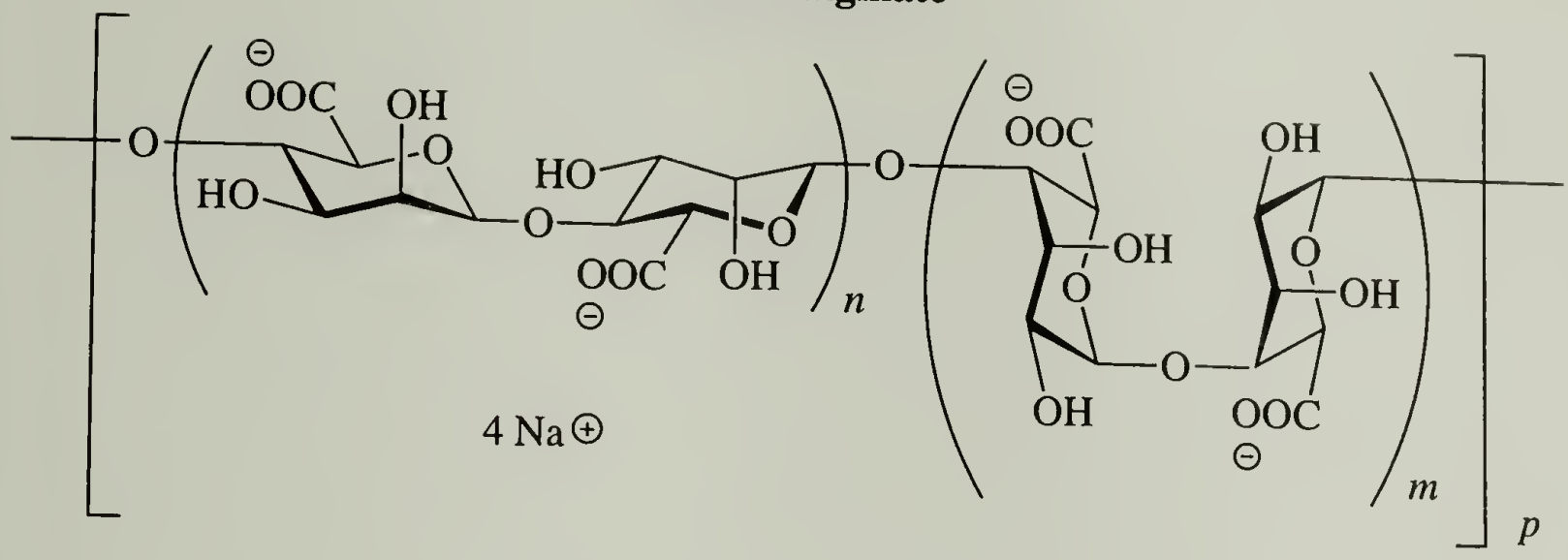


**Chitosan**

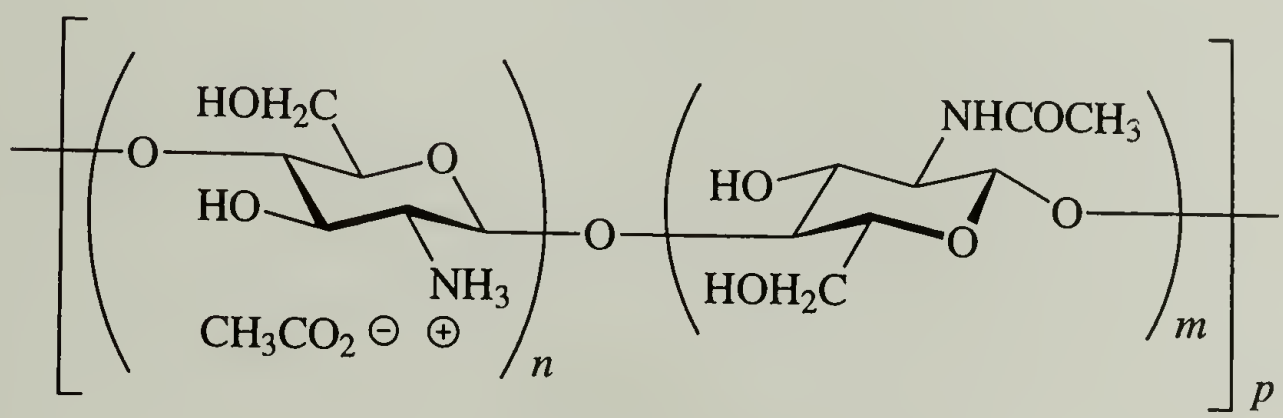


where $n > 70\%$

**Sodium dodecyl sulfate (SDS)**

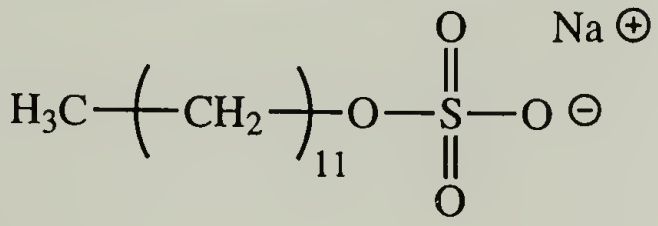


**Figure 3.1:** Structures of the polyelectrolytes and surfactants used for the polysaccharide–surfactant study. The structure of the cationic surfactant, CTAX, was shown in Figure 2.1.

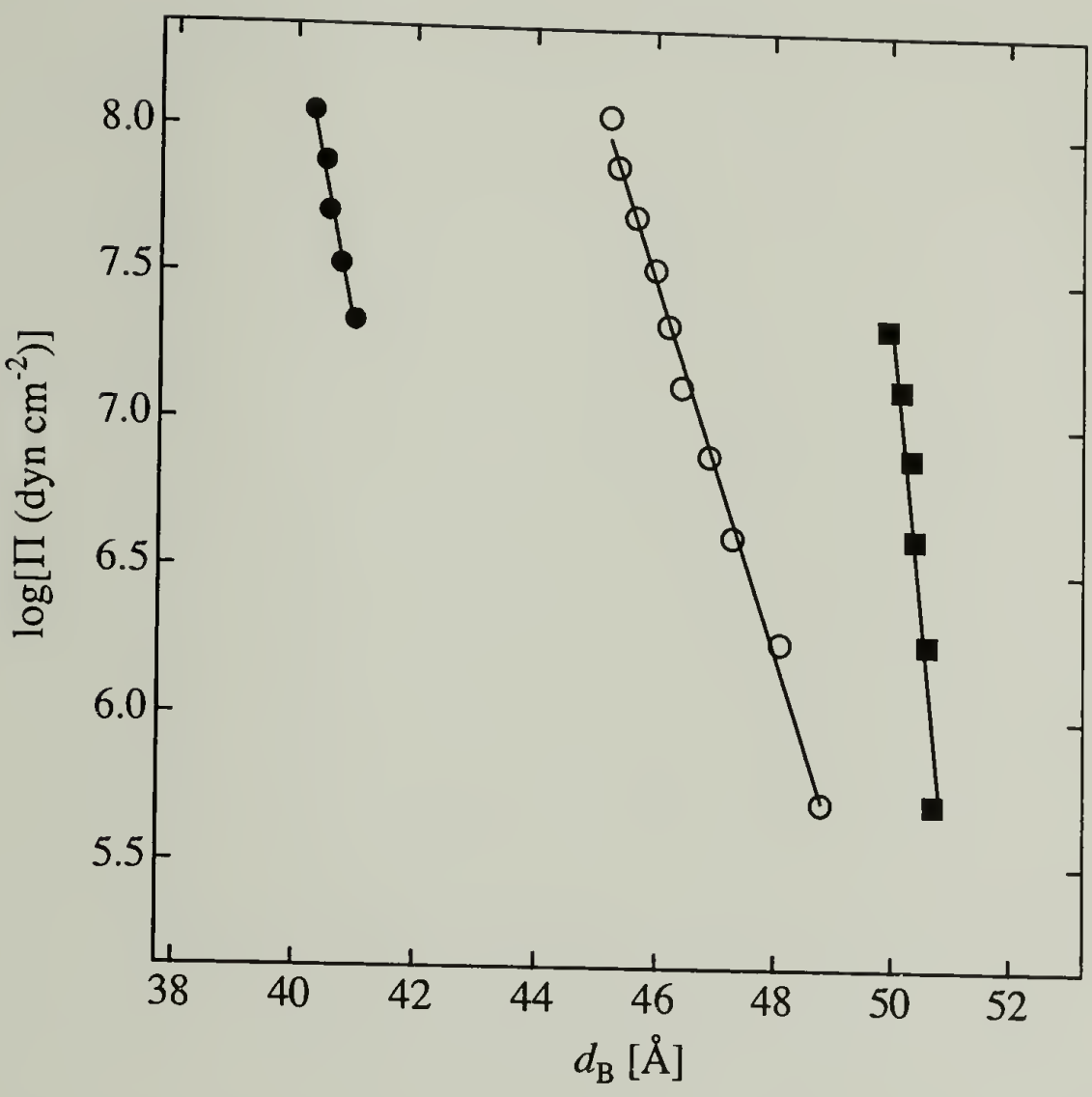


**Figure 3.2:** Phase diagram for alginate–CTABr complexes in 100 mM NaBr (filled symbols) and 100 mM NaBr (open symbols). The hcpc (●,○) and *Pm*3*n* cubic phases (■) were observed. Bragg spacings were calculated using the (100) hcpc and the (210) *Pm*3*n* cubic diffraction signals when those phases were present. Exponential decay lengths were determined by fitting the linear portion of each curve; these values are presented in Table 3.3.

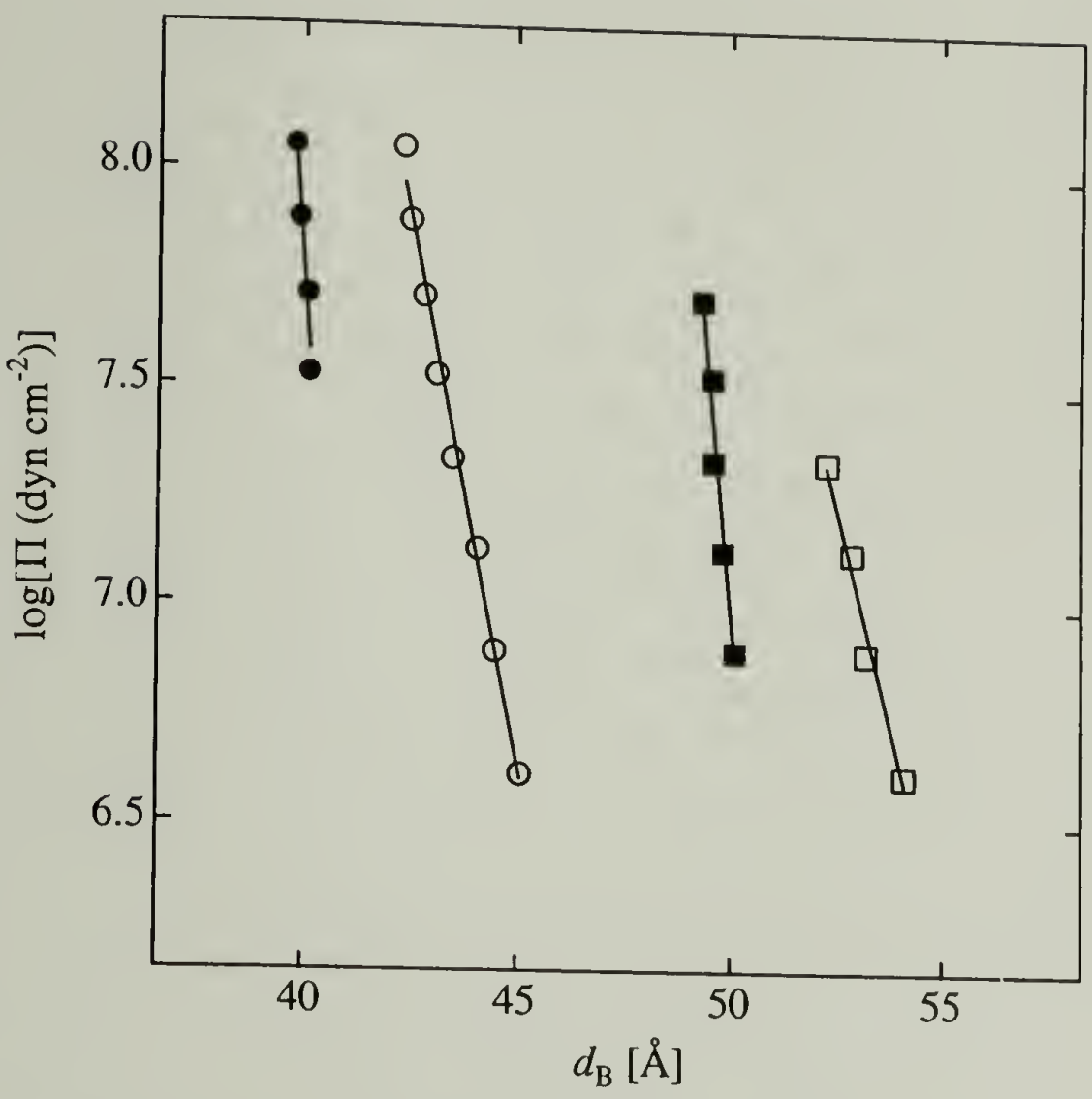


**Figure 3.3:** Phase diagram for alginate–CTABr complexes in 10 mM NaBr (filled symbols) and 100 mM NaBr (open symbols). The hcpc (●,○) and *Pm3n* cubic phases (■,□) were observed. Bragg spacings were calculated using the (100) hcpc and the (210) *Pm3n* cubic diffraction signals when those phases were present. Exponential decay lengths were determined by fitting the linear portion of each curve; these values are presented in Table 3.3.

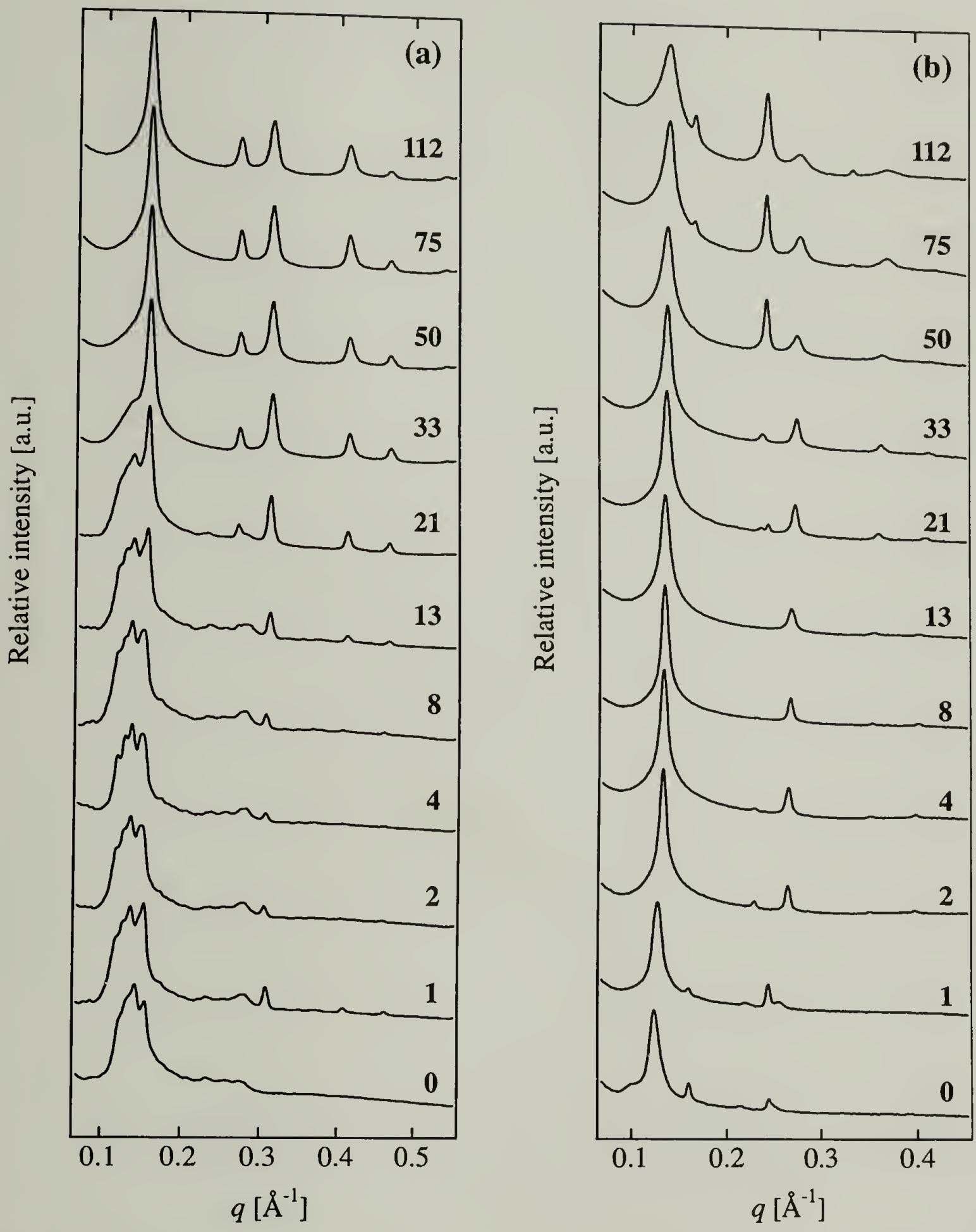


**Figure 3.4:** Angular-averaged scattering profiles for alginate–CTABr complexes in (a) 10 mM NaBr and (b) 100 mM NaBr under osmotic stress. Approximate osmotic pressure values in units of atm are associated with each curve.

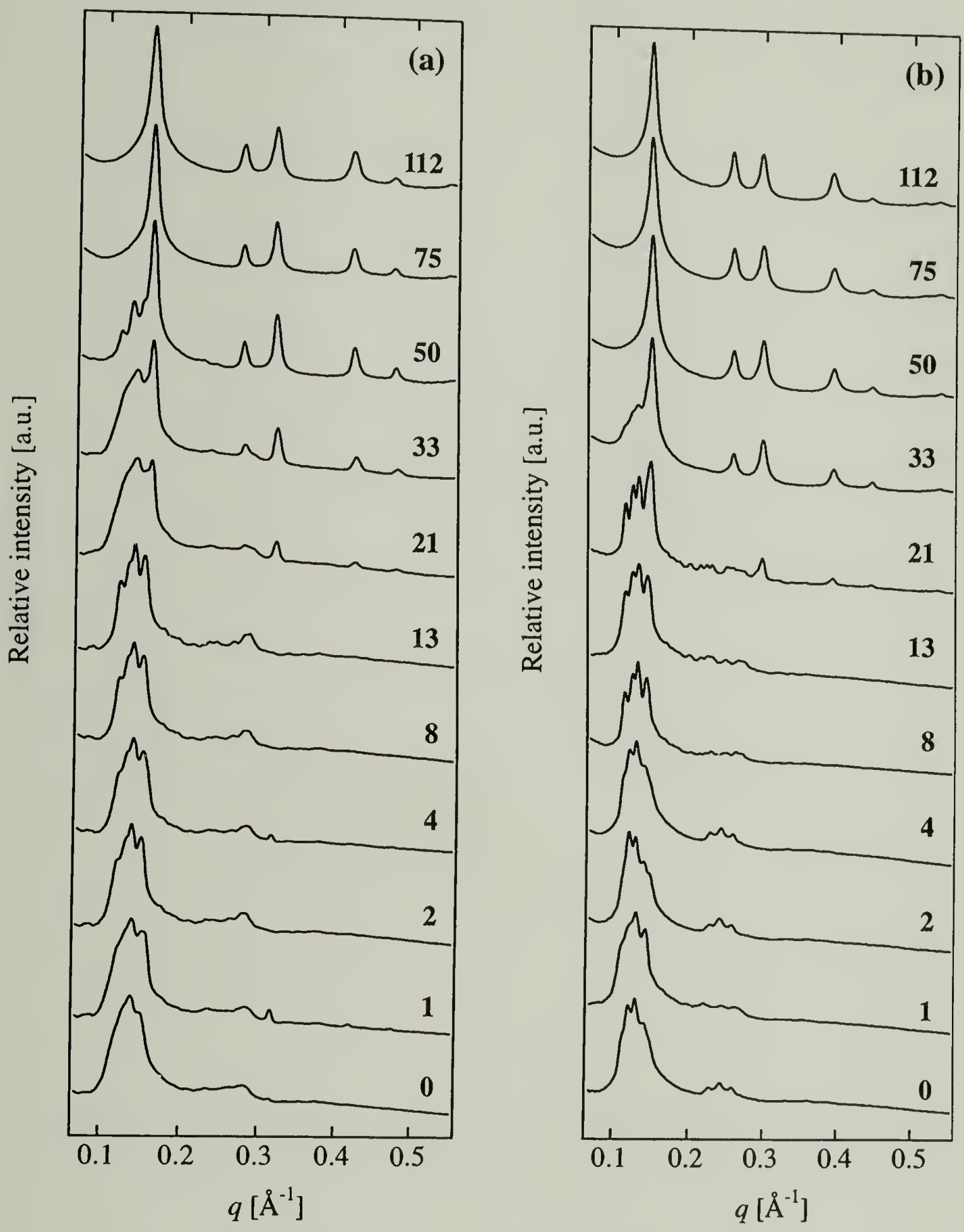


**Figure 3.5:** Angular-averaged scattering profiles for alginate–CTACl complexes in (a) 10 mM NaCl and (b) 100 mM NaCl under osmotic stress. Approximate osmotic pressure values in units of atm are associated with each curve.

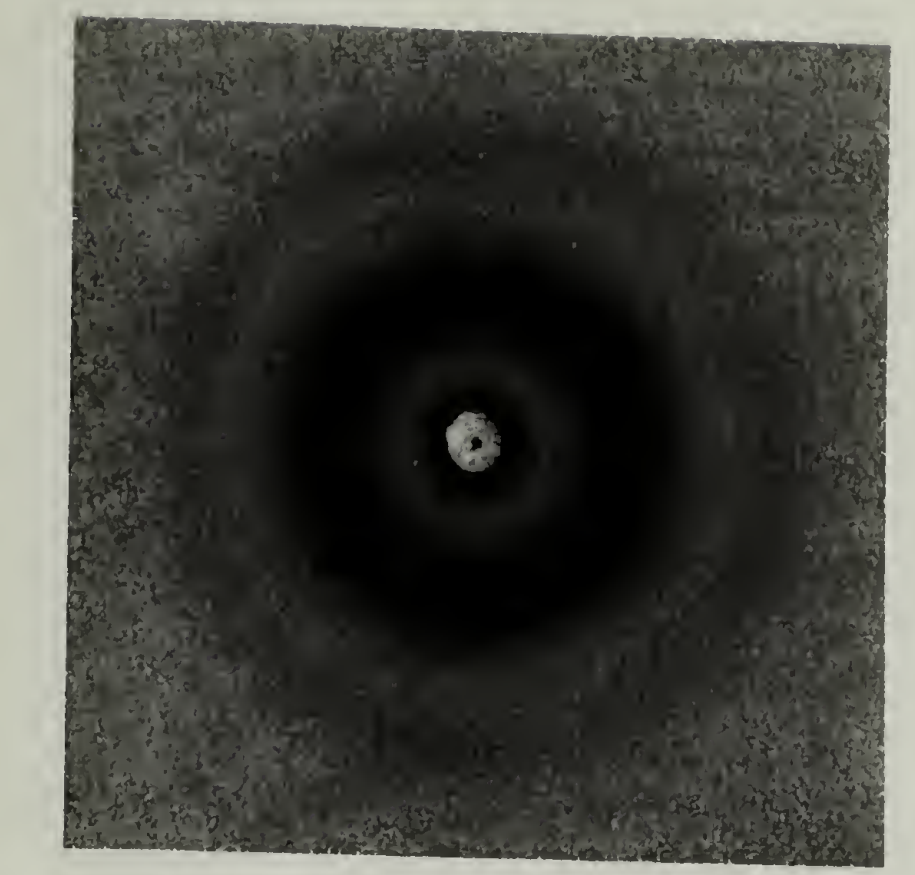

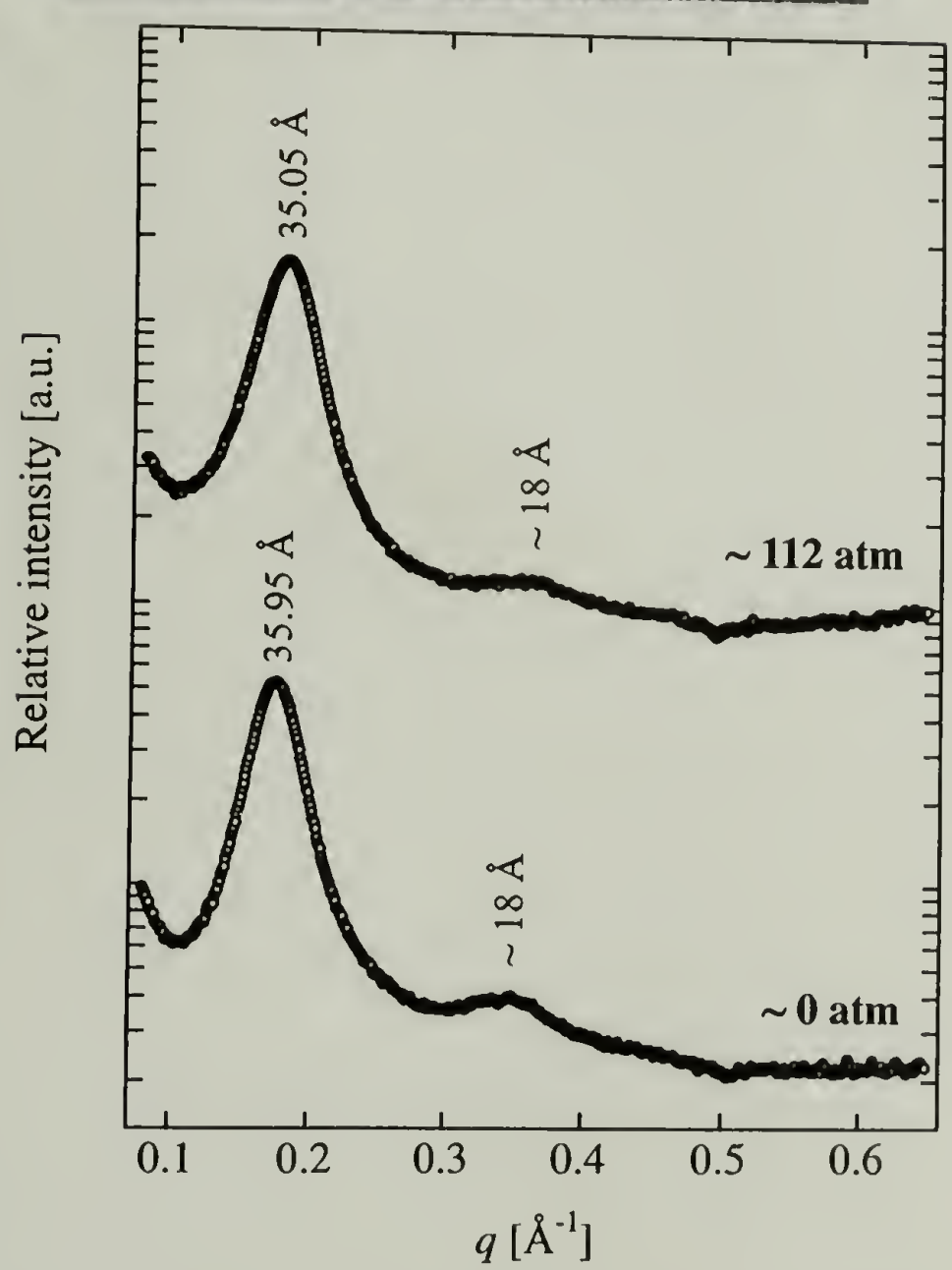


**Figure 3.6:** 2-D SAXS Image and angular-averaged scattering profiles for chitosan–SDS complexes in 100 mM NaCl at 2 osmotic pressures. These results are representative of those obtained in NaBr and at other ionic strengths.

## References


[1] Kamal, M.; Pfister, G.; Bahadir, M.; Lay, J. P. Uptake of C14-Simetryn by Duckweed (Lemna-Minor) During Release from a Polymer Matrix and the Consequent Herbicidal Effects. *J. Controlled Rel.* **1988,** *7,* 39-44.

[2] Posillico, E. G. Microencapsulation Technology for Large-Scale Antibody-Production. *Biotechnology* **1986,** *4,* 114-117.

[3] King, G. A.; Daugulis, A. J.; Faulkner, P.; Goosen, M. F. A. Alginate–Polylysine Microcapsules of Controlled Membrane Molecular-Weight Cutoff for Mammalian Cell Culture Engineering. *Biotechnol. Prog.* **1987,** *3,* 231-240.

[4] Kwok, K. K.; Groves, M. J.; Burgess, D. J. Production of 5-15 μm Diameter Alginate–Polylysine Microcapsules by an Air-Atomization Technique. *Pharm. Res.* **1991,** *8,* 341-344.

[5] Chandra, R.; Rustgi, R. Biodegradable Polymers. *Prog. Polym. Sci.* **1998,** *23,* 1273-1335.

[6] Hisano, N.; Morikawa, N.; Iwata, H.; Ikada, Y. Entrapment of islets into reversible disulfide hydrogels. *J Biomed Mater Res* **1998,** *40,* 113-123.

[7] Goosen, M. F. A.; O'Shea, G. M.; Gharapetian, H. M.; Chou, S.; Sun, A. M. Optimization of Microencapsulation Parameters–Semipermeable Microcapsules as a Bioartificial Pancreas. *Biotechnlol Bioeng* **1985,** *27,* 146-150.

[8] Hsu, B. R. S.; Ho, Y. S.; Fu, S. H. Membrane compactness affects the integrity and immunoprotection of alginate-poly-L-lysine-alginate microcapsules. *Transplant Proc* **1995,** *27,* 3227-3231.

[9] Hari, P. R.; Chandy, T.; Sharma, C. P. Chitosan/calcium-alginate beads for oral delivery of insulin. *J. Appl. Polym. Sci.* **1996,** *59,* 1795-1801.

[10] Kumar, M. N. V. R. A review of chitin and chitosan applications. *React. Funct. Polym.* **2000,** *46,* 1-27.

[11] Gupta, K. C.; Ravi Kumar, M. N. V. Structural Changes and Release Characteristics of Crosslinked Chitosan Beads in Response to Solution pH. *J.M.S.—Pure Appl. Chem.* **1999,** *A36,* 827-841.

[12] Jameela, S. R.; Jayakrishnana, A. Glutaraldehyde cross-linked chitosan microspheres as a long acting biodegradable drug delivery vehicle: studies on the *in vitro* release of mitoxantrone and *in vivo* degradation of microspheres in rat muscle. *Biomaterials* **1995,** *16,* 769-775.

[13] Genta, I.; Costantini, M.; Asti, A.; Conti, B.; Montanari, L. Influence of glutaraldehyde on drug release and mucoadhesive properties of chitosan microspheres. *Carbohydr. Polym.* **1998,** *36,* 81-88.

[14] Uchegbu, I. F.; Schätzlein, A. G.; Tetley, L.; Gray, A. I.; Sludden, J.; Siddique, S.; Mosha, E. Polymeric Chitosan-based Vesicles for Drug Delivery. *J. Pharm. Pharmacol.* **1998,** *50,* 453-458.

[15] Sludden, J.; Uchegbu, I. F.; Schätzlein, A. G. The Encapsulation of Bleomycin Within Chitosan Based Polymeric Vesicles Does Not Alter its Biodistribution. *J. Pharm. Pharmacol.* **2000,** *52,* 377-382.

[16] Oungbho, K.; Müller, B. W. Chitosan Sponges as Sustained Release Drug Carriers. *Int. J. Pharm.* **1997,** *156,* 229-237.

[17] Carreño-Gomez, B.; Duncan, R. Evaluation of the Biological Properties of Soluble Chitosan and Chitosan Microspheres. *Int. J. Pharm.* **1997,** *148,* 231-240.

[18] Tarsi, R.; Muzzarelli, R. A. A.; Guzman, C. A.; Pruzzo, C. Inhibition of *Streptococcus mutans* adsorption to hydroxyapatite by low-molecular-weight chitosans. *J. Dent. Res.* **1997,** *76,* 665-672.

[19] Tarsi, R.; Corbin, B.; Pruzzo, C.; Muzzarelli, R. A. A. Effect of low-molecular-weight chitosans on the adhesive properties of oral streptococci. *Oral Microbiol. Immunol.* **1998,** *13,* 217-224.

[20] Muzzarelli, R. A. A.; Muzzarelli, C.; Tarsi, R.; Miliani, M.; Gabbanelli, F.; Cartolari, M. Fungistatic activity of modified chitosans against *Saprolegnia parasitica*. *Biomacromolecules* **2001,** *2,* 165-169.

[21] Xie, W. M.; Xu, P. X.; Wang, W.; Liu, Q. Preparation of water-soluble chitosan derivatives and their antibacterial activity. *J. Appl. Polym. Sci.* **2002,** *85,* 1357-1361.

[22] Felse, P. A.; Panda, T. Production of microbial chitinases--A revisit. *Bioprocess Eng.* **2000,** *23,* 127-134.

[23] Coma, V.; Martial-Gros, A.; Garreau, S.; Copinet, A.; Salin, F.; Deschamps, A. Edible antimicrobial films based on chitosan matrix. *J. Food Sci.* **2002,** *67,* 1162-1169.

[24] Xie, W. M.; Xu, P. X.; Wang, W.; Liu, Q. Preparation and antibacterial activity of a water-soluble chitosan derivative. *Carbohydr. Polym.* **2002,** *50,* 35-40.

[25] Wei, Y. C.; Hudson, S. M. Binding of Sodium Dodecyl Sulfate to a Polyelectrolyte Based on Chitosan. *Macromolecules* **1993,** *26,* 4151-4154.

[26] Bae, H.-S.; Hudson, S. M. The Cooperative Binding Behavior of Sodium Dodecyl Sulfate to Crosslinked Chitosan Films. *J. Polym. Sci. A: Polym. Chem.* **1997,** *35,* 3755-3765.

[27] Thongngam, M.; McClements, D. J. Influence of pH, Ionic Strength, and Temperature on Self-Association and Interactions of Sodium Dodecyl Sulfate in the Absence and Presence of Chitosan. *Langmuir* **2005,** *21,* 79-86.

# CHAPTER 4

# ENERGETICS OF THE CUBIC-TO-HEXAGONAL TRANSITION IN POLYELECTROLYTE–SURFACTANT COMPLEXES

## 4.1 Introduction

The general phase sequence that we have observed for polyelectrolyte–surfactant complexes exemplifies the competition between spontaneous curvature and molecular packing constraints. The interplay between the elastic energy of the surfactant surfaces in the complex and the constraints of interfacial separation determines which structures will be preferentially formed under specific environmental conditions. In this chapter, we will investigate the energetics of the cubic-to-hexagonal phase transition for a PAAm–CTACl complex.

### 4.1.1 Energetics of Amphiphilic Monolayers

The structure of surfactant assemblies depends, in large measure, on the bending energy of the surfactant layers comprising the aggregates. This bending energy leads to the formation of structures with different radii of curvature, and therefore, different geometries. According to Helfrich[1], the total bending energy $F$ of the layers comprising a surfactant aggregate can be expressed in terms of deviations from the monolayer's spontaneous radius of curvature, $R_o$, as follows

$$F = \int dA \left[ \frac{1}{2} K \left( \frac{1}{R_1} + \frac{1}{R_2} - \frac{2}{R_o} \right)^2 + \bar{K} \left( \frac{1}{R_1 R_2} \right) \right] \tag{4.1}$$

where $R_1$ and $R_2$ are the principal radii of curvature, $K$ is the bending modulus, and $\overline{K}$ is the saddle-splay modulus, also known as the Gaussian curvature elastic constant. The bending modulus reflects the energy required to bend the monolayer away from its spontaneous radius of curvature, whereas the saddle-splay modulus reflects the topology of the structures formed and can be thought of as a coupling constant[2]. The bending energy depends on the many intermolecular forces between the amphiphiles in the monolayers, including hydrophobic interactions between alkyl chains[3-9], hydrogen bonding, electrostatic and steric repulsion of polar headgroups, van der Waals attractions, and solvation forces. Experimentally, it has been shown that the magnitude of $K$ at room temperature can range from a fraction of $k_BT$—where thermal energy can give rise to significant membrane fluctuations—to values tens or hundreds of times larger than $k_BT$ for very stiff systems, such as phospholipid bilayers. The experimentally-measured bending moduli for a variety of lipid–water systems are presented in Table 4.4 for illustrative purposes.

The phase transitions we have observed for polyelectrolyte–surfactant complexes are a consequence of the geometrically frustrated competition between the spontaneous curvature of the surfactant aggregates and the propensity of the hydrocarbon chains to remain shielded from water and the polar headgroups in contact with water (i.e. packing constraints). The structures we have observed therefore represent a compromise between the energetic cost to bend and the cost of uniformly

filling the hydrocarbon volume[10]. The lamellar-to-hexagonal ($L_\alpha$–$H_{II}$) phase transition in phospholipid bilayers is a very well-characterized[10-16] example of this concept.

### 4.1.2 Free Energy Measurement

In its most basic form, the osmotic stress method can be thought of as the controlled removal of water from a sample. We have shown that the phase sequence of polyelectrolyte–surfactant complexes is very sensitive to osmotic pressure. Since the neutral osmolyte does not interact with the complex during the equilibration process, it is simply the water content—and the associated curvature and packing constraints associated with it—that dictates the phase behavior of these systems. As such, it should be possible to access the same structures via controlled hydration of a completely dry sample. If the water volume change per surfactant molecule ($\Delta V_w$) and osmotic pressure associated with a phase transition are known, then the free energy of transition per surfactant molecule, $\Delta F/N$, can be determined from[17]

$$\frac{\Delta F}{N} = \int \Pi \, \Delta V_w \tag{4.4}$$

If this energy is attributed to curvature changes in the complex during the phase transition, then an estimate of the bending stiffness of the surfactant moieties can be made via eq 4.1.

Luzzati and Husson[18] were the first to demonstrate that controlled hydration of condensed lipid bilayers, in conjunction with X-ray scattering, provided a reasonable estimate of the average lipid area in these systems. Since then, many others have used

this method to explore the energetics of self-assembled soft matter systems[14,15,19-25]. In this work, we measured the free energy associated with the $Pm3n \leftrightarrow$ hcpc transition by combining the osmotic stress and controlled hydration methods. In particular, we focused on the 70% charge PAAm–CTACl system in 100 mM NaCl because it exhibited a rather narrow cubic–hexagonal coexistence region.

## 4.2 Experimental

### 4.2.1 Materials

Poly(acrylate-*co*-acrylamide) (PAAm, Polysciences, 70% carboxylate content, $M_n$ = 200,000 g mol$^{-1}$, sodium chloride (Mallinckrodt), cetyltrimethylammonium chloride (CTACl, Aldrich, 1.04 M aqueous solution), poly(ethylene glycol) (PEG, Fluka, $M_n$ = 8,000 g mol$^{-1}$), and ethylenediaminetetraacetic acid (EDTA, Sigma molecular biology grade) were used as received. Tris(hydroxymethylaminomethane) (TRIS base, Sigma molecular biology grade) was adjusted to pH 7.0 (HCl) before use. Concentrated solutions of PAAm (5 wt %) were prepared in 100 mM NaCl and were buffered in a mixture of 10 mM TRIS base/1 mM EDTA (10-1 TE). All aqueous solutions were prepared using water purified via reverse osmosis.

### 4.2.2 Methods

#### 4.2.2.1 Sample preparation

##### 4.2.2.1.1 Hydration experiments

PAAm–CTACl Complexes for use in the hydration experiments were prepared by combining 1.04 M CTACl solution with a stoichiometric amount (based on charge) of 5 wt % PAAm solution, followed by vigorous mixing. Immediately upon the addition of approximately 10 mL of water to these mixtures, a fine white precipitate formed. The precipitate was isolated by centrifugation, washed with three 50 mL aliquots of water to remove excess ions, and was allowed to air dry for approximately 8 hours. Pieces of the air-dried complexes were then vacuum-dried at room temperature for approximately 12 hours. Small amounts of the vacuum-dried complexes were quickly massed and placed in polyethylene Eppendorf tubes. Known amounts of 100 mM NaCl were added to each dehydrated sample such that a water-per-surfactant range of 8–28 was covered, as shown in Table 4.1. After adding the appropriate amounts of NaCl solution to the dehydrated complexes, the Eppendorf tubes were sealed and were subsequently allowed to equilibrate for 3 weeks. After this time, all of the added salt solution appeared to have fully penetrated the complexes such that each sample was qualitatively homogeneous.

Before adding the aforementioned aliquots of 100 mM NaCl to the dehydrated complexes, a rough estimate of water content at the transition point was made in the

following manner. The volume of a hexagonal unit cell with lattice parameter $a$ is $\sqrt{3}/2\ a^2L$, and the volume of surfactant comprising the cylinders is $\pi R^2 L$, where $R$ is the micellar radius. The volume of water $V_w$ associated with the unit cell is therefore

$$V_w = V_{total} - V_{surf} = L\left(\frac{\sqrt{3}}{2}a^2 - \pi R^2\right) \tag{4.5}$$

At the transition point between spheres and cylinders, the total area must be conserved such that

$$\frac{A_{sph}}{N_{sph}} = \frac{A_{cyl}}{N_{cyl}} \tag{4.6}$$

where $N$ is the surfactant aggregation number for either the sphere or cylinder. Since $A_{sph} = 4\pi R^2$ and $A_{cyl} = 2\pi RL$, we can write

$$L = 2R\frac{N_{sph}}{N_{cyl}} \tag{4.7}$$

Equation 4.5 can then be rewritten as

$$\frac{V_w}{N_{cyl}} = 2RN_{sph}\left(\frac{\sqrt{3}}{2}a^2 - \pi R^2\right) \tag{4.8}$$

For CTACl in 100 mM NaCl[26], $R \approx 26$ Å and $N_{sph} \approx 175$. From Table 2.3, $a \approx 50$ Å at the transition point. Substituting these values into eq 4.8, we find $V_w/N_{cyl} \approx 500$ Å$^3$. Since the molecular volume of water is 30 Å$^3$, $V_w = (n_w)$ (30 Å$^3$), the number of water molecules per surfactant molecule at the transition point was estimated to be

$$\frac{n_w}{n_{surf}} \approx \frac{500\ \text{Å}^3}{30\ \text{Å}^3} \approx 17 \tag{4.9}$$

#### 4.2.2.2.2 Osmotic stress experiments

Polyelectrolyte–surfactant complexes were prepared according to the procedure set forth in section 4.2.2.2.1. Pieces of the dried complexes were then placed in large reservoirs of aqueous 100 mM NaCl with PEG concentrations in each solution ranging from 30 wt % to 41 wt %, corresponding to an approximate osmotic pressure range of 20 to 55 atm. The choice of this pressure range was based on the data presented in Table 2.3 which showed that the $Pm3n \leftrightarrow$ hcpc transition for the 70% charge PAAm–CTACl system occurred between 21–50 atm at 100 mM ionic strength. Each of these solutions was buffered in 10-1 TE at a pH of 7. The samples were then allowed to equilibrate with the stressing solutions for one month at room temperature. During this time, samples were periodically vortexed to ensure PEG solution homogeneity during the dehydration process.

### 4.2.3 Measurements

Small angle X-ray scattering (SAXS) measurements were performed with a Rigaku RU-H3R rotating anode X-ray diffractometer operating at 1.2 kW. The diffractometer was equipped with a multilayer focusing optic (point focus = 100 $\mu m^2$; Osmic Inc., type CMF23-46Cu8) and a custom-built evacuated Statton-type scattering camera. The sample cells used for both the Luzzati and solution osmotic stress measurements consisted of a Teflon card sandwiched between thin Mylar windows which allowed the solid samples to remain in equilibrium with the stressing solutions during the measurements while isolating the samples from vacuum. The transfer of

each sample from its equilibrated environment to the sample holder was performed as quickly as possible, so as to minimize exposure to the external environment. Due to the small increments of water content and osmotic pressure required for this study, several replicate samples were analyzed for each experiment to establish reasonable statistics. The sample-to-detector distance was 460 mm, which corresponds to a $q$ range of 0.0698 $Å^{-1} \leq q \leq 0.625\ Å^{-1}$ with $q = (4\pi/\lambda)\sin(\theta/2)$, where $\theta$ is twice the Bragg angle, and the incident beam wavelength was 1.54 Å, corresponding to 8 keV Cu K$\alpha$ radiation. Scattering patterns were acquired with 10 cm × 15 cm Fuji ST-VA image plates in conjunction with a Fuji BAS-2500 image plate scanner. The scattering intensity profiles were obtained from radial averages of the scattering pattern intensities, using procedures developed by our research group for the Igor Pro software package (Wavemetrics, Inc.; Lake Oswego, OR). Crystallographic interpretation of SAXS data was performed according to the procedures set forth in section 2.2.4.

## 4.3 Results and Discussion

### 4.3.1 Osmotic Stress and Hydration Experiments

The controlled hydration of PAAm–CTACl complexes resulted in a transition from a distinct hcpc phase to a *Pm*3*n* phase via a 2-phase coexistence region, as shown in Figure 4.2. These results were highly correlated with the osmotic stress results, as shown by the selected SAXS profiles from the osmotic stress experiments in Figure 4.1. The hcpc and *Pm*3*n* unit cell sizes derived from the replicate SAXS measurements are

shown in Tables 4.2 and 4.3; note that the data obtained from both methods were quite precise, and that the coexistence region was successfully bracketed by both methods. In addition, the unit cell volumes of the $Pm3n$ ($V \sim a^3$) and hcpc ($V \sim a^2$) structures were found to increase linearly with increasing water content, as shown in Figure 4.3. This result confirms that the volume change accompanying the $Pm3n \leftrightarrow$ hcpc transition can indeed be attributed to the change in water content.

### 4.3.2 Energetics of the Transition

Phase diagrams derived from the osmotic pressure and hydration experiments are presented in Figures 4.4 and 4.5, respectively. Because we have characterized the $Pm3n \leftrightarrow$ hcpc phase transition as a function of both osmotic pressure and the change in water volume, we now have the basis for determining the free energy according to eq 4.4. The transition pressure was explicitly determined by using the relative intensities of the hcpc phase from the SAXS traces shown in Figure 4.1. These values were plotted in Figure 4.4a versus osmotic pressure and were fit to a sigmoid curve. The inflection point of this curve, which was calculated during the fitting procedure, was interpreted as the transition point. From Figure 4.4, we find that $\Pi = 3.89 \times 10^7$ dyn $cm^{-2}$ at the midpoint of the coexistence region, representing the transition pressure. Since 3 water molecules comprise the width of the coexistence region (Figure 4.5), the associated volume change was 3 $H_2O \times 30$ $Å^3 = 90$ $Å^3$; we assume that this volume change occurs at a constant transition pressure. Therefore, according to eq 4.4, the free energy of the $Pm3n \leftrightarrow$ hcpc transition was calculated as

$$\frac{\Delta F}{N} = (3.89 \times 10^{6}\ \mathrm{N/m^2})(9 \times 10^{-29}\ \mathrm{m^3}) = 3.50 \times 10^{-22}\ \mathrm{J} \qquad (4.10)$$

which is equivalent to 0.088 $k_BT$ per surfactant molecule. This value is significant because it represents the energetic cost of removing water from the cubic phase to form the hexagonal phase. The fact that the free energy change is small relative to $k_BT$ helps to explain why we have often observed coexisting *Pm*3*n* and hcpc phases in the PAAm–CTAX system; these two structures are very energetically similar and can be interconverted by thermal energy. For perspective, consider that the magnitude of this result is quite similar to the water binding energy determined for partially disordered, gel-phase dimyristoyl phosphatidylcholine bilayers[20].

As we alluded to earlier, the energetic cost of removing water from the PAAm–CTACl complex can be largely attributed to the bending of its constituent surfactant monolayers as the *Pm*3*n* phase is converted to the hcpc phase. It would therefore be useful to have an estimate of the bending stiffness of these amphiphilic aggregates at the transition point. The measured free energy change ($\Delta F = F_{\mathrm{hcpc}} - F_{Pm3n}$) can be attributed to a change in the monolayer curvature according to eq 4.1. We assume that the *Pm*3*n* phase includes mostly spherical aggregates such that

$$F_{Pm3n} = \int dA \left[ \frac{1}{2} K \left( \frac{1}{R_1} + \frac{1}{R_1} - \frac{2}{R_0} \right)^2 \right] \qquad (4.11)$$

For the hcpc phase, the free energy can be written in a similar fashion:

$$F_{\mathrm{hcpc}} = \int dA \left[ \frac{1}{2} K \left( \frac{1}{R_2} - \frac{2}{R_0} \right)^2 \right] \qquad (4.12)$$

We further assume that the radii of the surfactant aggregates are equal to the spontaneous radius of curvature throughout the phase transition such that $R_1 = R_2 = R_0$. Therefore, $F_{Pm3n} = 0$ and $\Delta F = F_{\text{hcpc}}$. On a per-surfactant basis, the free energy change can be written as follows:

$$\frac{\Delta F}{N} = \frac{A_{\text{cyl}}}{N_{\text{cyl}}}\left(\frac{1}{2}K\frac{1}{R_0^2}\right) = \frac{2\pi R_2 L}{N_{\text{cyl}}(L)}\left(\frac{1}{2}K\frac{1}{R_0^2}\right) \tag{4.13}$$

We can write $N_{\text{cyl}}(L)/L$ in terms of the density, $\rho = N/V$, which we assume remains constant throughout the phase transition:

$$\frac{N_{\text{cyl}}(L)}{L} = \frac{\rho V_{cyl}}{L} \tag{4.14}$$

Since $V_{\text{cyl}} = \pi R^2 L$, eq 4.13 can then be rewritten as

$$\frac{\Delta F}{N} = \frac{2}{\rho R_2}\left(\frac{1}{2}K\frac{1}{R_0^2}\right) \tag{4.15}$$

Again, we assume that the densities of the spherical and cylindrical phases are identical such that $\rho = 3N/4\pi R_0^3$. Substituting $\rho$ into eq 4.15 yields our working expression for the free energy in terms of the bending stiffness, $K$:

$$\frac{\Delta F}{N} = \frac{4\pi R_2^2}{N}\left(\frac{1}{3}K\frac{1}{R_0^2}\right) = \frac{1}{3}K\frac{A}{N}\frac{1}{R_0^2} \tag{4.16}$$

In this expression, $A/N$ is the area per surfactant molecule in a spherical aggregate. Roelants has shown that the aggregation number for CTACl micelles can vary widely as ionic strength is varied[26]: For example, $N$ was shown to increase from 136 to 176 as ionic strength was increased from 104 to 155 mM. Using those data as a starting point,

we assume that the aggregation number for surfactant moieties within a polyelectrolyte–surfactant complex will be larger than that of the analogous pure surfactant system due to additional screening from the polyelectrolyte . For this analysis, we estimated that the aggregation number for surfactant moieties in the PAAm–CTACl system was in the range of 150 to 200. Once the aggregation number is known, $R_0$ can then be estimated from[26]:

$$R_0 = \left[ \frac{3N(V_H + V_C)}{4\pi} \right]^{1/3} \tag{4.17}$$

where $V_H$ and $V_C$ are the surfactant headgroup and hydrophobic tail volumes, respectively. For CTACl, Roelants[26] found that $V_H = 170$ Å$^3$ and $V_C = 458$ Å$^3$. Thus, $R_0$ was calculated to be 28.2 Å and 31.1 Å for aggregation numbers of 150 and 200, respectively. Substituting these values into eq 4.16, along with $\Delta F/N$ (determined from eq 4.4) we estimate the bending modulus $K$ to span a range of 3.2 to 4.2 $k_BT$. From the spectrum of bending moduli presented in Table 4.4, we note that the magnitude of this value is very similar those obtained from nonionic surfactant systems with similar chain lengths in oil–water microemulsions. However, we cannot make a direct comparison of our result to the bending moduli of other polyelectrolyte–surfactant systems; these values are difficult to measure and, in this context, we are not aware of any previously-reported work.

As mentioned in Chapter 2, the thermodynamically well-defined conditions under which osmotic stress experiments are carried out strictly prohibit phase coexistence at equilibrium. It is interesting, then, to consider how the magnitude of

$\Delta F/N$ might relate to the unexpected presence of cubic–hexagonal coexistence regions in the PAAm–CTACl phase diagram. If the *Pm3n* and hcpc phases can be interconverted by thermal energy at room temperature, then the energy required to transform at least one CTACl micelle into a cylinder should be on the order of $k_BT$. However, the results presented here indicate that the transition energy is much larger than $k_BT$. Using our measured value of $\Delta F/N$ (0.088 $k_BT$) and a conservative estimate of the micellar aggregation number for CTACl (150), we estimate the total free energy to be roughly 13 $k_BT$. Clearly, this value is too large to explain the phase coexistence we have observed. As such, the complexes studied here have likely not reached their true equilibrium states, possibly due to large kinetic barriers that may be associated with the transition.

## 4.4 Conclusions

The cubic-to-hexagonal phase transition in polyelectrolyte–surfactant complexes exemplifies the geometrically frustrated competition between spontaneous curvature and molecular packing constraints. Using a combination of osmotic stress and controlled hydration experiments, the energetic cost of removing water from the *Pm3n* cubic phase to form the hcpc phase in the PAAm–CTACl system at 100 mM ionic strength was found to be 0.088 of $k_BT$ per surfactant at room temperature. Under these conditions, the bending stiffness of the surfactant monolayers within the complex was estimated to be in the range of 3 to 4 $k_BT$, which is consummate with values obtained for nonionic surfactant–oil–water microemulsions with similar surfactant chain lengths.

## Tables

**Table 4.1: Sample Preparation Data for Hydration Experiments**

| Sample mass [mg] | $V_w$[a] [μL] | $n_w$/surfactant[b] |
|---|---|---|
| 208.1 | 75.9 | 8 |
| 256.3 | 140.1 | 12 |
| 237.2 | 140.5 | 13 |
| 257.0 | 163.9 | 14 |
| 230.0 | 157.2 | 15 |
| 274.7 | 200.3 | 16 |
| 267.0 | 206.8 | 17 |
| 287.5 | 235.8 | 18 |
| 220.9 | 191.2 | 19 |
| 231.9 | 211.3 | 20 |
| 256.2 | 280.2 | 24 |
| 228.1 | 291.0 | 28 |

[a]Denotes volume of 100 mM NaCl solution
[b]Based on the mass fraetion of CTACl in the complex

**Table 4.2: Structural Data from Replicate Hydration Experiments**

| | | hcpc | | | *Pm3n* | | |
|---|---|---|---|---|---|---|---|
| $n_w$ /surfactant | $N$ | $d_B$ [Å] | $a$ [Å] | RSD [%] | $d_B$ [Å] | $a$ [Å] | RSD [%] |
| 8 | 9 | 41.87 | 48.35 | 0.13 | — | — | — |
| 12 | 9 | 42.11 | 48.62 | 0.12 | — | — | — |
| 13 | 5 | 42.15 | 48.67 | 0.15 | — | — | — |
| 14 | 5 | 42.24 | 48.77 | 0.10 | 48.00 | 107.33 | 0.25 |
| 15 | 8 | 42.40 | 48.96 | 0.12 | 48.15 | 107.67 | 0.16 |
| 16 | 9 | 42.62 | 49.21 | 0.07 | 48.03 | 107.40 | 0.17 |
| 17 | 9 | 42.62 | 49.21 | 0.15 | 48.12 | 107.60 | 0.25 |
| 18 | 9 | — | — | — | 48.15 | 107.67 | 0.18 |
| 19 | 9 | — | — | — | 48.23 | 107.85 | 0.11 |
| 20 | 9 | — | — | — | 48.26 | 107.91 | 0.20 |
| 24 | 9 | — | — | — | 48.38 | 108.18 | 0.15 |
| 28 | 9 | — | — | — | 48.41 | 108.25 | 0.16 |

—, no structure observed

**Table 4.3: Structural Data from Replicate Osmotic Stress Experiments**

| | | hcpc | | | *Pm3n* | | |
|---|---|---|---|---|---|---|---|
| log[Π (dyn cm$^{-2}$)] | *N* | $d_B$ [Å] | *a* [Å] | RSD [%] | $d_B$ [Å] | *a* [Å] | RSD [%] |
| 7.34 | 6 | — | — | — | 48.11 | 107.58 | 0.12 |
| 7.38 | 4 | — | — | — | 48.12 | 107.60 | 0.09 |
| 7.42 | 5 | 42.51 | 49.08 | 0.04 | 48.04 | 107.43 | 0.13 |
| 7.45 | 5 | 42.48 | 49.05 | 0.02 | 48.01 | 107.35 | 0.09 |
| 7.49 | 4 | 42.47 | 49.04 | 0.03 | 48.00 | 107.33 | 0.08 |
| 7.53 | 4 | 42.46 | 49.03 | 0.04 | 47.93 | 107.16 | 0.07 |
| 7.57 | 4 | 42.33 | 48.88 | 0.05 | 47.93 | 107.17 | 0.14 |
| 7.60 | 5 | 42.30 | 48.84 | 0.07 | 47.91 | 107.12 | 0.05 |
| 7.64 | 4 | 42.22 | 48.75 | 0.01 | 47.90 | 107.12 | 0.01 |
| 7.67 | 4 | 42.21 | 48.74 | 0.03 | 47.79 | 106.86 | 0.11 |
| 7.71 | 5 | 42.18 | 48.71 | 0.15 | 47.81 | 106.91 | 0.13 |
| 7.74 | 6 | 42.17 | 48.69 | 0.16 | — | — | — |

—, no structure observed

**Table 4.4: Bending Moduli of Various Lipid–Water Systems**

| Reference | Charge[a] | $n_C$[b] | System[c] (plus water) | $K$ [$k_BT$] |
|---|---|---|---|---|
| DiMeglio *et. al.*[27] | Anionic | 12 | SDS/Pentanol | 0.16 |
| Sottmann *et. al.*[28] | Nonionic | 6 | $C_6E_2$/Octane | 0.44 |
| Vollmer *et. al.*[29] | Nonionic | 4 | $C_4E_1$/Octane | 0.5 |
| Sottmann *et. al.*[28] | Nonionic | 8 | $C_8E_3$/Octane | 0.57 |
| Vollmer *et. al.*[29] | Nonionic | 8 | $C_8E_3$/Octane | 0.6 |
| Tsapis *et. al.*[30] | Nonionic | 12 | $C_{12}E_4$/Decane | 0.7 |
| Sottmann *et. al.*[28] | Nonionic | 10 | $C_{10}E_4$/Octane | 0.73 |
| Vollmer *et. al.*[29] | Nonionic | 12 | $C_{12}E_5$/Octane | 0.8 |
| Sottmann *et. al.*[28] | Nonionic | 12 | $C_{12}E_5$/Octane | 0.92 |
| Safinya *et. al.*[31] | Anionic | 12 | SDS/Pentanol/Dd | $\approx 1$ |
| This work | Cationic | 16 | CTACl/PAAm | $\approx 3$ |
| Castro-Roman *et. al.*[32] | Cationic | 16 | CPCl/Octanol/F68 | $\approx 3$ |
| Jung *et. al.*[2] | Cationic | 16 | $CTABr/FC_7$ | $\approx 5$ |
| Fuller *et. al.*[33] | Anionic | — | DOPS/DOPE/Td | $\approx 10$ |
| Malinin *et. al.*[34] | Anionic | — | DOPS/DOPE/Ch | $\approx 11$ |
| Rand *et. al.*[14] | Anionic | — | DOPE/DOPC/Td | $\approx 40$ |
| Servuss *et. al.*[35] | Anionic | — | PC | $\approx 50$ |

[a]Denotes lipid charge type
[b]Denotes alkyl chain carbon count (reported only for single-chain lipids)
[c]Lipid and solvent abbreviations can be found in Table 4.5

**Table 4.5: Lipid and Solvent Abbreviations**

| Abbreviation | Full name |
|---|---|
| $C_nE_m$ | Alkyl poly(ethylene oxide) |
| SDS | Sodium dodecyl sulfate |
| CPCl | Cetylpyridinium chloride |
| CTACl | Cetyltrimethylammonium chloride |
| Dd | Dodecane |
| Td | Tetradecane |
| Ch | Cholesterol |
| $FC_7$ | Sodium perfluorooctanoate |
| F68 | Pluronics F68 (PEO-PPO-PEO) |
| PC | Phosphatidylcholine |
| DOPC | Dioleoylphosphatidylcholine |
| DOPS | Dioleoylphosphatidylserine |
| DOPE | Dioleoylphosphatidylethanolamine |

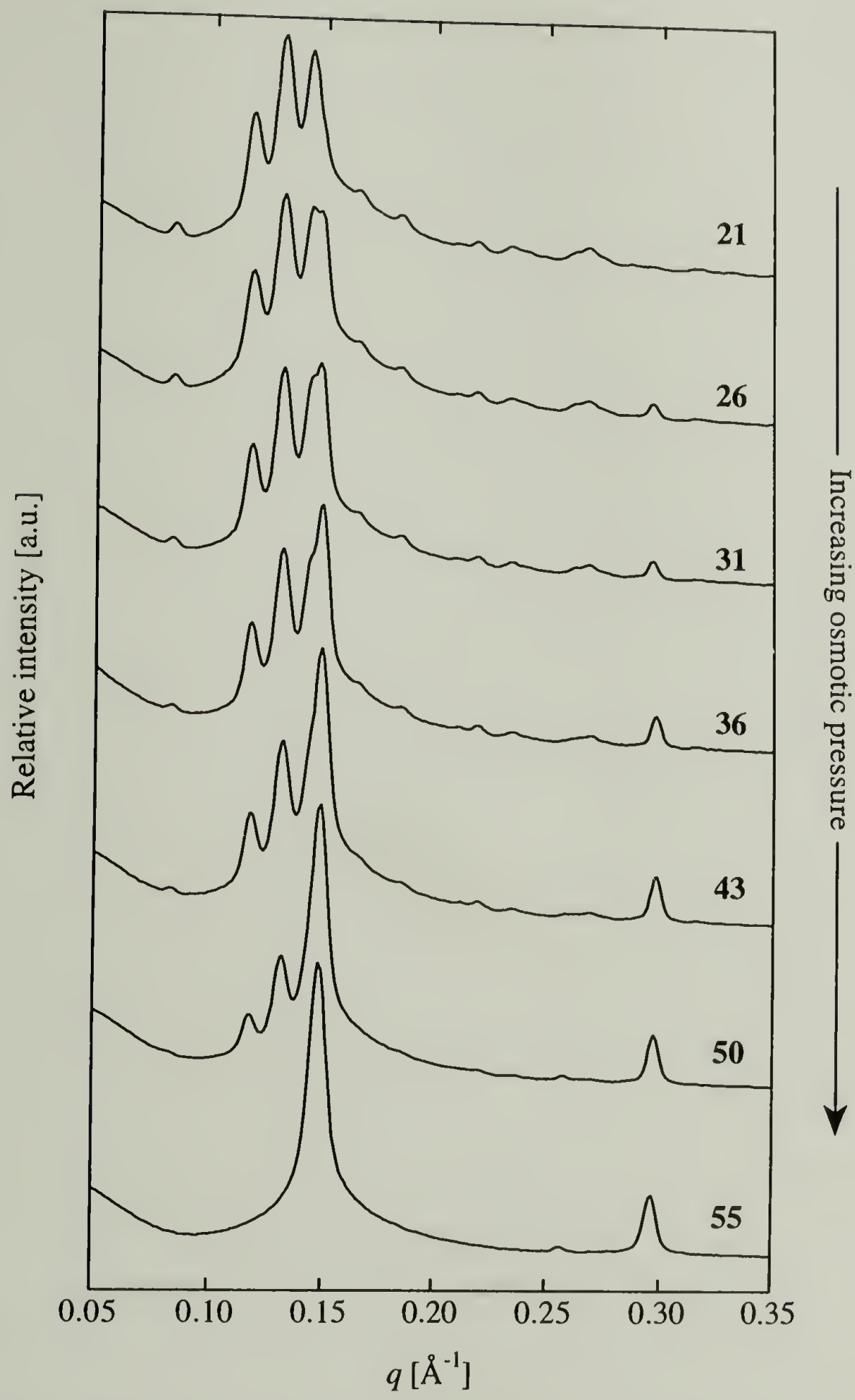


**Figure 4.1:** Angular-averaged SAXS profiles for 70% charge PAAm–CTACl complexes at 100 mM ionic strength under osmotic stress. Each curve represents the average of *N* replicate measurements, as reported in Table 4.3. Approximate osmotic pressure values in units of atm are associated with each curve.

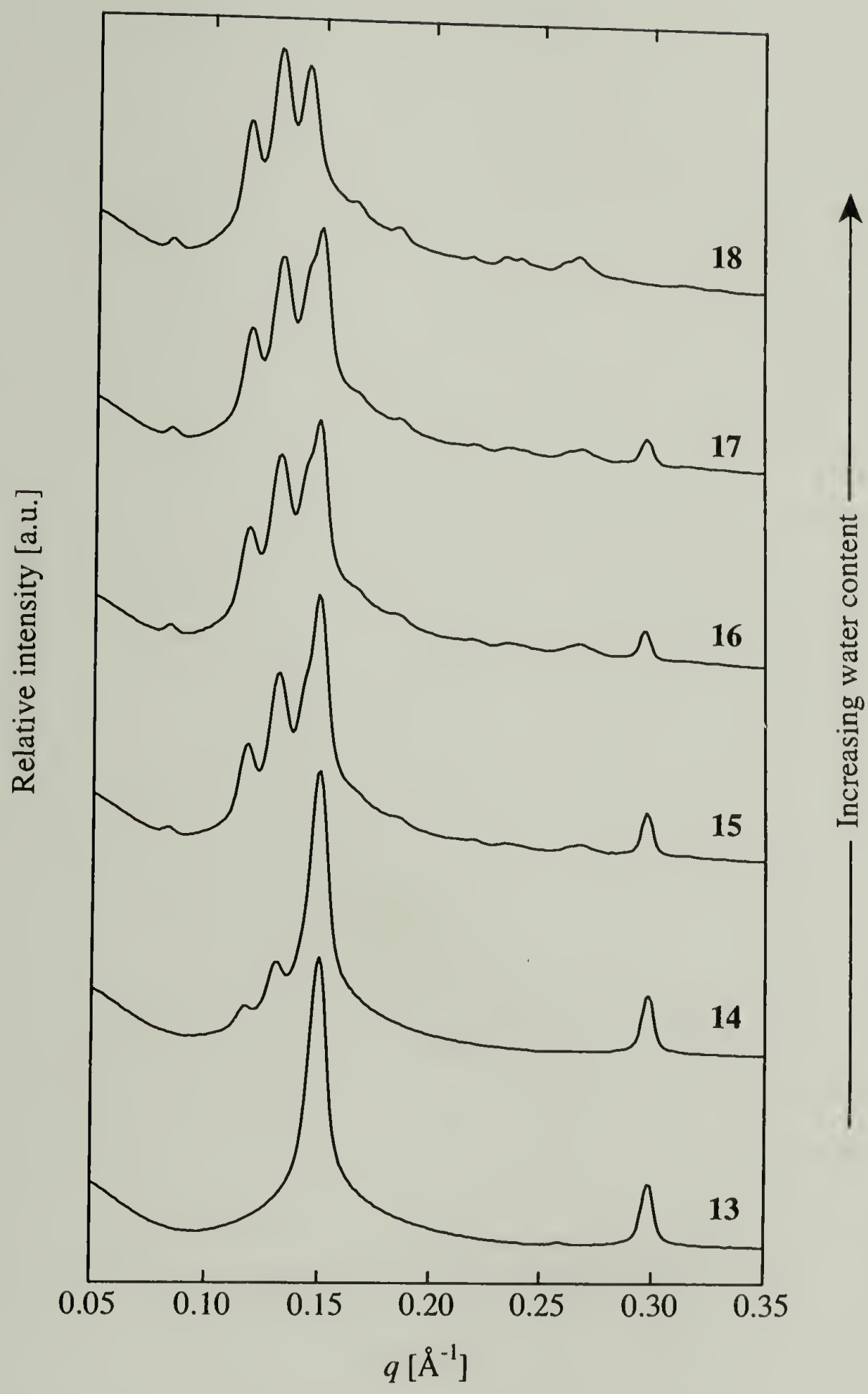


**Figure 4.2:** Angular-averaged SAXS profiles for 70% charge PAAm–CTACl complexes at 100 mM ionic strength under controlled hydration. Each curve represents the average of *N* replicate measurements, as reported in Table 4.2. Each curve is labeled with the corresponding number of water molecules per surfactant.

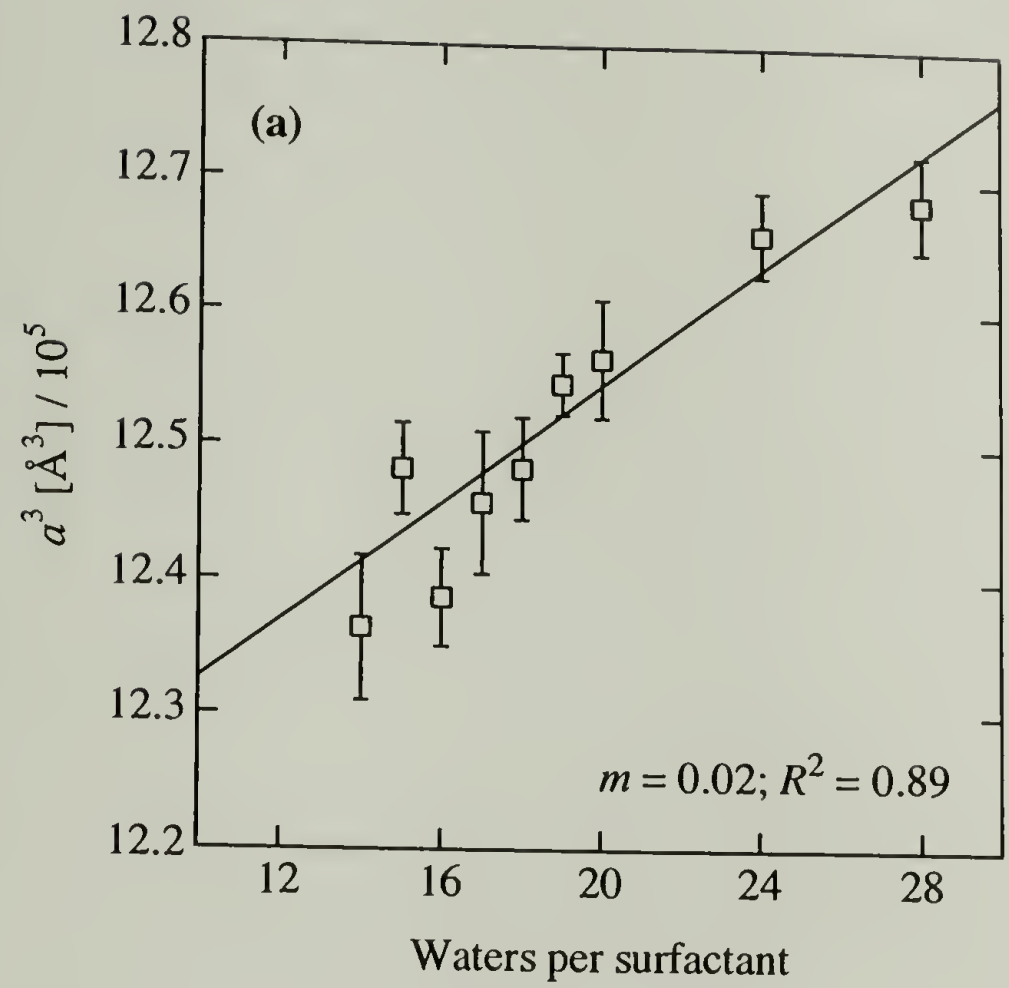


**Figure 4.3:** Unit cell volume versus water content for (a) *Pm*3*n* and (b) hcpc systems. Volume axes have been scaled by the indicated factors for more convenient presentation. Linear regression parameters are shown for each plot.

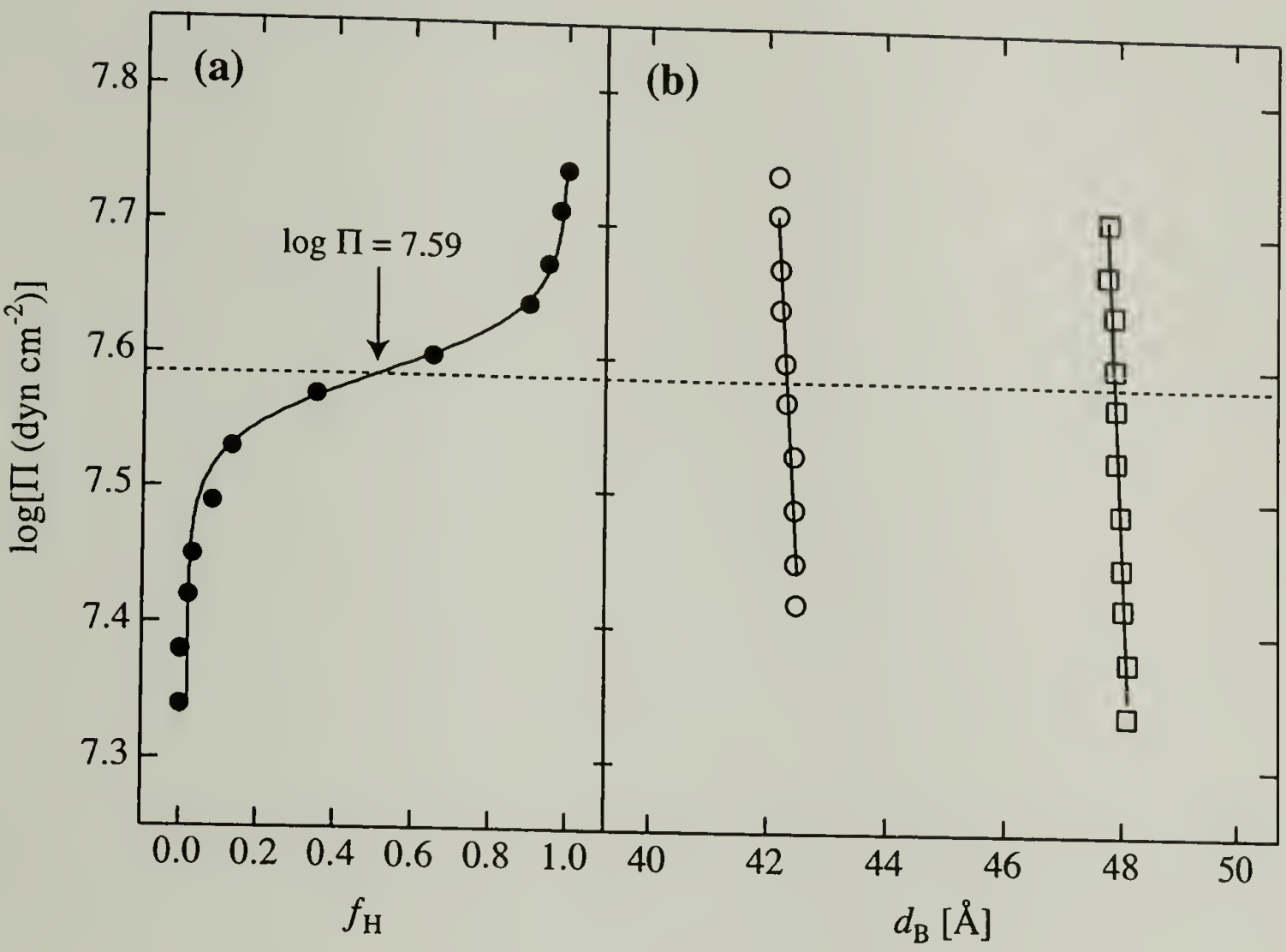


**Figure 4.4:** Characterization of the cubic-to-hexagonal transition in PAAm–CTACl complexes at 100 mM ionic strength under osmotic stress: (a) Increase of the hcpc phase fraction ($f_H$) with increasing osmotic pressure, as determined from relative SAXS intensities. The inflection point of the sigmoid fitting function was interpreted as the transition pressure (dashed line). (b) Phase diagram for PAAm–CTACl complexes at 100 mM ionic strength. Bragg spacings were calculated using the (100) hcpc (○) and the (210) *Pm*3*n* cubic (□) diffraction signals when those phases were present.

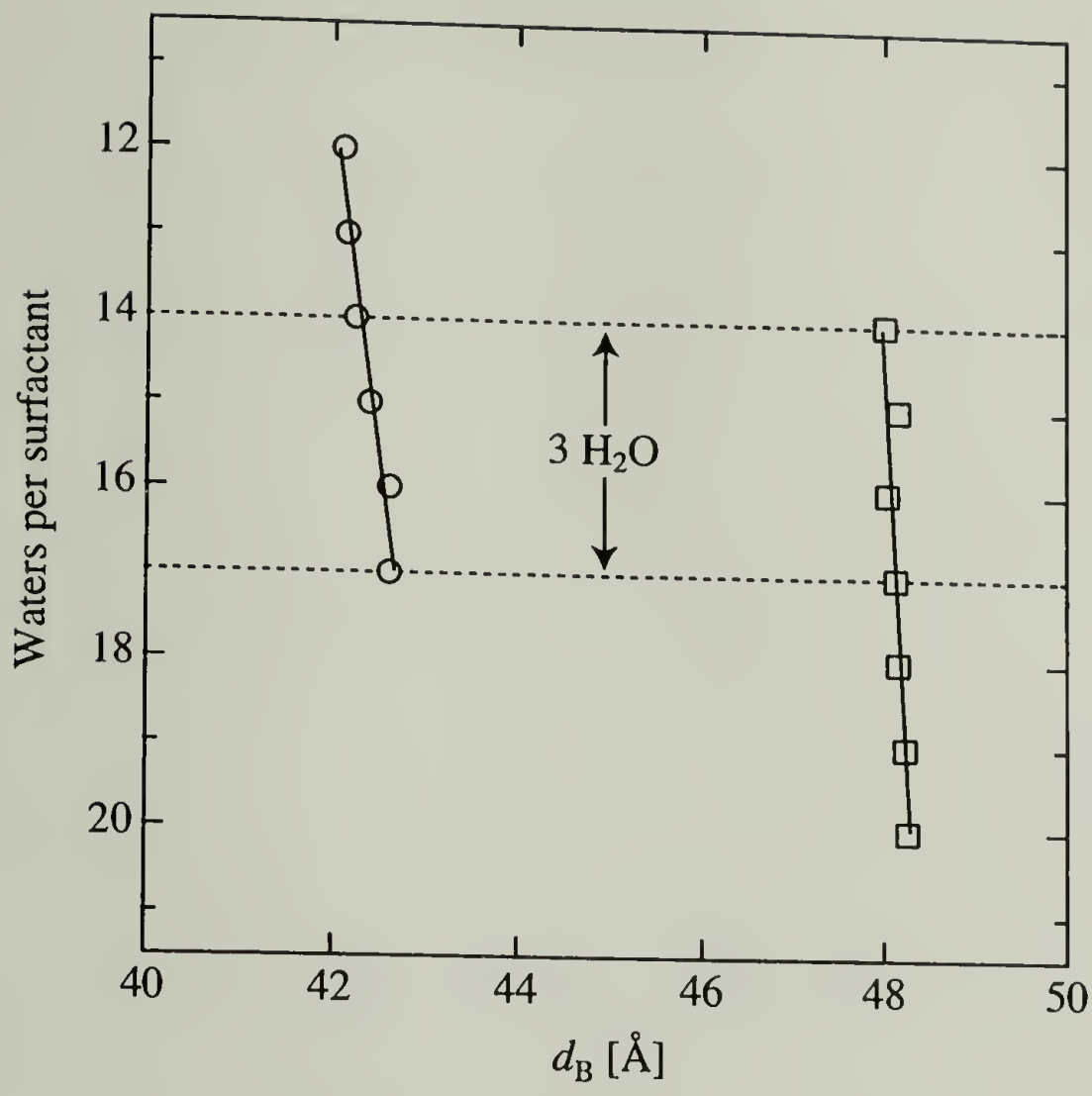


**Figure 4.5:** Water content versus Bragg spacing for PAAm–CTACl complexes at 100 mM ionic strength. Bragg spacings were calculated using the (100) hcpc (○) and the (210) *Pm*3*n* cubic (□) diffraction signals when those phases were present. The width of the coexistence region was used to calculate the volume change associated with the transition, which was assumed to occur at constant osmotic pressure.

## References


[1] Helfrich, W. Elastic Properties of Lipid Bilayers. *Z. Naturforsch., C: Biosci.* **1973,** *28,* 693-703.

[2] Jung, H.-T.; Lee, S. Y.; Kaler, E. W.; Coldren, B.; Zasadzinski, J. A. Gaussian Curvature and the Equilibrium among Bilayer Cylinders, Spheres, and Discs. *Proc. Natl. Acad. Sci. U.S.A.* **2002,** *99,* 15318-15322.

[3] Gradzielski, M.; Langevin, D.; Farago, B. Experimental investigation of the structure of nonionic microemulsions and their relation to the bending elasticity of the amphiphilic film. *Phys. Rev. E* **1996,** *53,* 3900-3919.

[4] Gradzielski, M.; Langevin, D.; Sottmann, T.; Strey, R. Droplet microemulsions at the emulsification boundary: The influence of the surfactant structure on the elastic constants of the amphiphilic film. *J. Chem. Phys.* **1997,** *106,* 106-119.

[5] Hellweg, T.; Langevin, D. Bending elasticity of the surfactant monolayer in droplet microemulsions: Determination by a combination of dynamic light scattering and neutron spin-echo spectroscopy. *Phys. Rev. E* **1998,** *57,* 6825-6834.

[6] Rekvig, L.; Hafskjold, B.; Smit, B. Chain Length Dependencies of the Bending Modulus of Surfactant Monolayers. *Phys. Rev. Lett.* **2004,** *92,* 116101.

[7] Safinya, C. R.; Sirota, E. B.; Roux, D.; Smith, G. S. Universality in Interacting Membranes: The Effect of Cosurfactants on the Interfacial Rigidity. *Phys. Rev. Lett.* **1989,** *62,* 1134-1137.

[8] Szleifer, I.; Kramer, D.; Ben-Shaul, A. Curvature Elasticity of Pure and Mixed Surfactant Films. *Phys. Rev. Lett.* **1988,** *60,* 1966-1969.

[9] Würger, A. Bending Elasticity of Surfactant Films: The Role of the Hydrophobic Tails. *Phys. Rev. Lett.* **2000,** *85,* 337-340.

[10] Gruner, S. M. Soft Materials and Biomaterials Under Pressure: Putting the Squeeze on Biology. In *High-Pressure Crystallography*; Katrusiak, A., McMillan, P., Eds.; Kluwer Academic Publishers: Dordrecht, The Netherlands, 2004; pp 543-556.

[11] Gruner, S. M. Stability of Lyotropic Phases with Curved Interfaces. *J. Phys. Chem.* **1989,** *93,* 7562-7570.

[12] Gruner, S. M. Intrinsic Curvature Hypothesis for Biomembrane Lipid Compositions: A Role for Nonbilayer Lipids. *Proc. Natl. Acad. Sci. U.S.A.* **1985,** *82,* 3665-3669.

[13] Gruner, S. M. Nonlamellar lipid phases. *Cell Membranes* **1991,** *5,* 1-57.

[14] Rand, R. P.; Fuller, N. L.; Gruner, S. M.; Parsegian, V. A. Membrane Curvature, Lipid Segregation, and Structural Transitions for Phospholipids under Dual-Solvent Stress. *Biochemistry* **1990,** *29,* 76-87.

[15] Gawrisch, K.; Parsegian, V. A.; Hajduk, D. A.; Tate, M. W.; Gruner, S. M.; Fuller, N. L.; Rand, R. P. Energetics of a Hexagonal–Lamellar–Hexagonal-Phase Transition Sequence in Dioleoylphosphatidylethanolamine Membranes. *Biochemistry* **1992,** *31,* 2856-2864.

[16] Rappolt, M.; Hickel, A.; Bringezu, F.; Lohner, K. Mechanism of the Lamellar/Inverse Hexagonal Phase Transition Examined by High Resolution X-Ray Diffraction. *Biophys J.* **2003,** *84,* 3111-3122.

[17] Parsegian, V. A.; Rand, R. P.; Fuller, N. L.; Rau, D. C. Osmotic Stress for the Direct Measurement of Intermolecular Forces. In *Methods in Enzymology*; Packer, L., Ed.; Academic Press, Inc., 1986; Vol. 127; pp 400-416.

[18] Luzzati, V.; Husson, F. Structure of Liquid-Crystalline Phases of Lipid-Water Systems. *J. Cell. Biol.* **1962,** *12,* 207-216.

[19] Gruner, S. M.; Parsegian, V. A.; Rand, R. P. Directly Measured Deformation Energy of Phospholipid $H_{II}$ Hexagonal Phases. *Faraday Discuss. Chem. Soc.* **1986,** *81,* 29-37.

[20] Hung, W. C.; Chen, F. Y. Osmotic Threshold and Water Association for Phospholipid Gel Phase Bilayers. *Chin. J. Phys.* **2000,** *38,* 882-892.

[21] Hung, W. C.; Chen, F. Y. The Hydrophobic-Hydrophilic Interface of Phospholipid Membranes Studied by Lamellar X-Ray Diffraction. *Chin. J. Phys.* **2003,** *41,* 85-91.

[22] Chen, F. Y.; Hung, W. C.; Huang, H. W. Critical Swelling of Phospholipid Bilayers. *Phys. Rev. Lett.* **1997,** *79,* 4026-4029.

[23] Costigan, S. C.; Booth, P.; Templer, R. H. Swelling Series and Bilayer Defects Due to Sample Preparation. *Mol. Cryst. Liq. Cryst.* **2000,** *352,* 59-66.

[24] Seddon, J. M.; Robins, J.; Gulik-Krzywicki, T.; Delacroix, H. Inverse micellar phases of phospholipids and glycolipids. *Phys. Chem. Chem. Phys.* **2000,** *2,* 4485-4493.

[25] Smith, G. S.; Sirota, E. B.; Safinya, C. R.; Clark, N. A. Structure of the $L_\beta$ Phases in a Hydrated Phosphatidylcholine Multimembrane. *Phys. Rev. Lett.* **1988,** *60,* 813-816.

[26] Roelants, E.; De Schryver, F. C. Parameters Affecting Aqueous Micelles of CTAC, TTAC, and DTAC Probed by Fluorescence Quenching. *Langmuir* **1987,** *3,* 209-214.

[27] Di Meglio, J.-M.; Dvolaitzky, M.; Taupin, C. Determination of the Rigidity Constant of the Amphiphilic Film in "Birefringent Microemulsions": The Role of the Cosurfactant. *J. Phys. Chem.* **1985,** *89,* 871-874.

[28] Sottmann, T.; Strey, R.; Chen, S.-H. A small-angle neutron scattering study of nonionic surfactant molecules at the water-oil interface: Area per molecule, microemulsion domain size, and rigidity. *J. Chem. Phys.* **1997,** *106,* 6483-6491.

[29] Vollmer, D.; Vollmer, J. Bending free energy and spontaneous curvature for micelles and microemulsions with weak and strong surfactants. *Eur. Phys. J. E* **2001,** *4,* 153-159.

[30] Tsapis, N.; Ober, R.; Urbach, W. Modification of Elastic Constants by Charge Addition to a Nonionic Lamellar Phase. *Langmuir* **2000,** *16,* 2968-2974.

[31] Safinya, C. R.; Roux, D.; Smith, G. S.; Sinha, S. K.; Dimon, P.; Clark, N. A.; Bellocq, A. M. Steric Interactions in a Model Multimembrane System: A Synchrotron X-Ray Study. *Phys. Rev. Lett.* **1986,** *57,* 2718-2721.

[32] Castro-Roman, F.; Porte, G.; Ligoure, C. Smectic Phase of Fluid Membranes Decorated by Amphiphilic Copolymer. *Langmuir* **2001,** *17,* 5045-5058.

[33] Fuller, N. L.; Benatti, C. R.; Rand, R. P. Curvature and Bending Constants for Phosphatidylserine-Containing Membranes. *Biophys J.* **2003,** *85,* 1667-1674.

[34] Malinin, V. S.; Lentz, B. R. On the Analysis of Elastic Deformations in Hexagonal Phases. *Biophys J.* **2004,** *86,* 3324-3328.

[35] Servuss, R. M.; Harbich, W.; Helfrich, W. Measurement of Curvature-Elastic Modulus of Egg Lecithin Bilayers. *Biochim. Biophys. Acta* **1976,** *436,* 900-903.

# APPENDIX

# TEMPERATURE DEPENDENCE OF POLYELECTROLYTE–SURFACTANT COMPLEX STRUCTURE

## A.1 Introduction

Many macromolecular self-assembly processes are known to be sensitive to temperature. Examples from biology and biochemistry include self-ordered arrays of $Mn^{2+}$–DNA helices[1], spontaneous association of hydroxypropyl cellulose polymers[2], organization of collagen into helical fibers[3-6], and the formation of actin filaments[7]. Synthetic systems, such as nanotubes consisting of functionalized crown ethers[8], adamantane encapsulates[9], and carboxylate–guanidiniocarbonyl pyrrole oligomers[10] are also formed by temperature-dependent self-assembly processes. At the root of these processes is the attraction between either hydrophobic or hydrophilic surfaces, which is driven by the entropically favorable release of surface-bound solvent molecules. As an illustration, consider a system consisting of polar surfaces (e.g. collagen). At low temperatures, water molecules will become ordered close to these polar surfaces such that there is a structurally important difference in the in the entropy of this water compared to that of the bulk solution. At higher temperatures, the entropic penalty these water molecules must incur to remain closely bound to the polar surfaces increases significantly, and eventually, they are released into the bulk and the surfaces move closer together. This entropically-driven release of structured solvent molecules

and the concomitant decrease in the degree of surface separation is known as temperature favored assembly.

The influence of temperature on polyelectrolyte–surfactant complex structure was not studied extensively as part of this thesis work. However, a preliminary investigation of PAAm–CTAX phase behavior as a function of temperature was conducted. This small study was limited to only 2 charge densities at fixed ionic strength.

## A.2 Experimental

All materials, methods, instrumentation, and data analysis procedures were identical to those described in section 2.2. The two polyelectrolyte–surfactant complexes chosen for this study were the PA–CTACl and PAAm–CTABr systems at 100 mM ionic strength. Each complex was studied in PEG-free salt solutions and in salt solutions with 5 wt % PEG. A custom-built brass sample cell was used for the temperature-dependent SAXS measurements. This cell was equipped with a water-jacketed cooling system, a brass capillary tube holder, and a Peltier thermoelectric heating device. The temperature of the sample cell was regulated by an external controller and spanned a range of 10–70 °C. All samples were sealed in 1 mm glass capillary tubes prior to the SAXS measurements; these capillaries were placed in thermal contact with the sample cell using a heat-conducting paste. Samples were allowed to equilibrate for 15 minutes after adjusting the cell temperature, and a 10-minute exposure time was used.

## A.3 Results and Discussion

Both of the polyelectrolyte–surfactant complexes chosen for these measurements exhibited coexistence regions of *Pm*3*n* cubic and hcpc phases at 10 °C, as shown by the lowermost traces in Figure A.1. The *Pm*3*n* cubic phase dominated the coexistence region for the 70% charge PAAm–CTABr complex, whereas the hcpc phase was predominant in the PA–CTACl coexistence region. The predominance of the hcpc phase in the 100% charge system versus the 70% charge system at this temperature is consistent with the earlier observation that higher polyelectrolyte charge densities bring about more compact phases (section 2.3.2.3). As the temperature was increased, both complexes underwent a transition to a hcpc phase, which persisted throughout the remainder of the heating process; these transitions can be seen explicitly in Figure A.1. From these data, the transition temperature for the PA–CTACl complex appeared to be between 15 and 20 °C, whereas the transition point for the 70% charge PAAm–CTABr complex was between 10 and 25 °C.

The temperature-driven transition from coexisting *Pm*3*n* and hcpc structures to a distinct hcpc phase was accompanied by a linear decrease in the unit cell sizes for both the PAAm–CTABr and PA–CTACl complexes, as shown in Figures A.2 and A.3, respectively. The Bragg spacings shown in these figures represent only the (100) hcpc diffraction signals—the *Pm*3*n* spacings, when that phase was present, were not considered as part of this analysis. From these data, we see that the 70% charge system was more compressible as a function of temperature than the 100% charge complex, and that the unit cell sizes at each temperature were smaller for the 100% charge

complex than for the 70% charge system. This result is consistent with previous observations regarding unit cell size and complex compressibility as functions of polyelectrolyte charge density (section 2.3).

For samples that were equilibrated in 5 wt % PEG, it is important to mention that the corresponding osmotic pressure—approximately 1 atm at 25 °C—was assumed to remain constant throughout the heating/cooling cycles shown in Figures A.2 and A.3. It is well known that increasing temperature results in a lowering of osmotic pressure at constant PEG concentration[11]. However, this effect is most pronounced at high PEG concentrations (> 5 wt %) and was not expected to significantly influence the structural trends with temperature that we have observed in these particular systems.

It is interesting to note that the compression of the hcpc phase in both complexes was completely reversible over the experimental temperature range; no hysteresis was observed during the cooling step, as shown in Figure A.4. In addition, the structure of the complex before heating was identical to the structure obtained after the cooling step, as shown by the angular-averaged SAXS profiles in Figure A.5. Note that the same degree of *Pm*3*n*–hcpc coexistence was qualitatively observed at both stages.

## A.4 Conclusions

The data presented here clearly show that PAAm–CTAX complexes undergo temperature favored assembly. Increasing the temperature results in compression of the complex, which in turn, brings about an overall decrease in the curvature of the system. In this particular case, the decrease in curvature was sufficient to give rise to a transition

from coexisting *Pm*3*n* and hcpc structures to a distinct hcpc phase at both charge densities studied. In this context, increasing the temperature had the same effect on polyelectrolyte–surfactant complex structure as did increasing polyelectrolyte charge density and/or osmotic pressure as described in Chapter 2. However, it is the entropically-driven release of structured water from the polar surfaces of the complexes that is responsible for the attractive interactions observed in this example.

## Figures

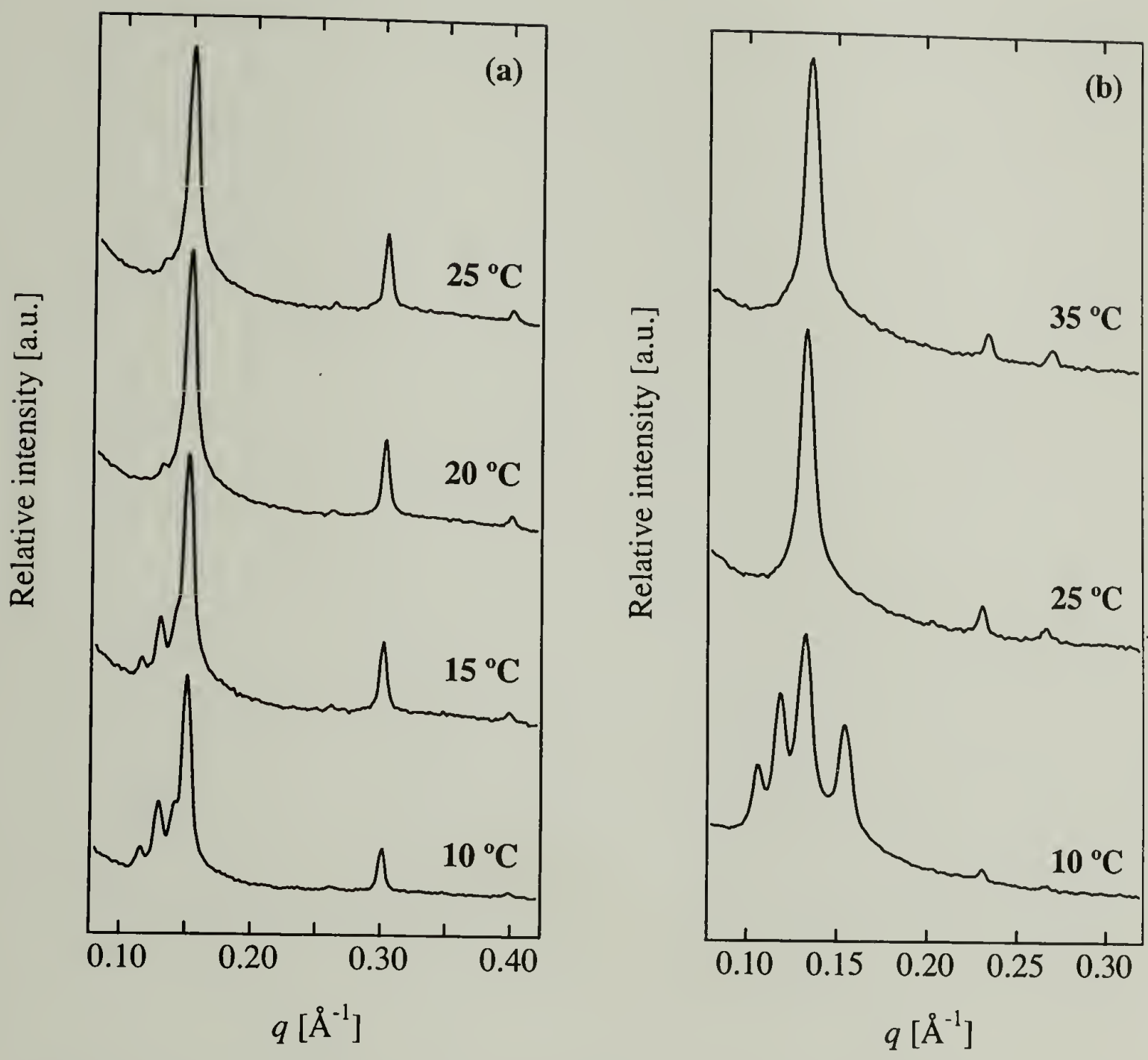


**Figure A.1:** Temperature-dependent, angular-averaged scattering profiles for (a) PA–CTACl and (b) 70% charge PAAm–CTABr complexes at 100 mM ionic strength and 5 wt % PEG.

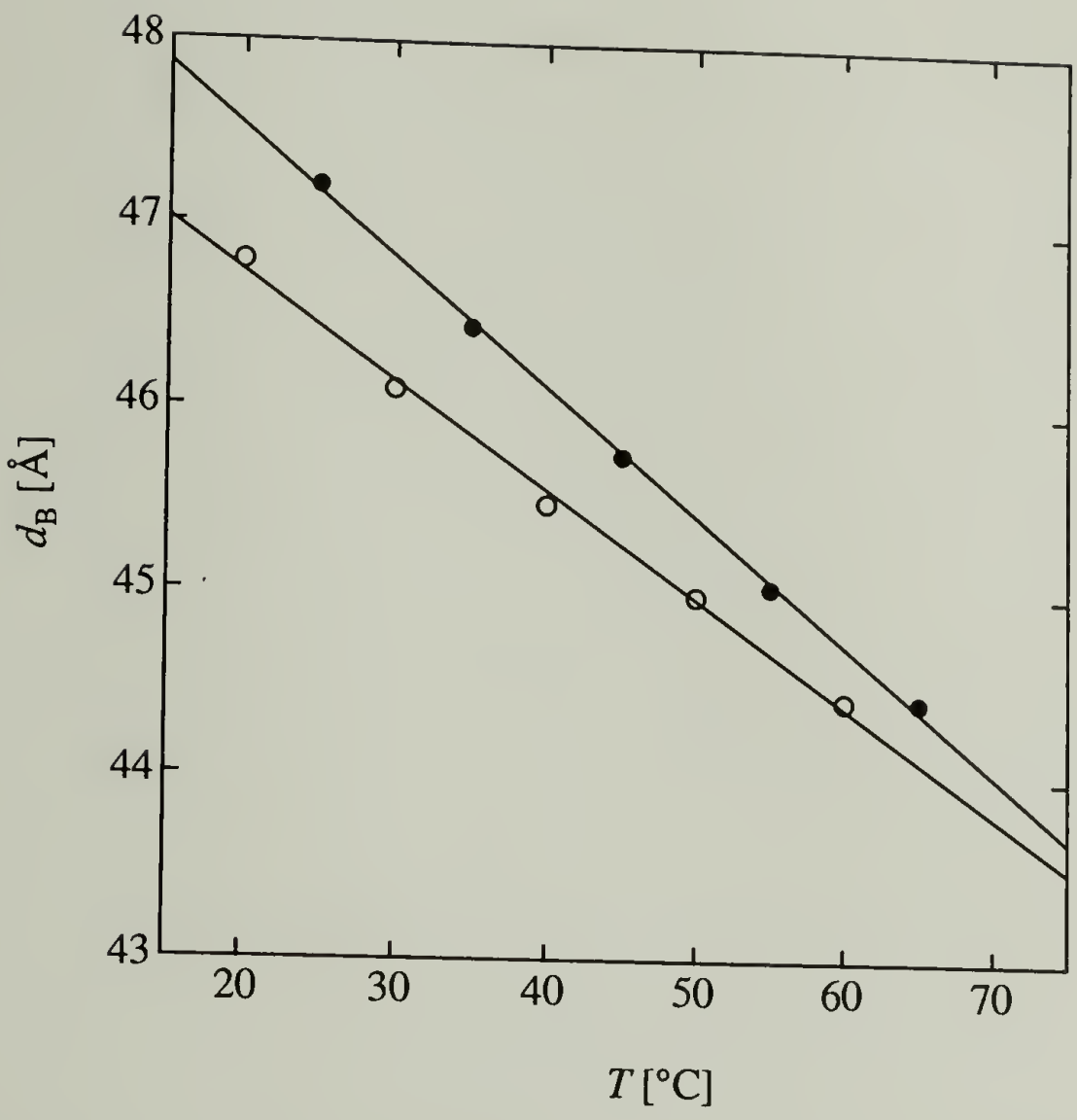


**Figure A.2:** Temperature-dependent Bragg spacings for 70% charge PAAm–CTABr complexes at 100 mM ionic strength. The PEG concentration was set at 0 wt % (filled symbols) and 5 wt % (open symbols).

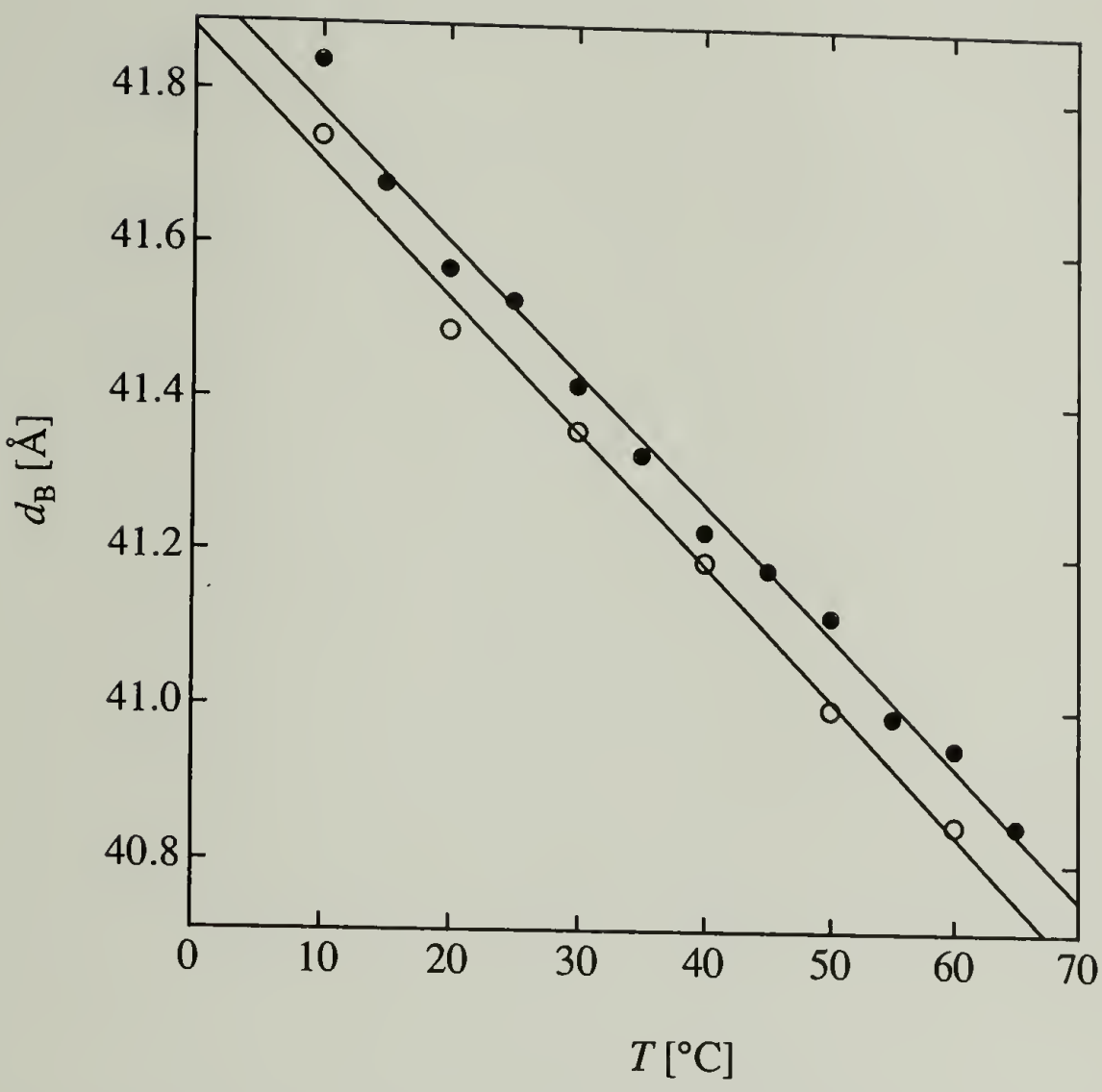


**Figure A.3:** Temperature-dependent Bragg spacings for PA–CTACl complexes at 100 mM ionic strength. The PEG concentration was set at 0 wt % (filled symbols) and 5 wt % (open symbols).

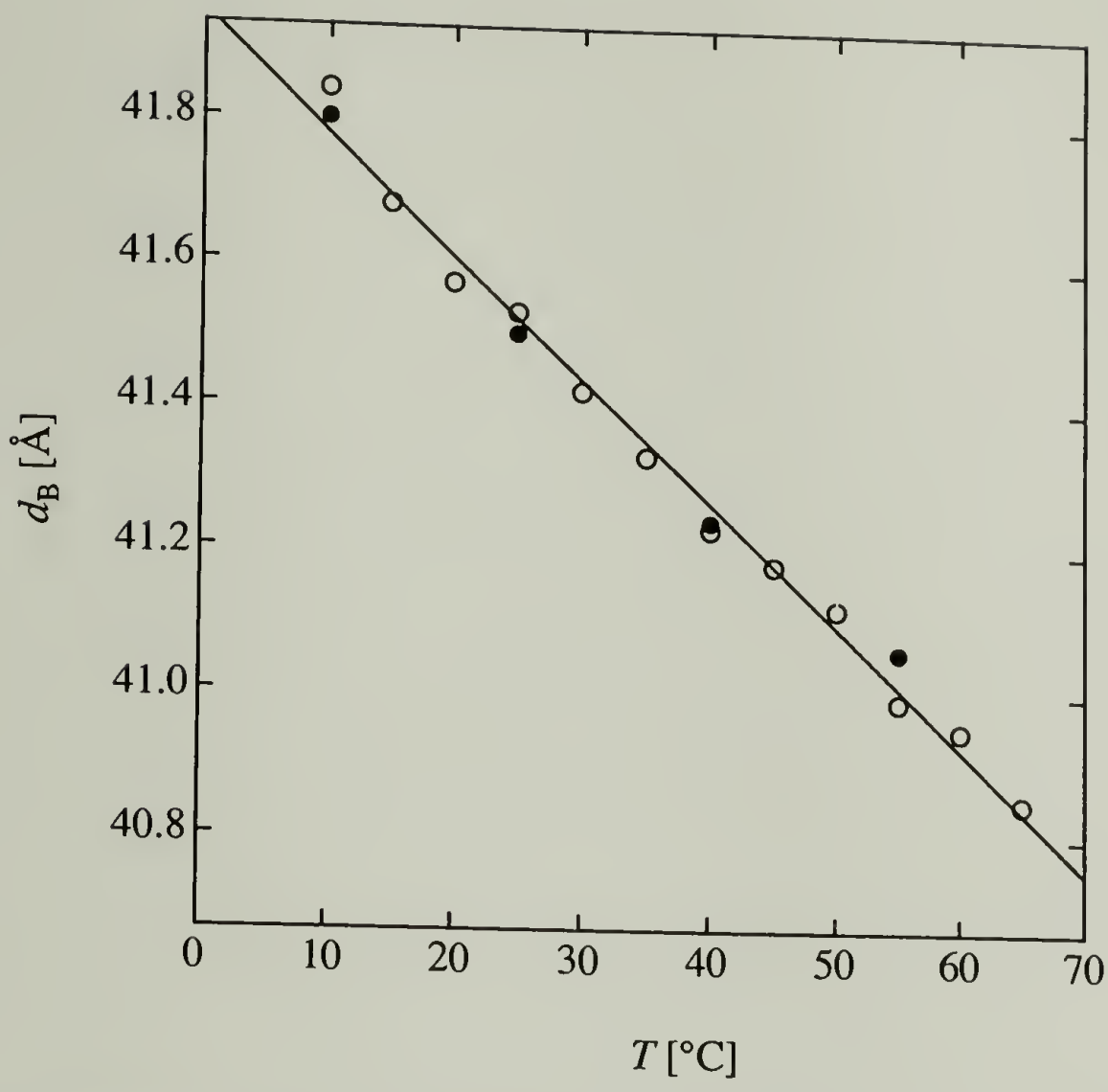


**Figure A.4:** Bragg spacings for PA–CTACl complex at 100 mM ionic strength (no added PEG) throughout a temperature cycle: heating step (open symbols), cooling step (filled symbols).

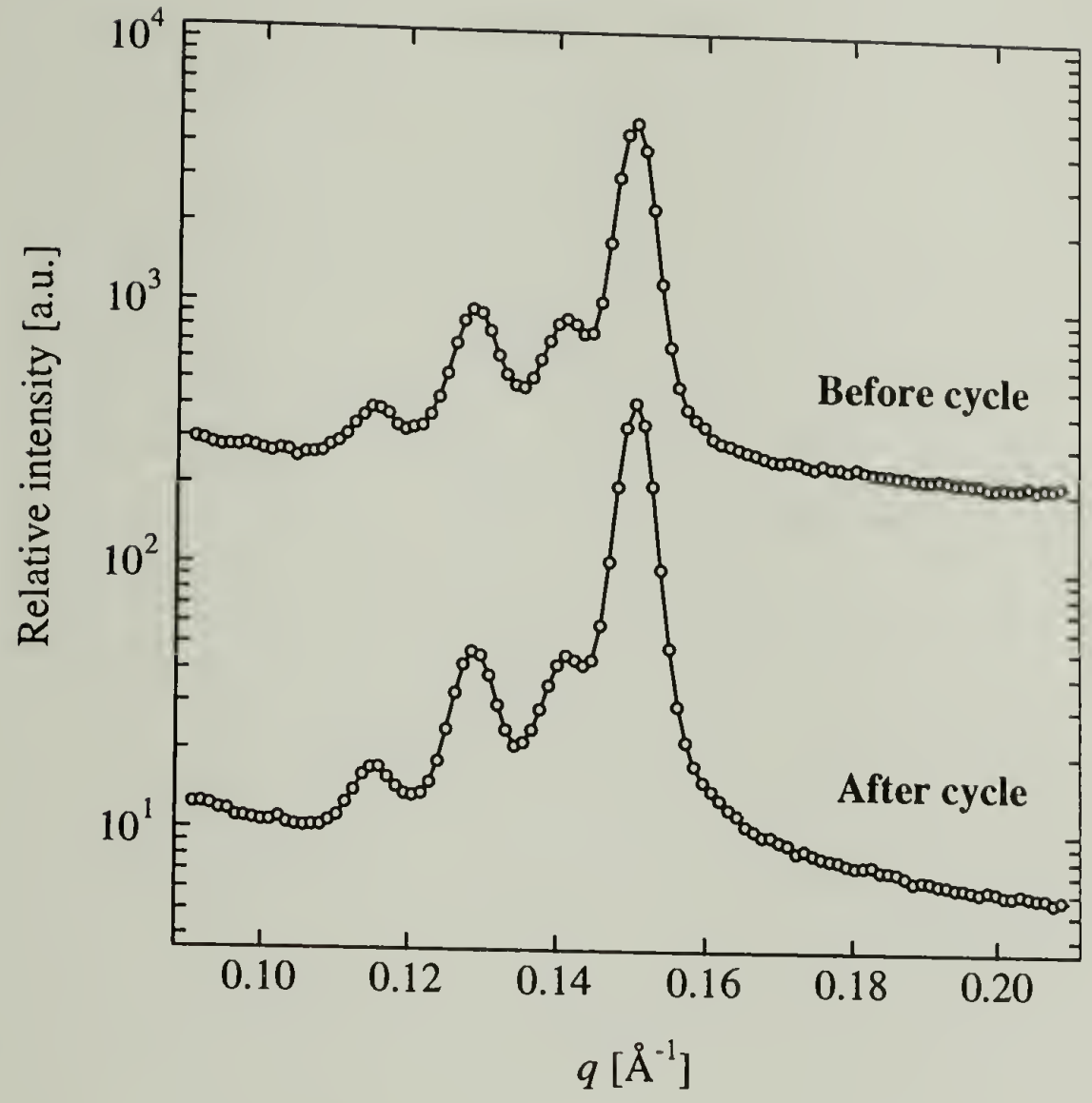


**Figure A.5:** Angular-averaged scattering profiles for PA–CTACl complexes at 100 mM ionic strength (no added PEG) at the beginning and end of a temperature cycle.

## References


[1] Leikin, S.; Rau, D. C.; Parsegian, V. A. Measured entropy and enthalpy of hydration as a function of distance between DNA double helices. *Phys. Rev. A* **1991,** *44,* 5272-5278.

[2] Bonnet-Gonnet, C.; Leikin, S.; Chi, S.; Rau, D. C.; Parsegian, V. A. Measurement of Forces between Hydroxypropylcellulose Polymers: Temperature Favored Assembly and Salt Exclusion. *J. Phys. Chem. B* **2001,** *105,* 1877-1886.

[3] Friedhoff, P.; Schneider, A.; Mandelkow, E.-M.; Mandelkow, E. Rapid Assembly of Alzheimer-like Paired Helical Filaments from Microtubule-Associated Protein Tau Monitored by Fluorescence in Solution. *Biochemistry* **1998,** *37,* 10223-10230.

[4] Leikin, S.; Rau, D. C.; Parsegian, V. A. Direct Measurement of Forces Between Self-Assembled Proteins - Temperature-Dependent Exponential Forces Between Collagen Triple Helices. *Proc. Natl. Acad. Sci. U.S.A.* **1994,** *91,* 276-280.

[5] Kadler, K. E.; Hojima, Y.; Prockop, D. J. Assembly of Collagen Fibrils *de Novo* by Cleavage of the Type I pC-Collagen with Procollagen C-Proteinase. *J. Biol. Chem.* **1987,** *260,* 15696-15701.

[6] Kadler, K. E.; Hojima, Y.; Prockop, D. J. Assembly of Type I Collagen Fibrils *de Novo*. *J. Biol. Chem.* **1988,** *263,* 10517-10523.

[7] Wong, G. C. L.; Tang, J. X.; Lin, A.; Li, Y.; Janmey, P. A.; Safinya, C. R. F-Actin and Cationic Lipid Complexes: Stacked Three-Layer Tubule Networks. *Science* **2000,** *288,* 2035-2039.

[8] Fenniri, H.; Deng, B.-L.; Ribbe, A. E.; Hallenga, K.; Jacob, J.; Thiyagarajan, P. Entropically driven self-assembly of multichannel rosette nanotubes. *Proc. Natl. Acad. Sci. U.S.A.* **2002,** *99,* 6487-6492.

[9] Kang, J.; Rebek, J. Entropically driven binding in a self-assembling molecular capsule. *Nature* **1996,** *382,* 239-241.

[10] Schmuck, C. Self-assembly of 2-(guanidiniocarbonyl)-pyrrole-4-carboxylate in dimethyl sulfoxide: an entropy driven oligomerization. *Tetrahedron* **2001,** *37,* 3063-3067.

[11] Stanley, C. B.; Strey, H. H. Measuring Osmotic Pressure of Poly(ethylene glycol) Solutions by Sedimentation Equilibrium Ultracentrifugation. *Macromolecules* **2003,** *36,* 6888-6893.

## BIBLIOGRAPHY


Aksay, I. A.; Trau, M.; Manne, S.; Homma, I.; Yao, N.; Zhou, L.; Fenter, P.; Eisenberger, P. M.; Gruner, S. M. Biomimetic Pathways for Assembling Inorganic Thin Films. *Science* **1996,** *273,* 892-898.

Allen, R. J.; Warrent, P. B. Phase behaviour of oppositely charged polymer/surfactant mixtures. *Europhys. Lett.* **2003,** *64,* 468-474.

Almgren, M.; Hansson, P.; Mukhtar, E.; van Stam, J. Aggregation of Alkyltrimethylammonium Surfactants in Aqueous Poly(styrenesulfonate) Solutions. *Langmuir* **1992,** *8,* 2405-2412.

Andelman, D.; Kozlov, M. M.; Helfrich, W. Phase Transitions betweeen Vesicles and Micelles Driven by Competing Curvatures. *Europhys. Lett.* **1994,** *25,* 231-236.

Angelov, B.; Angelova, A.; Ollivon, M.; Bourgaux, C.; Campitelli, A. Diamond-Type Lipid Cubic Phase with Large Water Channels. *J. Am. Chem. Soc.* **2003,** *125,* 7188-7189.

Antonietti, M. Structure and dynamics of polyelectrolyte-surfactant complexes as revealed by solid state NMR. *Macromol. Chem. Phys.* **1996,** *197,* 2713-2727.

Antonietti, M.; Burger, C.; Conrad, J.; Kaul, A. Polyelectrolyte-surfactant complexes: highly ordered microphase-separated polymers. *Macromol. Symp.* **1996,** *106,* 1-8.

Antonietti, M.; Burger, C.; Effing, J. Mesomorphous Polyelectrolyte-Surfactant Complexes. *Adv. Mat.* **1995,** *7,* 751-753.

Antonietti, M.; Conrad, J. Synthesis of Very Highly Ordered Liquid Crystalline Phases by Complex Formation of Polyacrylic Acid with Cationic Surfactants. *Angew. Chem. Int. Ed. Engl.* **1994,** *33,* 1869-1870.

Antonietti, M.; Conrad, J.; Thünemann, A. Polyelectrolyte-Surfactant Complexes: A New Type of Solid, Mesomorphous Material. *Macromolecules* **1994,** *27,* 6007-6011.

Antonietti, M.; Kaul, A.; Thünemann, A. Complexation of Lecithin with Cationic Polyelectrolytes: "Plastic Membranes" as Models for the Structure of the Cell Membrane? *Langmuir* **1995,** *11,* 2633-2638.

Antonietti, M.; Maskos, M. Fine-Tuning of Phase Structures and Thermoplasticity of Polyelectrolyte-Surfactant Complexes: Copolymers of Ionic Monomers with *N*-Alkylacrylamides. *Macromolecules* **1996,** *29,* 4199-4205.

Antonietti, M.; Thünemann, A. Polyelectrolyte-Lipid Complexes as Membrane Mimetic Systems. *Current Opinion in Colloid and Interface Science* **1996,** *1,* 667-671.

Antonietti, M.; Wenzel, A. Structure control of polyelectrolyte-lipid complexes by variation of charge density and addition of cholesterol. *Colloids Surf. A* **1998,** *135,* 141-147.

Ashbaugh, H. S.; Lindman, B. Swelling and Structural Changes of Oppositely Charged Polyelectrolyte Gel-Mixed Surfactant Complexes. *Macromolecules* **2001,** *34,* 1522-1525.

Atkins, E. D. T. University of Massachusetts Amherst, Amherst, MA. Lecture notes from Polymer Morphology course (PSE 721), 1999.

Atkins, P. W. *Physical Chemistry,* 5th ed.; W.H. Freeman and Company: New York, 1994.

Auvray, X.; Petipas, C.; Anthore, R.; Rico, I.; Lattes, A. X-Ray Diffraction Study of Mesophases of Cetyltrimethylammonium Bromide in Water, Formamide, and Glycerol. *J. Phys. Chem.* **1989,** *93,* 7458-7464.

Babak, V. G.; Merkovich, E. A.; Desbrières, J.; Rinaudo, M. Formation of an ordered nanostructure in surfactant-polyelectrolyte complexes formed by interfacial diffusion. *Polym. Bull.* **2000,** *45,* 77-81.

Bae, H.-S.; Hudson, S. M. The Cooperative Binding Behavior of Sodium Dodecyl Sulfate to Crosslinked Chitosan Films. *J. Polym. Sci. A: Polym. Chem.* **1997,** *35,* 3755-3765.

Bai, G.; Santos, L. M. N. B. F.; Nichifor, M.; Lopes, A.; Bastos, M. Thermodynamics of the Interaction between a Hydrophobically Modified Polyelectrolyte and Sodium Dodecyl Sulfate in Aqueous Solution. *J. Phys. Chem. B* **2004,** *108,* 405-413.

Bakeev, K. N.; Ponomarenko, E. A.; Shishkanova, T. y. V.; Tirrell, D. A.; Zezin, A. B.; Kabanov, V. A. Complexation of Amphiphilic Polyelectrolytes with Surfactants of the Same Charge in Water Solutions. *Macromolecules* **1995,** *28,* 2886-2892.

Bakshi, M. S.; Sachar, S. Surfactant polymer interactions between strongly interacting cationic surfactants and anionic polyelectrolytes from conductivity and turbidity measurements. *Colloid Polym. Sci.* **2004,** *282,* 993-999.

Beck, J. S.; Vartulli, J. C.; Roth, W. J.; Leonowicz, M. E.; Kresge, C. T.; Schmitt, K. D.; Chu, C. T.-W.; Olson, D. H.; Sheppard, E. W.; McCullen, S. B.; Higgins, J. B.; Schlenker, J. L. A New Family of Mesoporous Molecular Sieves Prepared with Liquid Crystal Templates. *J. Am. Chem. Soc.* **1992,** *114,* 10834-10843.

Bergström, M. Derivation of expressions for the spontaneous curvature, mean and Gaussian bending constants of thermodynamically open surfactant monolayers and bilayers. *J. Chem. Phys.* **2003,** *118,* 1440-1452.

Bergström, M. L.; Kjellin, U. R. M.; Claesson, P. M. Small-Angle Neutron Scattering Study of Mixtures of Cationic Polyelectrolyte and Anionic Surfactant: Effect of Polyelectrolyte Charge Density. *J. Phys. Chem. B* **2004,** *108,* 1874-1881.

Bergström, M. L.; Kjellin, U. R. M.; Claesson, P. M.; Pedersen, J. S.; Nielsen, M. M. A Small-Angle X-ray Scattering Study of Complexes Formed in Mixtures of a Cationic Polyelectrolyte and an Anionic Surfactant. *J. Phys. Chem. B* **2002,** *106,* 11412-11419.

Berr, S. S.; Caponetti, E.; Johnson, J. S. J.; Jones, R. R. M.; Magid, L. J. Small-Angle Neutron Scattering from Hexadecyltrimethylammonium Bromide Micelles in Aqueous Solutions. *J. Phys. Chem.* **1986,** *90,* 5766-5770.

Berret, J.-F.; Vigolo, B.; Eng, R.; Hervé, P. Electrostatic Self-Assembly of Oppositely Charged Copolymer and Surfactants: A Light, Neutron, and X-ray Scattering Study. *Macromolecules* **2004,** *37,* 4922-4930.

Blankschtein, D.; Puvvada, S. Theoretical and Experimental Investigations of Micellar Properties of Aqueous Solutions Containing Binary Mixtures of Nonionic Surfactants. *J. Phys. Chem.* **1992,** *96,* 5579-5592.

Bloomfield, V. A. DNA Condensation. *Curr. Opin. Struc. Biol.* **1996,** *6,* 334-341.

Bonnet-Gonnet, C.; Leikin, S.; Chi, S.; Rau, D. C.; Parsegian, V. A. Measurement of Forces between Hydroxypropylcellulose Polymers: Temperature Favored Assembly and Salt Exclusion. *J. Phys. Chem. B* **2001,** *105,* 1877-1886.

Boström, M.; Kunz, W.; Ninham, B. W. Hofmeister Effects in Surface Tension of Aqueous Electrolyte Solution. *Langmuir* **2005,** *21,* 2619-2623.

Camejo, G.; Fager, G.; Rosengren, B.; Hurtcamejo, E.; Bondjers, G. Binding of Low-Density Lipoproteins by Proteoglycans Synthesized by Proliferating and Quiescent Human Arterial Smooth-Muscle Cells. *J. Biol. Chem.* **1993,** *268,* 14131-14137.

Camejo, G.; Lopez, A.; Lopez, F.; Quinones, J. Interaction of Low-Density Lipoproteins with Arterial Proteoglycans - the Role of Charge and Sialic-Acid Content. *Atherosclerosis* **1985,** *55,* 93-105.

Cantor, R. S. Statistical thermodynamics of curvature elasticity in surfactant monolayer films: A molecular approach. *J. Chem. Phys.* **1993,** *99,* 7124-7149.

Cárdenas, M.; Campos-Terán, J.; Nylander, T.; Lindman, B. DNA and Cationic Surfactant Complexes at Hydrophilic Surfaces. An Ellipsometry and Surface Force Study. *Langmuir* **2004,** *20,* 8597-8603.

Carnali, J. O. (Polymer/Polymer)-Like Phase Behavior in the System Tetradecyltrimethylammonium Bromide/Sodium Polyacrylate/Water. *Langmuir* **1993,** *9,* 2933-2941.

Carreño-Gomez, B.; Duncan, R. Evaluation of the Biological Properties of Soluble Chitosan and Chitosan Microspheres. *Int. J. Pharm.* **1997,** *148,* 231-240.

Castro-Roman, F.; Porte, G.; Ligoure, C. Smectic Phase of Fluid Membranes Decorated by Amphiphilic Copolymer. *Langmuir* **2001,** *17,* 5045-5058.

Cegile, A.; Colafemmina, G.; Della Monica, M.; Olsson, U.; Jönsson, B. Shape and Size of Micelles in the Sodium Dodecyl Sulfate–Formamide System. *Langmuir* **1993,** *9,* 1449-1455.

Chandra, R.; Rustgi, R. Biodegradable Polymers. *Prog. Polym. Sci.* **1998,** *23,* 1273-1335.

Chandy, T.; Mooradian, D. L.; Rao, G. H. R. Evaluation of Modified Alginate-Chitosan-Polyethylene Glycol Microcapsules for Cell Encapsulation. *Artif. Organs* **1999,** *23,* 894-903.

Chen, F. Y.; Hung, W. C.; Huang, H. W. Critical Swelling of Phospholipid Bilayers. *Phys. Rev. Lett.* **1997,** *79,* 4026-4029.

Chen, J.; Heitmann, J. A.; Hubbe, M. A. Dependency of polyelectrolyte comples stoichiometry on the order of addition 1. Effect of salt concentration during streaming current titrations with strong poly-acid and poly-base. *Colloids Surf. A* **2003,** *223,* 215-230.

Chen, J.; Hubbe, M. A.; Heitmann, J. A.; Argyropoulos, D. S.; Rojas, O. J. Dependency of polyelectrolyte complex stoichiometry on the order of addition 2. Aluminum chloride and poly-vinylsulfate. *Colloids Surf. A* **2004,** *246,* 71-79.

Chen, Z.; Rand, R. P. The influence of cholesterol on phospholipid membrane curvature and bending elasticity. *Biophys J.* **1997,** *73,* 267-276.

Chu, D.-y.; Thomas, J. K. Effect of Cationic Surfactants on the Conformational Transition of Poly(methacrylic acid). *J. Am. Chem. Soc.* **1986,** *108,* 6270-6276.

Ciesla, U.; Schüth, F. Ordered mesoporous materials. *Microporous Mesoporous Mat.* **1999,** *27,* 131-149.

Collins, K. D. Ions from the Hofmeister series and osmolytes: effects on proteins in solution and in the crystallization process. *Methods* **2004,** *34,* 300-311.

Coma, V.; Martial-Gros, A.; Garreau, S.; Copinet, A.; Salin, F.; Deschamps, A. Edible antimicrobial films based on chitosan matrix. *J. Food Sci.* **2002,** *67,* 1162-1169.

Corma, A. From Microporous to Mesoporous Molecular Sieve Materials and Their Use in Catalysis. *Chem. Rev.* **1997,** *97,* 2373-2419.

Costigan, S. C.; Booth, P.; Templer, R. H. Swelling Series and Bilayer Defects Due to Sample Preparation. *Mol. Cryst. Liq. Cryst.* **2000,** *352,* 59-66.

Darnell, J.; Lodish, H.; Baltimore, D. *Molecular Cell Biology,* Second ed.; Scientific American Books: New York, 1990.

De Smedt, S. C.; Demeester, J.; Hennink, W. E. Cationic Polymer Based Gene Delivery Systems. *Pharm. Res.* **2000,** *17,* 113-126.

Dedinaite, A.; Ernstsson, M. Chitosan–SDS Interactions at a Solid–Liquid Interface: Effects of Surfactant Concentration and Ionic Strength. *J. Phys. Chem. B* **2003,** *107,* 8181-8188.

Dembo, A. T.; Yakunin, A. N.; Zaitsev, V. S.; Mironov, A. V.; Starodoubtsev, S. G.; Khokhlov, A. R.; Chu, B. Regular Microstructures in Gel-Surfactant Complexes: Influence of Water Content and Comparison with the Surfactant Structure in Water. *J. Polym. Sci. B: Polym. Phys.* **1996,** *34,* 2893-2898.

Di Meglio, J.-M.; Dvolaitzky, M.; Taupin, C. Determination of the Rigidity Constant of the Amphiphilic Film in "Birefringent Microemulsions": The Role of the Cosurfactant. *J. Phys. Chem.* **1985,** *89,* 871-874.

Diamant, H.; Andelman, D. Onset of self-assembly in polymer-surfactant systems. *Europhys. Lett.* **1999,** *48,* 170-176.

Diamant, H.; Andelman, D. Self-Assembly in Mixtures of Polymers and Small Associating Molecules. *Macromolecules* **2000,** *33,* 8050-8061.

Diamant, H.; Witten, T. A.; Gopal, A.; Lee, K. Y. C. Unstable topography of biphasic surfactant monolayers. *Europhys. Lett.* **2000,** *52,* 171-177.

Dobrynin, A. V.; Deshkovski, A.; Rubinstein, M. Adsorption of Polyelectrolytes at an Oppositely Charged Surface. *Phys. Rev. Lett.* **2000,** *84,* 3101-3104.

Dubois, M.; Zemb, T.; Fuller, N. L.; Rand, R. P.; Parsegian, V. A. Equation of state of a charged bilayer system: Measure of the entropy of the lamellar–lamellar transition in DDABr. *J. Chem. Phys.* **1998,** *108,* 7855-7869.

Dumitriu, S.; Chornet, E. Inclusion and release of proteins from polysaccharide-based polyion complexes. *Adv. Drug Deliv. Rev.* **1998,** *31,* 223-246.

Eastoe, J.; Summers, M.; Heenan, R. K. Control over Phase Curvature Using Mixtures of Polymerizable Surfactants. *Chem. Mater.* **2000,** *12,* 3533-3537.

Edler, K. J.; Brennan, T.; Roser, S. J.; Mann, S.; Richardson, R. M. Formation of CTAB-templated mesophase silicate films from acidic solutions. *Microporous Mesoporous Mat.* **2003,** *62,* 165-175.

El-Gibaly Development and *in vitro* evaluation of novel floating chitosan microcapsules for oral use: comparison with non-floating chitosan. *Int. J. Pharm.* **2002,** *249,* 7-21.

Evans, D. F.; Mitchell, D. J.; Ninham, B. W. Ion Binding and Dressed Micelles. *J. Phys. Chem.* **1984,** *88,* 6344-6348.

Evans, D. F.; Mitchell, D. J.; Ninham, B. W. Oil, Water, and Surfactant: Properties and Conjectured Structure of Simple Microemulsions. *J. Phys. Chem.* **1986,** *90,* 2817-2825.

Evans, D. F.; Ninham, B. W. Ion Binding and the Hydrophobic Effect. *J. Phys. Chem.* **1983,** *87,* 5025-5032.

Evans, E.; Rawicz, W. Entropy-Driven Tension and Bending Elasticity in Condensed-Fluid Membranes. *Phys. Rev. Lett.* **1990,** *64,* 2094-2097.

Faul, C. F. J.; Antonietti, M. Ionic Self-Assembly: Facile Synthesis of Supramolecular Materials. *Adv. Mat.* **2003,** *15,* 673-683.

Faul, C. F. J.; Antonietti, M.; Sanderson, R.; Hentze, H.-P. Directed Polymerization in Mesophases of Polyelectrolyte–Surfactant Complexes. *Langmuir* **2001,** *17,* 2031-2035.

Felse, P. A.; Panda, T. Production of microbial chitinases–A revisit. *Bioprocess Eng.* **2000,** *23,* 127-134.

Fendler, J. H. Self-Assembled Nanostructured Materials. *Chem. Mater.* **1996,** *8,* 1616-1624.

Fenniri, H.; Deng, B.-L.; Ribbe, A. E.; Hallenga, K.; Jacob, J.; Thiyagarajan, P. Entropically driven self-assembly of multichannel rosette nanotubes. *Proc. Natl. Acad. Sci. U.S.A.* **2002,** *99,* 6487-6492.

Fischer, T. M. Bending stiffness of lipid bilayers. II. Spontaneous curvature of the monolayers. *J. Phys. II France* **1992,** *2,* 327-336.

Fischer, T. M. Bending stiffness of lipid bilayers. III. Gaussian curvature. *J. Phys. II France* **1992,** *2,* 337-343.

Fischer, T. M. Bending stiffness of lipid bilayers. V. Comparison of two formulations. *J. Phys. II France* **1993,** *3,* 1795-1805.

Fontell, K. Cubic phases in surfactant and lipid-containing systems. *Colloid Polym. Sci.* **1990,** *268,* 264-285.

Fontell, K.; Fox, K. K.; Hansson, E. On the Structure of the Cubic Phase I1 in Some Lipid–Water Systems. *Mol. Cryst. Liq. Cryst.* **1985,** *1,* 9-17.

Friedhoff, P.; Schneider, A.; Mandelkow, E.-M.; Mandelkow, E. Rapid Assembly of Alzheimer-like Paired Helical Filaments from Microtubule-Associated Protein Tau Monitored by Fluorescence in Solution. *Biochemistry* **1998,** *37,* 10223-10230.

Fuller, N. L.; Benatti, C. R.; Rand, R. P. Curvature and Bending Constants for Phosphatidylserine-Containing Membranes. *Biophys J.* **2003,** *85,* 1667-1674.

Funari, S. S.; Rapp, G. A continuous topological change during phase transitions in amphiphile/water systems. *Proc. Natl. Acad. Sci. U.S.A.* **1999,** *96,* 7756-7759.

Ganeva, D.; Antonietti, M.; Faul, C. F. J.; Sanderson, R. Polymerization of the Organized Phases of Polyelectrolyte–Surfactant Complexes. *Langmuir* **2003,** *19,* 6561-6565.

Gawrisch, K.; Parsegian, V. A.; Hajduk, D. A.; Tate, M. W.; Gruner, S. M.; Fuller, N. L.; Rand, R. P. Energetics of a Hexagonal–Lamellar–Hexagonal-Phase Transition Sequence in Dioleoylphosphatidylethanolamine Membranes. *Biochemistry* **1992,** *31,* 2856-2864.

Genta, I.; Costantini, M.; Asti, A.; Conti, B.; Montanari, L. Influence of glutaraldehyde on drug release and mucoadhesive properties of chitosan microspheres. *Carbohydr. Polym.* **1998,** *36,* 81-88.

Giasson, S.; Kuhl, T. L.; Israelachvili, J. N. Adsorption and Interaction Forces of Micellar and Microemulsion Solutions in Ultrathin Films. *Langmuir* **1998,** *14,* 891-898.

Gleeson, J. T.; Polcyn, A. D.; Gruner, S. M. Structure of Phospholipid Suspensions under Negative Pressure. *J. Colloid Interface Sci.* **1993,** *156,* 430-432.

Goddard, E. D. Polymer-Surfactant Interaction Part II. Polymer and Surfactant of Opposite Charge. *Colloids Surf.* **1986,** *19,* 301-329.

Gonzalez, A. P. Curvature elasticity of mixed amphiphilic bilayers. *J. Chem. Phys.* **2004,** *120,* 11267-11284.

Goosen, M. F. A.; O'Shea, G. M.; Gharapetian, H. M.; Chou, S.; Sun, A. M. Optimization of Microencapsulation Parameters–Semipermeable Microcapsules as a Bioartificial Pancreas. *Biotechnlol Bioeng* **1985,** *27,* 146-150.

Gradzielski, M.; Langevin, D.; Farago, B. Experimental investigation of the structure of nonionic microemulsions and their relation to the bending elasticity of the amphiphilic film. *Phys. Rev. E* **1996,** *53,* 3900-3919.

Gradzielski, M.; Langevin, D.; Sottmann, T.; Strey, R. Droplet microemulsions at the emulsification boundary: The influence of the surfactant structure on the elastic constants of the amphiphilic film. *J. Chem. Phys.* **1997,** *106,* 106-119.

Gruner, S. M. Intrinsic Curvature Hypothesis for Biomembrane Lipid Compositions: A Role for Nonbilayer Lipids. *Proc. Natl. Acad. Sci. U.S.A.* **1985,** *82,* 3665-3669.

Gruner, S. M. Stability of Lyotropic Phases with Curved Interfaces. *J. Phys. Chem.* **1989,** *93,* 7562-7570.

Gruner, S. M. Nonlamellar lipid phases. *Cell Membranes* **1991,** *5,* 1-57.

Gruner, S. M. Soft Materials and Biomaterials Under Pressure: Putting the Squeeze on Biology. In *High-Pressure Crystallography*; Katrusiak, A., McMillan, P., Eds.; Kluwer Academic Publishers: Dordrecht, The Netherlands, 2004; pp 543-556.

Gruner, S. M.; Parsegian, V. A.; Rand, R. P. Directly Measured Deformation Energy of Phospholipid $H_{II}$ Hexagonal Phases. *Faraday Discuss. Chem. Soc.* **1986,** *81,* 29-37.

Gu, G.; Yan, H.; Chen, W.; Wang, W. Observation of Micelle Formation and Micellar Structural Transition from Sphere to Rod by Microcalorimetry. *J. Colloid Interface Sci.* **1996,** *178,* 614-619.

Guillot, S.; McLoughlin, D.; Jain, N.; Delsanti, M.; Langevin, D. Polyelectrolyte–surfactant complexes at interfaces and in bulk. *J. Phys.: Condens. Matter* **2003,** *15,* S219-S224.

Guinier, A. *X-Ray Diffraction in Crystals, Imperfect Crystals, and Amorphous Bodies*; Dover: New York, 1994.

Gupta, K. C.; Ravi Kumar, M. N. V. Structural Changes and Release Characteristics of Crosslinked Chitosan Beads in Response to Solution pH. *J.M.S.—Pure Appl. Chem.* **1999,** *A36,* 827-841.

Hansson, P. Surfactant Self-Assembly in Polyelectrolyte Gels: Aggregation Numbers and Their Relation to the Gel Collapse and the Appearance of Ordered Structures in the NaPa/$C_{12}$TAB System. *Langmuir* **1998,** *14,* 4059-4064.

Hansson, P. Self-Assembly of Ionic Surfactants in Polyelectrolyte Solutions: A Model for Mixtures of Opposite Charge. *Langmuir* **2001,** *17,* 4167-4180.

Hansson, P.; Schneider, S.; Lindman, B. Phase Separation in Polyelectrolyte Gels Interacting with Surfactants of Opposite Charge. *J. Phys. Chem. B* **2002,** *106,* 9777-9793.

Harden, J. L.; Marques, C.; Joanny, J.-F.; Andelman, D. Membrane Curvature Elasticity in Weakly Charged Lamellar Phases. *Langmuir* **1992,** *8,* 1170-1175.

Hari, P. R.; Chandy, T.; Sharma, C. P. Chitosan/calcium-alginate beads for oral delivery of insulin. *J. Appl. Polym. Sci.* **1996,** *59,* 1795-1801.

Harries, D.; May, S.; Gelbart, W. M.; Ben-Shaul, A. Structure, Stability, and Thermodynamics of Lamellar DNA–Lipid Complexes. *Biophys J.* **1998,** *75,* 159-173.

Helfrich, W. Elastic Properties of Lipid Bilayers. *Z. Naturforsch., C: Biosci.* **1973,** *28,* 693-703.

Hellweg, T.; Langevin, D. Bending elasticity of the surfactant monolayer in droplet microemulsions: Determination by a combination of dynamic light scattering and neutron spin-echo spectroscopy. *Phys. Rev. E* **1998,** *57,* 6825-6834.

Hentze, H.-P.; Antonietti, M. Template synthesis of porous organic polymers. *Curr. Opin. Solid St. M.* **2001,** *5,* 343-353.

Hisano, N.; Morikawa, N.; Iwata, H.; Ikada, Y. Entrapment of islets into reversible disulfide hydrogels. *J Biomed Mater Res* **1998,** *40,* 113-123.

*Electrostatic Effects in Soft Matter and Biophysics*; Holm, C.; Kékicheff, P.; Podgornik, R., Eds.; Kluwer Academic Publishers: Dordrecht, The Netherlands, 2001.

Howells, M. R.; Cambie, D.; Duarte, R. M.; Irick, S.; MacDowell, A. A.; Padmore, H. A.; Renner, T. R.; Rah, S.; Sandler, R. Theory and practice of elliptically bent X-ray mirrors. *Opt. Eng.* **2000,** *39,* 2748-2762.

Hsu, B. R. S.; Ho, Y. S.; Fu, S. H. Membrane compactness affects the integrity and immunoprotection of alginate-poly-L-lysine-alginate microcapsules. *Transplant Proc* **1995,** *27,* 3227-3231.

Hung, W. C.; Chen, F. Y. Osmotic Threshold and Water Association for Phospholipid Gel Phase Bilayers. *Chin. J. Phys.* **2000,** *38,* 882-892.

Hung, W. C.; Chen, F. Y. The Hydrophobic-Hydrophilic Interface of Phospholipid Membranes Studied by Lamellar X-Ray Diffraction. *Chin. J. Phys.* **2003,** *41,* 85-91.

Ilekti, P.; Martin, T.; Cabane, B.; Piculell, L. Effects of Polyelectrolytes on the Structures and Interactions of Surfactant Aggregates. *J. Phys. Chem. B* **1999,** *103,* 9831-9840.

Ilekti, P.; Piculell, L.; Tournilhac, F.; Cabane, B. How to Concentrate and Aqueous Polyelectrolyte/Surfactant Mixture by Adding Water. *J. Phys. Chem. B* **1998,** *102,* 344-351.

Imae, T.; Kamiya, R.; Ikeda, S. Formation of Spherical and Rod-like Micelles of Cetyltrimethylammonium Bromide in Aqueous NaBr Solutions. *J. Colloid Interface Sci.* **1985,** *108,* 215-225.

Isogai, N.; Narita, T.; Chen, L.; Hirata, M.; Gong, J.; Osada, Y. Polymer-surfactant interactions: their cooperativity and stoichiometry. *Colloids Surf. A* **1999,** *147,* 189-201.

Jameela, S. R.; Jayakrishnana, A. Glutaraldehyde cross-linked chitosan microspheres as a long acting biodegradable drug delivery vehicle: studies on the *in vitro* release of mitoxantrone and *in vivo* degradation of microspheres in rat muscle. *Biomaterials* **1995,** *16,* 769-775.

Jerke, G.; Pedersen, J. S.; Egelhaaf, S. U.; Schurtenberger, P. Flexibility of Charged and Uncharged Polymer-like Micelles. *Langmuir* **1998,** *14,* 6013-6024.

Joanny, J.-F.; Castelnovo, M.; Netz, R. Adsorption of charged polymers. *J. Phys.: Condens. Matter* **2000,** *12,* A1-A7.

Jung, H.-T.; Lee, S. Y.; Kaler, E. W.; Coldren, B.; Zasadzinski, J. A. Gaussian Curvature and the Equilibrium among Bilayer Cylinders, Spheres, and Discs. *Proc. Natl. Acad. Sci. U.S.A.* **2002,** *99,* 15318-15322.

Kadler, K. E.; Hojima, Y.; Prockop, D. J. Assembly of Collagen Fibrils *de Novo* by Cleavage of the Type I pC-Collagen with Procollagen C-Proteinase. *J. Biol. Chem.* **1987,** *260,* 15696-15701.

Kadler, K. E.; Hojima, Y.; Prockop, D. J. Assembly of Type I Collagen Fibrils *de Novo*. *J. Biol. Chem.* **1988,** *263,* 10517-10523.

Kamal, M.; Pfister, G.; Bahadir, M.; Lay, J. P. Uptake of C14-Simetryn by Duckweed (Lemna-Minor) During Release from a Polymer Matrix and the Consequent Herbicidal Effects. *J. Controlled Rel.* **1988,** *7,* 39-44.

Kang, J.; Rebek, J. Entropically driven binding in a self-assembling molecular capsule. *Nature* **1996,** *382,* 239-241.

Kankia, B. I.; Buckin, V.; Bloomfield, V. A. Hexamminecobalt(III)-induced condensation of calf thymus DNA: circular dichroism and hydration measurements. *Nucl. Acid. Res.* **2001,** *29,* 2795-2801.

Kawase, M.; Yashi, N.; Nakashima, Y.; Kurikawa, N.; Yagi, K.; Mizoguchi, T. Application of Glutaraldehyde-Crosslinked Chitosan as a Scaffold for Hepatocyte Attachment. *Biol. Pharm. Bull.* **1997,** *20,* 108-710.

Kayitmazer, A. B.; Seyrek, E.; Dubin, P. L.; Staggemeier, B. A. Influence of Chain Stiffness of the Interaction of Polyelectrolytes with Oppositely Charges Micelles and Proteins. *J. Phys. Chem. B* **2003,** *107,* 8158-8165.

Kékicheff, P.; Grabielle-Madelmont, C.; Ollivon, M. Phase Diagram of Sodium Dodecyl Sulfate-Water System. *J. Colloid Interface Sci.* **1989,** *131,* 112-132.

Khandurina, Y. V.; Dembo, A. T.; Rogacheva, V. B.; Zezin, A. B.; Kabanov, V. A. Structure of Polycomplexes Composed of Cross-Linked Sodium Polyacrylate and Cationic Micelle-Forming Surfactants. *Polym. Sci.* **1994,** *36,* 235-240.

Kiefer, J. J.; Somasundaran, P.; Ananthapadmanabhan, K. P. Interaction of Tetradecyltrimethylammonium Bromide with Poly(acrylic acid) and Poly(methacrylic acid). Effect of Charge Density. *Langmuir* **1993,** *9,* 1187-1192.

Kim, B.; Ishizawa, M.; Gong, J.; Osada, Y. Molecular and Supramolecular Structures of Complexes Formed by Polyelectrolyte-Surfactant Interactions: Effects of Charge Density and Compositions. *J. Polym. Sci. A: Polym. Chem.* **1999,** *37,* 635-644.

Kim, Y. W.; Sung, W. Membrane curvature induced by polymer adsorption. *Phys. Rev. E* **2001,** *63,* 041910.

Kim, Y. W.; Sung, W. Effects of charge and its fluctuation on membrane undulation and stability. *Europhys. Lett.* **2002,** *58,* 147-153.

King, G. A.; Daugulis, A. J.; Faulkner, P.; Goosen, M. F. A. Alginate–Polylysine Microcapsules of Controlled Membrane Molecular-Weight Cutoff for Mammalian Cell Culture Engineering. *Biotechnol. Prog.* **1987,** *3,* 231-240.

Kirk, G. L.; Gruner, S. M. Lyotropic Effects of Alkanes and Headgroup Composition on the $L_\alpha$–$H_{II}$ Lipid Liquid Crystal Phase Transition—Hydrocarbon Packing versus Intrinsic Curvature. *J. Phys.* **1985,** *46,* 761-769.

Kogej, K. Study of the Effect of Polyion Charge Density on Structural Properties of Complexes between Poly(acrylic acid) and Alkylpyridinium Surfactants. *J. Phys. Chem. B* **2003,** *107,* 8003-8010.

Kogej, K.; Evmenenko, G.; Theunissen, E.; Berghmans, H.; Reynaers, H. Investigation of Structures in Polyelectrolyte/Surfactant Complexes by X-ray Scattering. *Langmuir* **2001,** *17,* 3175-3184.

Kogej, K.; Evmenenko, G.; Theunissen, E.; Berghmans, H.; Skerjanc, J.; Reynaers, H.; Bras, W. Formation of ordered microstructures in polyelectrolyte/surfactant systems: linear anionic polyelectrolytes and cetylpyridinium chloride. *Macromol. Rapid Commun.* **2000,** *21,* 1226-1233.

Kogej, K.; Theunissen, E.; Reynaers, H. Effect of Polyion Charge Density on the Morphology of Nanostructures in Polyelectrolyte-Surfactant Complexes. *Langmuir* **2002,** *18,* 8799-8805.

Konop, A. J.; Colby, R. H. Role of Condensed Counterions in the Thermodynamics of Surfactant Micelle Formation with and without Oppositely Charged Polyelectrolytes. *Langmuir* **1999,** *15,* 58-65.

Kosmella, S.; Kötz, J.; Shirahama, K.; Liu, J. Cooperative Nature of Complex Formation in Mixed Polyelectrolyte-Surfactant Systems. *J. Phys. Chem. B* **1998,** *102,* 6459-6464.

Kríz, J.; Dybal, J.; Kurková, D. Energy versus Entropy in Cooperative Electrostatic Interactions: Comparative Study of Binding of Sodium Poly(Styrenesulfonate), Dodecylbenzenesulfonate, and Methylbenzenesulfonate to Polycations. *J. Phys. Chem.* **2002,** *106,* 2175-2185.

Kumar, M. N. V. R. A review of chitin and chitosan applications. *React. Funct. Polym.* **2000,** *46,* 1-27.

Kumar, S.; Naqvi, A. Z.; ud-Din, K. Micellar Morphology in the Presence of Salts and Organic Additives. *Langmuir* **2000,** *16,* 5252-5256.

Kwok, K. K.; Groves, M. J.; Burgess, D. J. Production of 5-15 μm Diameter Alginate–Polylysine Microcapsules by an Air-Atomization Technique. *Pharm. Res.* **1991,** *8,* 341-344.

Kwon, S. Y.; Kim, M. W. Structure and Growth Control of a Nonionic Surfactant Micelle by Adding a Phospholipid. *Langmuir* **2001,** *17,* 8016-8023.

Langevin, D. Dynamics of surfactant layers. *Current Opinion in Colloid and Interface Science* **1998,** *3,* 600-607.

Lapeña, A. M.; Gross, A. F.; Tolbert, S. H. Examining the Role of Surfactant Packing in Phase Transformations of Periodic Templated Silica/Surfactant Composites. *Langmuir* **2005,** *21,* 470-480.

Lau, A. W. C.; Pincus, P. Charge-Fluctuation-Induced Nonanalytic Bending Rigidity. *Phys. Rev. Lett.* **1998,** *81,* 1338-1341.

Leaver, M. S.; Olsson, U.; Wennerström, H.; Strey, R. Emulsification failure in a ternary system. *J. Phys. II France* **1994,** *4,* 515-531.

Leaver, M. S.; Rajagopalan, V.; Olsson, U.; Mortensen, K. Non-spherical micelles in an oil-in-water cubic phase. *Phys. Chem. Chem. Phys.* **2000,** *2,* 2951-2958.

Leikin, S.; Rau, D. C.; Parsegian, V. A. Measured entropy and enthalpy of hydration as a function of distance between DNA double helices. *Phys. Rev. A* **1991,** *44,* 5272-5278.

Leikin, S.; Rau, D. C.; Parsegian, V. A. Direct Measurement of Forces Between Self-Assembled Proteins - Temperature-Dependent Exponential Forces Between Collagen Triple Helices. *Proc. Natl. Acad. Sci. U.S.A.* **1994,** *91,* 276-280.

LeNeveu, D. M.; Rand, R. P.; Gingell, D.; Parsegian, V. A. Measurement and modification of forces between lecithin bilayers. *Biophys J.* **1977,** *18,* 209-230.

Leonard, M.; Hong, H. M.; Easwar, N.; Strey, H. H. Soft matter under osmotic stress. *Polymer* **2001,** *42,* 235-239.

Leonard, M. J.; Strey, H. H. Phase Diagrams of Stoichiometric Polyelectrolyte–Surfactant Complexes. *Macromolecules* **2003,** *36,* 9549-9558.

Li, D. Curvature effects on the phase rule. *Fluid Phase Equilib.* **1994,** *98,* 13-34.

Li, D.; Gaydos, J.; Neumann, A. W. The Phase Rule for Systems Containing Surfaces and Lines, 1. Moderate Curvature. *Langmuir* **1989,** *5,* 1133-1140.

Li, Y.; Dubin, P. L.; Havel, H. A.; Edwards, S. L.; Dautzenberg, H. Complex Formation between Polyelectrolyte and Oppositely Charged Mixed Micelles: Soluble Complexes vs Coacervation. *Langmuir* **1995,** *11,* 2486-2492.

*CRC Handbook of Chemistry and Physics;* 73rd ed.; Lide, D. R., Ed.; CRC Press: Boca Raton, FL, 1993.

Lim, P. F. C.; Chee, L. Y.; Chen, S. B. Study of Interaction between Cetyltrimethylammonium Bromide and Poly(acrylic acid) by Rheological Measurements. *J. Phys. Chem. B* **2003,** *107,* 6491-6496.

Lindblom, G.; Rilfors, L. Cubic phases and isotropic structures formed by membrane lipids - possible biological relevance. *Biochim. Biophys. Acta* **1989,** *988,* 221-256.

Lis, L. J.; McAlister, M.; Fuller, N. L.; Rand, R. P.; Parsegian, V. A. Interactions between neutral phospholipid bilayer membranes. *Biophys J.* **1982,** *37,* 657-665.

Liu, T.; Burger, C.; Chu, B. Nanofabrication in polymer matrices. *Prog. Polym. Sci.* **2003,** *28,* 5-26.

Luzzati, V.; Husson, F. Structure of Liquid-Crystalline Phases of Lipid-Water Systems. *J. Cell. Biol.* **1962,** *12,* 207-216.

Macdonald, P. M. $^{2}$H NMR and polyelectrolyte-surfactant interactions: from micelles to monolayers to membranes. *Colloids Surf. A* **1999,** *147,* 115-131.

Macdonald, P. M.; Strashko, V. A Thermotropic Phase Transition in Polyelectrolyte-Surfactant Complexes As Characterized by Deuterium NMR. *Langmuir* **1998,** *14,* 4758-4764.

MacKnight, W. J.; Ponomarenko, E. A.; Tirrell, D. A. Self-Assembled Polyelectrolyte-Surfactant Complexes in Nonaqueous Solvents and in the Solid State. *Acc. Chem. Res.* **1998,** *31,* 781-787.

Magid, L. J. The Surfactant-Polyelectrolyte Analogy. *J. Phys. Chem. B* **1998,** *102,* 4064-4074.

Malinin, V. S.; Lentz, B. R. Energetics of Vesicle Fusion Intermediates: Comparison of Calculations with Observed Effects of Osmotic and Curvature Stresses. *Biophys J.* **2004,** *86,* 2951-2964.

Malinin, V. S.; Lentz, B. R. On the Analysis of Elastic Deformations in Hexagonal Phases. *Biophys J.* **2004,** *86,* 3324-3328.

Manning, G. S. Counterion binding in polyelectrolyte theory. *Acc. Chem. Res.* **1979,** *12,* 443-449.

Mariani, P.; Luzzati, V.; Delacroix, H. Cubic Phases of Lipid-Containing Systems: Structure Analysis and Biological Implications. *J. Mol. Biol.* **1988,** *204,* 165-189.

May, S. Curvature elasticity and thermodynamic stability of electrically charged membranes. *J. Chem. Phys.* **1996,** *105,* 8314-8323.

May, S.; Ben-Shaul, A. Spontaneous curvature and thermodynamic stability of mixed amphiphilic layers. *J. Chem. Phys.* **1995,** *103,* 3839-3848.

May, S.; Bohbot, Y.; Ben-Shaul, A. Molecular Theory of Bending Elasticity and Branchin of Cylindrical Micelles. *J. Phys. Chem. B* **1997,** *101,* 8648-8657.

McGrath, K. M.; Dabbs, D. M.; Yao, N.; Aksay, I. A.; Gruner, S. M. Formation of a Silicate $L_3$ Phase with Continuously Adjustable Pore Sizes. *Science* **1997,** *277,* 552-556.

Meier-Koll, A. A.; Fleck, C. C.; Grünberg, v. The counterion-release interaction. *J. Phys.: Condens. Matter* **2004,** *16,* 6041-6052.

Merta, J.; Garamus, V. M.; Willumeit, R.; Stenius, P. Structure of Complexes Formed by PDADMAC and Sodium Palmitate. *Langmuir* **2002,** *18,* 7272-7278.

Merta, J.; Torkkeli, M.; Ikonen, T.; Serimaa, R.; Stenius, P. Structure of Cationic Starch (CS) / Anionic Surfactant Complexes Studied by Small-Angle X-ray Scattering (SAXS). *Macromolecules* **2001,** *34,* 2937-2946.

Michel, B. E. Evaluation of the water potentials of solutions of polyethylene glycol-8000 both in the absence and presence of other solutes. *Plant Physiol.* **1983,** *72,* 66-70.

Michel, B. E.; Kaufmann, M. R. Osmotic potential of polyethylene-glycol 6000. *Plant Physiol.* **1973,** *51,* 914-916.

Michiotti, P.; Bonicelli, M. G.; Cafarelli, P.; Ceccaroni, G.; Ferragina, C.; La Mesa, C. Complexes of octadecyltrimethylammonium polyacrylate: properties in solution, gel and solid forms. *Colloid Polym. Sci.* **2003,** *281,* 431-438.

Mironov, A. V.; Starodoubtsev, S. G.; Khokhlov, A. R.; Dembo, A. T.; Yakunin, A. N. Ordered Nonstoichiometric Polymer Gel-Surfactant Complexes in Aqueous Medium with High Ionic Strength. *Macromolecules* **1998,** *31,* 7698-7705.

Mironov, A. V.; Starodoubtsev, S. G.; Khokhlov, A. R.; Dembo, A. T.; Yakunin, A. N. Structural study of surfactant aggregates in polyelectrolyte gel. *Colloids Surf. A* **1999,** *147,* 213-220.

Miyake, M.; Kakizawa, Y. Study on the interaction between polyelectrolytes and oppositely charged ionic surfactants. Solubilized state of the complexes in the postprecipitation region. *Colloid Polym. Sci.* **2002,** *280,* 18-23.

Monnier, A.; Schüth, F.; Huo, Q.; Kumar, D.; Margolese, D.; Maxwell, R. S.; Stucky, G. D.; Krishnamurty, M.; Petroff, P.; Firouzi, A.; Janicke, M.; Chmelka, B. F. Cooperative Formation of Inorganic–Organic Interfaces in the Synthesis of Silicate Mesostructures. *Science* **1993,** *261,* 1299-1303.

Muzzarelli, R. A. A.; Muzzarelli, C.; Tarsi, R.; Miliani, M.; Gabbanelli, F.; Cartolari, M. Fungistatic activity of modified chitosans against *Saprolegnia parasitica*. *Biomacromolecules* **2001,** *2,* 165-169.

Naor, A.; Puvvada, S.; Blankschtein, D. An Analytical Expression for the Free Energy of Micellization. *J. Phys. Chem.* **1992,** *96,* 7830-7832.

Naves, A.; Petri, D. F. S. The effect of molecular weight and degree of substitution on the interactions between carboxymethyl cellulose and cetyltrimethylammonium bromide. *Colloids Surf. A* **2005,** *254,* 207-214.

Netz, R. Buckling and nonlocal elasticity of charged membranes. *Phys. Rev. E* **2001,** *64,* 051401.

Neumann, M. G.; Schmitt, C. C.; Iamazaki, E. T. A fluorescence study of the interactions between sodium alginate and surfactants. *Carbohydr. Res.* **2003,** *338,* 1109-1113.

Nizri, G.; Magdassi, S.; Schmidt, J.; Cohen, Y.; Talmon, Y. Microstructural Characterization of Micro- and Nanoparticles Formed by Polymer–Surfactant Interactions. *Langmuir* **2004,** *20,* 4380-4385.

Ober, C. K.; Wegner, G. Polyelectrolyte-Surfactant Complexes in the Solid State: Facile Building Blocks for Self-Organizing Materials. *Adv. Mat.* **1997,** *9,* 17-31.

Odian, G. *Principles of Polymerization,* 3rd ed.; Wiley: New York, 1991.

Okuyama, K.; Noguchi, K.; Miyazawa, T.; Yui, T. Molecular and Crystal Structure of Hydrated Chitosan. *Macromolecules* **1997,** *30,* 5849-5855.

Orädd, G.; Gustafsson, J.; Almgren, M. Intermediate Phases in the System Egg Lecithin/CTAC/Brine. SAXS and NMR Studies. *Langmuir* **2001,** *17,* 3227-3234.

Oungbho, K.; Müller, B. W. Chitosan Sponges as Sustained Release Drug Carriers. *Int. J. Pharm.* **1997,** *156,* 229-237.

Ozeki, S.; Ikeda, S. The Sphere-Rod Transition of Micelles and the Two-Step Micellization of Dodecyltrimethylammonium Bromide in Aqueous NaBr Solutions. *J. Colloid Interface Sci.* **1982,** *87,* 424-435.

Pantazis, C. C.; Trikalitis, P. N.; Pomonis, P. J.; Hudson, M. J. A method of synthesis of silicious inorganic ordered materials (MCM-41–SBA-1) employing polyacrylic acid–$C_n$TAB–TEOS nanoassemblies. *Microporous Mesoporous Mat.* **2003,** *66,* 37-51.

Parsegian, V. A.; Fuller, N. L.; Rand, R. P. Measured Work of Deformation and Repusion of Lecithin Bilayers. *Proc. Natl. Acad. Sci. U.S.A.* **1979,** *76,* 2750-2754.

Parsegian, V. A.; Rand, R. P.; Fuller, N. L.; Rau, D. C. Osmotic Stress for the Direct Measurement of Intermolecular Forces. In *Methods in Enzymology*; Packer, L., Ed.; Academic Press, Inc., 1986; Vol. 127; pp 400-416.

Philip, J.; Gnanaprakash, G.; Jayakumar, T.; Kalyanasundaram, P.; Raj, B. Three Distinct Scenarios under Polymer, Surfactant, and Colloidal Interaction. *Macromolecules* **2003,** *36,* 9230-9236.

Pileni, M.-P. The role of soft colloidal templates in controlling the size and shape of inorganic nanocrystals. *Nat. Mater.* **2003,** *2,* 145-150.

Podgornik, R.; Strey, H. H.; Parsegian, V. A. Colloidal DNA. *Curr. Opin. Colloid In.* **1998,** *3,* 534-539.

Ponomarenko, E. A. Self-Assembled Polypeptide-Surfactant Complexes in Organic Solvents and in the Solid State: A New Class of Comb-Shaped Polypeptides. Ph.D. Dissertation, University of Massachusetts Amherst, 1997.

Ponomarenko, E. A.; Tirrell, D. A.; MacKnight, W. J. Stoichiometric Complexes of Synthetic Polypeptides and Oppositely Charged Surfactants in Organic Solvents and in the Solid State. *Macromolecules* **1996,** *29,* 8751-8758.

Ponomarenko, E. A.; Tirrell, D. A.; MacKnight, W. J. Water-Insoluble Complexes of Poly(L-Lysine) with Mixed Alkyl Sulfates: Composition-Controlled Solid State Structures. *Macromolecules* **1998,** *31,* 1584-1589.

Ponomarenko, E. A.; Waddon, A. J.; Bakeev, K. N.; Tirrell, D. A.; MacKnight, W. J. Self-Assembled Complexes of Synthetic Polypeptides and Oppositely Charged Low Molecular Weight Surfactants. Solid State Properties. *Macromolecules* **1996,** *29,* 4340-4345.

Ponomarenko, E. A.; Waddon, A. J.; Tirrell, D. A.; MacKnight, W. J. Structure and Properties of Stoichiometric Complexes Formed by Sodium Poly($\alpha$,L-glutamate) and Oppositely Charged Surfactants. *Langmuir* **1996,** *12,* 2169-2172.

Posillico, E. G. Microencapsulation Technology for Large-Scale Antibody-Production. *Biotechnology* **1986,** *4,* 114-117.

Puvvada, S.; Blankschtein, D. Thermodynamic Description of Micellization, Phase Behavior, and Phase Separation of Aqueous Solutions of Surfactant Mixtures. *J. Phys. Chem.* **1992,** *96,* 5567-5579.

Rançon, Y.; Charvolin, J. Epitaxial Relationships during Phase Transformations in a Lytropic Liquid Crystal. *J. Phys. Chem.* **1988,** *92,* 2646-2651.

Rand, R. P.; Fuller, N. L.; Gruner, S. M.; Parsegian, V. A. Membrane Curvature, Lipid Segregation, and Structural Transitions for Phospholipids under Dual-Solvent Stress. *Biochemistry* **1990,** *29,* 76-87.

Rand, R. P.; Parsegian, V. A. Hydration forces between phospholipid bilayers. *Biochim. Biophys. Acta* **1989,** *988,* 351-376.

Rappolt, M.; Hickel, A.; Bringezu, F.; Lohner, K. Mechanism of the Lamellar/Inverse Hexagonal Phase Transition Examined by High Resolution X-Ray Diffraction. *Biophys J.* **2003,** *84,* 3111-3122.

Rau, D. C.; Parsegian, V. A. Direct Measurement of Forces Between Linear Polysaccharides Xanthan and Schizophyllan. *Science* **1990,** *249,* 1278-1281.

Ray, B.; El Hasri, S.; Guenet, J.-M. Effect of polymer tacticity on the molecular structure of polyelectrolyte/surfactant stoichiometric complexes in solution and gels. *Eur. Phys. J. E* **2003,** *11,* 315-323.

Rekvig, L.; Hafskjold, B.; Smit, B. Chain Length Dependencies of the Bending Modulus of Surfactant Monolayers. *Phys. Rev. Lett.* **2004,** *92,* 116101.

Roelants, E.; De Schryver, F. C. Parameters Affecting Aqueous Micelles of CTAC, TTAC, and DTAC Probed by Fluorescence Quenching. *Langmuir* **1987,** *3,* 209-214.

Rowley, J. A.; Madlambayan, G.; Mooney, D. J. Alginate hydrogels as synthetic extracellular matrix materials. *Biomaterials* **1999,** *20,* 45-53.

Safinya, C. R.; Roux, D.; Smith, G. S.; Sinha, S. K.; Dimon, P.; Clark, N. A.; Bellocq, A. M. Steric Interactions in a Model Multimembrane System: A Synchrotron X-Ray Study. *Phys. Rev. Lett.* **1986,** *57,* 2718-2721.

Safinya, C. R.; Sirota, E. B.; Roux, D.; Smith, G. S. Universality in Interacting Membranes: The Effect of Cosurfactants on the Interfacial Rigidity. *Phys. Rev. Lett.* **1989,** *62,* 1134-1137.

Sasaki, S.; Koga, S. Order–Disorder Phase Transition of Polyelectrolyte Gel–Surfactant Complexes. *Macromolecules* **2004,** *37,* 3809-3814.

Sasaki, S.; Koga, S.; Sugiyama, M.; Annaka, M. Nanostructures of polyelectrolyte gel–surfactant complexes in uniaxially stretched networks. *Phys. Rev. E* **2003,** *68,* 021504.

Schmuck, C. Self-assembly of 2-(guanidiniocarbonyl)-pyrrole-4-carboxylate in dimethyl sulfoxide: an entropy driven oligomerization. *Tetrahedron* **2001,** *37,* 3063-3067.

Schüth, F. Non-siliceous Mesostructured and Mesoporous Materials. *Chem. Mater.* **2001,** *13,* 3184-3195.

Schwarz, H.-H.; Richau, K.; Apostel, R. The Combination of Ionic Surfactants with Polyelectrolytes-A New Material for Membranes? *Macromolecular Symposium* **1997,** *126,* 95-104.

Schwarz, U. S.; Gompper, G. Bending Frustration of Lipid–Water Mesophases Based on Cubic Minimal Surfaces. *Langmuir* **2001,** *17,* 2084-2096.

Schwarz, U. S.; Swamy, K.; Gompper, G. The lamellar-to-isotropic transition in ternary amphiphilic systems. *Europhys. Lett.* **1996,** *36,* 117-122.

Seddon, J. M. Structure of the inverted hexagonal ($H_{II}$) phase, and non-lamellar phase transitions of lipids. *Biochim. Biophys. Acta* **1990,** *1031,* 1-69.

Seddon, J. M.; Robins, J.; Gulik-Krzywicki, T.; Delacroix, H. Inverse micellar phases of phospholipids and glycolipids. *Phys. Chem. Chem. Phys.* **2000,** *2,* 4485-4493.

Sens, P.; Joanny, J.-F. Counterion Release and Electrostatic Adsorption. *Phys. Rev. Lett.* **2000,** *84,* 4862-4865.

Servuss, R. M.; Harbich, W.; Helfrich, W. Measurement of Curvature-Elastic Modulus of Egg Lecithin Bilayers. *Biochim. Biophys. Acta* **1976,** *436,* 900-903.

Shimizu, T. Changes in pH and counterion activity during the binding process of cationic surfactants to carboxylic polyions. *Colloids Surf. A* **1994,** *84,* 239-248.

Shtykova, E. V.; Shtykova, E. V.; Volkov, V. V.; Konarev, P. V.; Dembo, A. T.; Makhaeva, E. E.; Ronova, I. A.; Khokhlov, A. R.; Reynaers, H.; Svergun, D. I. Small-angle X-ray scattering reveals hollow nanostructures in ι- and κ-carrageenan/surfactant complexes. *J. Appl. Cryst.* **2003,** *36,* 669-673.

Skepö, M.; Linse, P. Dissolution of a polyelectrolyte-macroion complex by addition of salt. *Phys. Rev. E* **2002,** *66,* 051807.

Sludden, J.; Uchegbu, I. F.; Schätzlein, A. G. The Encapsulation of Bleomycin Within Chitosan Based Polymeric Vesicles Does Not Alter its Biodistribution. *J. Pharm. Pharmacol.* **2000,** *52,* 377-382.

Smith, G. S.; Sirota, E. B.; Safinya, C. R.; Clark, N. A. Structure of the $L_\beta$ Phases in a Hydrated Phosphatidylcholine Multimembrane. *Phys. Rev. Lett.* **1988,** *60,* 813-816.

So, P. T. C.; Gruner, S. M.; Erramilli, S. Pressure-Induced Topological Phase Transitions in Membranes. *Phys. Rev. Lett.* **1993,** *70,* 3455-3458.

Sokolov, E. L.; Yeh, F.; Khokhlov, A. R.; Chu, B. Nanoscale Supramolecular Ordering in Gel-Surfactant Complexes: Sodium Alkyl Sulfates in Poly(diallyldimethylammonium Chloride). *Langmuir* **1996,** *12,* 6229-6234.

Sokolov, E. L.; Yeh, F.; Khokhlov, A. R.; Grinberg, V. Y.; Chu, B. Nanostructure Formation in Polyelectrolyte-Surfactant Complexes. *J. Phys. Chem. B* **1998,** *102,* 7091-7098.

Sorci, G. A.; Reed, W. F. Electrostatic and Association Phenomena in Aggregates of Polymers and Micelles. *Langmuir* **2002,** *18,* 353-357.

Sottmann, T.; Strey, R.; Chen, S.-H. A small-angle neutron scattering study of nonionic surfactant molecules at the water-oil interface: Area per molecule, microemulsion domain size, and rigidity. *J. Chem. Phys.* **1997,** *106,* 6483-6491.

Stanley, C. B.; Strey, H. H. Measuring Osmotic Pressure of Poly(ethylene glycol) Solutions by Sedimentation Equilibrium Ultracentrifugation. *Macromolecules* **2003,** *36,* 6888-6893.

Stoyanov, S. D.; Paunovv, V. N.; Kuhn, H.; Rehage, H. A General Method for Calculating Bending Moduli and Spontaneous Curvature of Polymer Brushes in Terms of Local Density Functional Theory. *Macromolecules* **2003,** *36,* 5032-5038.

Strey, H. H.; Hoagland, D. A. University of Massachusetts Amherst, Amherst, MA. Lecture notes from Biopolymers course (PSE 742), 1999.

Strey, H. H.; Parsegian, V. A.; Podgornik, R. Equation of State for DNA Liquid Crystals: Fluctuation Enhanced Electrostatic Double Layer Repulsion. *Phys. Rev. Lett.* **1997,** *78,* 895-898.

Strey, H. H.; Parsegian, V. A.; Podgornik, R. Equation of State for Lyotropic Polymer Liquid Crystals: Theory and Experiment. *Phys. Rev. E* **1999,** *59,* 999-1008.

Strey, H. H.; Podgornik, R.; Rau, D. C.; Parsegian, V. A. DNA-DNA interactions. *Curr. Opin. Struc. Biol.* **1998,** *8,* 309-313.

Svensson, A.; Piculell, L.; Cabane, B.; Ilekti, P. A New Approach to the Phase Behavior of Oppositely Charged Polymers and Surfactants. *J. Phys. Chem. B* **2002,** *106,* 1013-1018.

Svensson, A.; Sjöström, J.; Scheel, T.; Piculell, L. Phases and structures of a polyion–surfactant ion complex salt in aqueous mixtures: cationic hydroxyethyl cellulose with dodecylsulfate counterions. *Colloids Surf. A* **2003,** *228,* 91-106.

Svensson, A.; Topgaard, D.; Piculell, L.; Söderman, O. Molecular Self-Diffusion in Micellar and Discrete Cubic Phases of an Ionic Surfactant with Mixed Monovalent/Polymeric Counterions. *J. Phys. Chem. B* **2003,** *107,* 13241-13250.

Szleifer, I.; Kramer, D.; Ben-Shaul, A. Curvature Elasticity of Pure and Mixed Surfactant Films. *Phys. Rev. Lett.* **1988,** *60,* 1966-1969.

Tanford, C. Micelle Shape and Size. *J. Phys. Chem.* **1972,** *76,* 3020-3024.

Tanford, C. Thermodynamics of Micelle Formation: Prediction of Micelle Size and Size Distribution. *Proc. Natl. Acad. Sci. U.S.A.* **1974,** *71,* 1811-1815.

Tao, C.; Li, J. Synthesis and Characterization of Wormlike Mesoporous Silica by Using Polyelectrolyte/Surfactant Complexes as Templates. *Langmuir* **2003,** *19,* 10353-10356.

Tarsi, R.; Corbin, B.; Pruzzo, C.; Muzzarelli, R. A. A. Effect of low-molecular-weight chitosans on the adhesive properties of oral streptococci. *Oral Microbiol. Immunol.* **1998,** *13,* 217-224.

Tarsi, R.; Muzzarelli, R. A. A.; Guzman, C. A.; Pruzzo, C. Inhibition of *Streptococcus mutans* adsorption to hydroxyapatite by low-molecular-weight chitosans. *J. Dent. Res.* **1997,** *76,* 665-672.

Thalberg, K.; Lindman, B. Gel Formation in Aqueous Systems of a Polyanion and an Oppositely Charged Surfactant. *Langmuir* **1991,** *7,* 277-283.

Thalberg, K.; Lindman, B. Segregation in aqueous systems of a polyelectrolyte and an ionic surfactant. *Colloids Surf. A* **1993,** *76,* 283-288.

Thalberg, K.; Lindman, B.; Bergfeldt, K. Phase Behavior of Systems of Polyelectrolyte and Cationic Surfactants. *Langmuir* **1991,** *7,* 2893-2898.

Thalberg, K.; Lindman, B.; Karlström, G. Phase Diagram of a System of Cationic Surfactant and Anionic Polyelectrolyte: Tetradecyltrimethylammonium Bromide–Hyaluronan–Water. *J. Phys. Chem.* **1990,** *94,* 4289-4295.

Thalberg, K.; Lindman, B.; Karlström, G. Phase Behavior of a System of Cationic Surfactant and Anionic Polyelectrolyte: The Effect of Salt. *J. Phys. Chem.* **1991,** *95,* 6004-6011.

Thalberg, K.; Lindman, B.; Karlström, G. Phase Behavior of Systems of Cationic Surfactant and Anionic Polyelectrolyte: Influence of Surfactant Chain Length and Polyelectrolyte Molecular Weight. *J. Phys. Chem.* **1991,** *95,* 3370-3376.

Thongngam, M.; McClements, D. J. Influence of pH, Ionic Strength, and Temperature on Self-Association and Interactions of Sodium Dodecyl Sulfate in the Absence and Presence of Chitosan. *Langmuir* **2005,** *21,* 79-86.

Thünemann, A. Polyelectrolyte–surfactant complexes (synthesis, structure and materials aspects). *Prog. Polym. Sci.* **2002,** *27,* 1473-1572.

Toombes, G. E. S.; Finnefrock, A. C.; Tate, M. W.; Gruner, S. M. Determination of Lamellar-Hexagonal Phase Transition Temperature for 1,2-Dioleoyl-sn-Glycero-3-Phosphatidylethanolamine. *Biophys J.* **2002,** *82,* 2504-2510.

Tsapis, N.; Ober, R.; Urbach, W. Modification of Elastic Constants by Charge Addition to a Nonionic Lamellar Phase. *Langmuir* **2000,** *16,* 2968-2974.

Uchegbu, I. F.; Schätzlein, A. G.; Tetley, L.; Gray, A. I.; Sludden, J.; Siddique, S.; Mosha, E. Polymeric Chitosan-based Vesicles for Drug Delivery. *J. Pharm. Pharmacol.* **1998,** *50,* 453-458.

Vaknin, D.; Dahlke, S.; Travesset, A.; Nizri, G.; Magdassi, S. Induced Crystallization of Polyelectrolyte–Surfactant Complexes at the Gas-Water Interface. *Phys. Rev. Lett.* **2004,** *93,* 218302.

Vargas, R.; Mariani, P.; Gulik, A.; Luzzati, V. Cubic Phases of Lipid-Containing Systems–The Structure of Phase-Q223 (Space Group *Pm3n*)– An X-Ray Scattering Study. *J. Mol. Biol.* **1992,** *225,* 137-145.

Vårum, K. M.; Anthonsen, M. W.; Grasdalen, H.; Smidsrød, O. Determination of the degree of *N*-acetylation and the distribution of *N*-acetyl groups in partially *N*-deacetylated chitins (chitosans) by high-field n.m.r. spectroscopy. *Carbohydr. Res.* **1991,** *211,* 17-23.

Vollmer, D. How to calculate phase diagrams for microemulsions–a simple rule. *Fett/Lipid* **1999,** *101,* 379-388.

Vollmer, D.; Strey, R. Latent Heat of Spontaneous-Curvature-Induced Lamellar-to-Microemulsion Transitions. *Europhys. Lett.* **1995,** *32,* 693-698.

Vollmer, D.; Vollmer, J. Bending free energy and spontaneous curvature for micelles and microemulsions with weak and strong surfactants. *Eur. Phys. J. E* **2001,** *4,* 153-159.

Vollmer, D.; Vollmer, J.; Strey, R. Temperature-dependent phase transitions in water-oil-surfactant mixtures: Experiment and theory. *Phys. Rev. E* **1996,** *54,* 3028-3031.

von Ferber, C.; Löwen, H. Complexes of polyelectrolytes and oppositely charged ionic surfactants. *J. Chem. Phys.* **2003,** *118,* 10774-10779.

Wagner, K.; Harries, D.; May, S.; Kahl, V.; Rädler, J. O.; Ben-Shaul, A. Direct Evidence for Counterion Release upon Cationic Lipid-DNA Condensation. *Langmuir* **2000,** *16,* 303-306.

Wallin, T.; Linse, P. Polyelectrolyte-Induced Micellization of Charged Surfactantts. Calculations Based on a Self-Consistent Field Model. *Langmuir* **1998,** *14,* 2940-2949.

Wang, C.; Tam, K. C. New Insights on the Interaction Mechanism within Oppositely Charged Polymer/Surfactant Systems. *Langmuir* **2002,** *18,* 6484-6490.

Wang, C.; Tam, K. C. Interaction between Polyelectrolyte and Oppositely Charged Surfactant: Effect of Charge Density. *J. Phys. Chem. B* **2004,** *108,* 8976-8982.

Wang, C.; Tam, K. C.; Jenkins, R. D.; Tan, C. B. Interactions between Methacrylic Acid/Ethyl Acrylate Copolymers and Dodecyltrimethylammonium Bromide. *J. Phys. Chem. B* **2003,** *107,* 4667-4675.

Wang, C.; Tong, Z.; Zeng, F.; Ren, B.; Liu, X. Binding on strong polyelectrolytes of mixed ionic and nonionic surfactants below their critical micelle concentration observed by fluorescence. *Colloid Polym. Sci.* **2003,** *282,* 141-148.

Wang, W.; McConaghy, A. M.; Tetley, L.; Uchegbu, I. F. Controls on Polymer Molecular Weight May Be Used To Control the Size of Palmitoyl Glycol Chitosan Polymeric Vesicles. *Langmuir* **2001,** *17,* 631-636.

Wang, X.; Wang, J.; Wang, Y.; Yan, H. Salt Effect on the Complex Formation between Cationic Gemini Surfactant and Anionic Polyelectrolyte in Aqueous Solution. *Langmuir* **2004,** *20,* 9014-9018.

Wei, Y. C.; Hudson, S. M. Binding of Sodium Dodecyl Sulfate to a Polyelectrolyte Based on Chitosan. *Macromolecules* **1993,** *26,* 4151-4154.

Winter, R.; Köhling, R. Static and time-resolved synchrotron small-angle X-ray scattering studies of lyotropic lipid mesophases, model biomembranes and proteins in solution. *J. Phys.: Condens. Matter* **2004,** *16,* S327-S352.

Witten, T. A. Insights from soft condensed matter. *Rev. Mod. Phys.* **1999,** *71,* S367-S373.

Wong, G. C. L.; Tang, J. X.; Lin, A.; Li, Y.; Janmey, P. A.; Safinya, C. R. F-Actin and Cationic Lipid Complexes: Stacked Three-Layer Tubule Networks. *Science* **2000,** *288,* 2035-2039.

Wu, C.; Zhou, S. Effects of Surfactants on the Phase Transition of Poly(*N*-isopropylacrylamide) in Water. *J. Polym. Sci. B: Polym. Phys.* **1996,** *34,* 1597-1604.

Wu, C.-M.; Liou, W.; Chen, H.-L.; Lin, T.-L.; Jeng, U.-S. Self-Assembled Structure of the Binary Complex of DNA with Cationic Lipid. *Macromolecules* **2004,** *37,* 4974-4980.

Würger, A. Bending Elasticity of Surfactant Films: The Role of the Hydrophobic Tails. *Phys. Rev. Lett.* **2000,** *85,* 337-340.

Xie, W. M.; Xu, P. X.; Wang, W.; Liu, Q. Preparation of water-soluble chitosan derivatives and their antibacterial activity. *J. Appl. Polym. Sci.* **2002,** *85,* 1357-1361.

Xie, W. M.; Xu, P. X.; Wang, W.; Liu, Q. Preparation and antibacterial activity of a water-soluble chitosan derivative. *Carbohydr. Polym.* **2002,** *50,* 35-40.

Yeh, F.; Sokolov, E. L.; Khokhlov, A. R.; Chu, B. Nanoscale Supramolecular Structures in the Gels of Poly(Diallyldimethylammonium Chloride) Interacting with Sodium Dodecyl Sulfate. *J. Am. Chem. Soc.* **1996,** *118,* 6615-6618.

Yeom, C. K.; Lee, K. H. Characterization of Sodium Alginate Membrane Crosslinked with Glutaraldehyde in Pervaporation Separation. *J. Appl. Polym. Sci.* **1998,** *67,* 209-219.

Ying, J. Y.; Mehnert, C. P.; Wong, M. S. Synthesis and Applications of Supramolecular-Templated Mesoporous Materials. *Angew. Chem. Int. Ed. Engl.* **1999,** *38.*

Yu, Q.; Frömmel, J.; Wolff, T.; Procházka, K. Ionene-surfactant complexes: temperature and humidity sensitive materials. *Colloid Polym. Sci.* **2004,** *282,* 1039-1043.

Yuet, P. K.; Blankschtein, D. Molecular-Thermodynamic Modeling of Mixed Cationic/Anionic Vesicles. *Langmuir* **1996,** *12,* 3802-3818.

Zhao, D.; Feng, J.; Huo, Q.; Melosh, N.; Fredrickson, G. H.; Chmelka, B. F.; Stucky, G. D. Triblock Copolymer Synthesis of Mesoporous Silica with Periodic 50 to 300 Angstrom Pores. *Science* **1998,** *279,* 548-552.

Zhou, S.; Burger, C.; Yeh, F.; Chu, B. Charge Density Effect of Polyelectrolyte Chains on the Nanostructures of Polyelectrolyte-Surfactant Complexes. *Macromolecules* **1998,** *31,* 8157-8163.

Zhou, S.; Hu, H.; Burger, C.; Chu, B. Phase Structural Transitions of Polyelectrolyte-Surfactant Complexes between Poly(vinylamine hydrochloride) and Oppositely Charged Sodium Alkyl Sulfate. *Macromolecules* **2001,** *34,* 1772-1778.

Zhou, S.; Xu, C.; Wang, J.; Golas, P.; Batteas, J. Phase Behavior of Cationic Hydroxyethyl Cellulose–Sodium Dodecyl Sulfate Mixtures: Effects of Molecular Weight and Ethylene Oxide Side Chain Length of Polymers. *Langmuir* **2004,** *20,* 8482-8489.

Zhou, S.; Yeh, F.; Burger, C.; Chu, B. Nanostructures of Polyelectrolyte Gel-Surfactant Complexes. *J. Polym. Sci. B: Polym. Phys.* **1999,** *37,* 2165-2172.

Zhou, S.; Yeh, F.; Burger, C.; Chu, B. Highly Ordered Supramolecular Structures from Self-Assembly of Ionic Surfactants in Oppositely Charged Polyelectrolyte Gels. *ACS Sym. Ser.* **2000,** *739,* 244-260.

Zhou, S.; Yeh, F.; Burger, C.; Hu, H.; Liu, T.; Chu, B. SAXS Study on Complexes Formed by Anionic Poly(sodium methacrylate-co-*N*-isopropylacrylamide) Gels with Cationic Surfactants. *Polym. Adv. Technol.* **2000,** *11,* 235-241.

Ziherl, P.; Kamien, R. D. Soap Froths and Crystal Structures. *Phys. Rev. Lett.* **2000,** *85,* 3528-3531.

Ziherl, P.; Kamien, R. D. Maximizing Entropy by Minimizing Area: Towards a New Principle of Self-Organization. *J. Phys. Chem. B* **2001,** *105,* 10147-10158.

Zilman, A.; Safran, S. A.; Sottmann, T.; Strey, R. Temperature Dependence of the Thermodynamics and Kinetics of Micellar Solutions. *Langmuir* **2004,** *20,* 2199-2207.